ON THE PREDICTABILITY OF THE NOTIONAL PERMEABILITY OF BREAKWATERS AS A FUNCTION OF CORE PROPERTIES

J.T. FRANKEN

A Numerical Study

September 2016

ON THE PREDICTABILITY OF THE NOTIONAL PERMEABILITY OF BREAKWATERS AS A FUNCTION OF CORE PROPERTIES

by

JACOBUS THOMAS FRANKEN

Master's thesis
In partial fulfilment of the requirements for the degree of

MASTER OF SCIENCE
in Civil Engineering

Delft University of Technology
faculty of Civil Engineering and Geosciences
department of Hydraulic Engineering

THESIS COMMITTEE:

Ir. J.P. van den Bos	TU Delft
Dr. ir. B. Hofland	TU Delft
Ir. S.A.H. van de Sande	Boskalis
Prof. dr. ir. W.S.J. Uijttewaal	TU Delft

PERSONAL INFORMATION:

Student number	1517147
E-mail adress	jochemfranken@gmail.com

ABSTRACT

Armour stone stability on a rubble mound breakwater slope is governed by complex processes. On the load side there is the water motion, influenced by wave breaking and turbulence for example. On the resistance side there is the structure, including all of its parameters and dimensions, some of which are more important than others for stability. The armour stones provide the first layer of resistance to the forces induced by the fluid motion and are thus an important design concern. The formulas as described by [Van der Meer, 1988] are based on empirical research and are the main design tool for armour stone stability. Its functionality is limited however: not every type of structure can be used as the formula is validated for only a select number of cases. The type of structure is taken into account using P, the so-called *notional permeability* parameter. Many research has already been performed to broaden the knowledge on this parameter. An important aspect is that P appears to depend on hydraulic conditions as well, rather than on structural properties only. That is contrary to the way its being used now. This raises doubts about the applicability of the parameter. A better idea would probably be to replace it with something that is able to better describe the interaction between fluid and structure, or replace the formula completely by advanced techniques or models.

Before that is possible, being able to predict P for structures that differ from the ones defined by [Van der Meer, 1988] is desired from an engineering perspective. Four hypotheses have been posed in previous research to do so. In this thesis, these are divided into direct- and indirect methods. The latter make use of interpolation of either a hypothetical flow into the core or measured reflection coefficient, between an impermeable structure ($P = 0.1$) and a permeable structure ($P = 0.5$). Between these bounds an intermediate-P region has been defined by altering core layer properties. The IH-2VOF numerical model has been used to simulate a range of structures in this region. All tests were done for varying wave periods.

With varying core thickness and nominal stone diameter of the core layer, predictions for P follow an expected trend. When both t_c and $D_{n50,c}$ are increased, an increase in P is obtained regardless of chosen method. Good agreement is observed between the two methods.

The results based on interpolation of Q show a clear trend and deviations for varying wave period are small. However, in the results

based on interpolation of K_r more scatter is noticed, resulting in a less clear trend. The source of this scatter in is the calculation of K_r, which seems to yield unexpected outliers in some cases. These values are not within the interpolation-range, making prediction of P impossible.

Relations for $K_r = f(\xi, D_{n50,c}, t_c)$ and $Q/\sqrt{gH^3} = f(\xi, t_c, D_{n50,c})$ were obtained by means of non-linear regression analysis. These functions can be used as an indication for the influence of changing core layer properties. Subsequently, relations for $P(Q) = f(\xi, D_{n50,c}, t_c)$ and $P(K_r) = f(\xi, D_{n50,c}, t_c)$ were acquired. These relations for *the predicted notional permeability based on interpolation* only slightly depend on ξ. A general formula for P was described in which ξ was discarded.

In practice, $P = 0.4$ can be used when designing a rubble mound breakwater with an armour layer ($t_a = 2 \cdot D_{n50,a}$), on top of a filter layer and porous core when $t_c/D_{n50,c} > 3$ and $D_{n50,c}/D_{n50,a} > 0.1$.

Now that an intermediate P-region of interest has been defined and predictions for P are quantified, the next step is to perform physical model tests. This is the original, verified way of obtaining values for the notional permeability parameter. Predictions obtained using interpolation of Q and K_r can be compared to these outcomes and the best method can be selected.

ACKNOWLEDGEMENTS

This thesis marks the completion of the Master's programme Hydraulic Engineering of the faculty Civil Engineering at the TU Delft. The research was performed in cooperation with Boskalis. I would like to express my thanks to several people who supported me during the process of writing this report:

First of all I wish to thank my graduation committee: Jeroen van den Bos, Bas Hofland, Stefan van de Sande and Wim Uijttewaal. Their constructive feedback and support was essential for completing the research.

At Boskalis, I would like to thank everyone for the nice time I had, and I am especially grateful to Stefan Aarninkhof and Jeroen van den Bos for giving me the opportunity to conduct my thesis there. It was an inspiring environment and I really enjoyed working at Boskalis.

I want to thank my friends, roommates and girlfriend for their support past months.

Without the unconditional support of my parents during my time in Delft I would never have been in the position to write this thesis. I am very grateful for the opportunities you gave me.

Jochem Franken
Delft, September 2016

CONTENTS

Nomenclature xv

1 INTRODUCTION 1
- 1.1 Background information . . . 1
- 1.2 Problem analysis . . . 2
- 1.3 Research scope . . . 3
- 1.4 Methodology . . . 3
- 1.5 Report structure . . . 4

2 LITERATURE STUDY 5
- 2.1 Previous studies . . . 5
- 2.2 General related literature . . . 17

3 METHODOLOGY 31
- 3.1 Research objective . . . 31
- 3.2 Selection of hypotheses . . . 31
- 3.3 Research set-up . . . 32
- 3.4 Numerical testing . . . 33
- 3.5 Calculating the governing parameters . . . 34

4 NUMERICAL MODEL TESTING 37
- 4.1 Introduction . . . 37
- 4.2 Overview of tested structures . . . 37
- 4.3 Test Programs . . . 42
- 4.4 Model set-up . . . 49

5 RESULTS 51
- 5.1 Framework tests . . . 51
- 5.2 Varying core thickness . . . 54
- 5.3 Sensitivities of model parameters . . . 59
- 5.4 Varying nominal diameter of the core layer . . . 61
- 5.5 Analysis of results . . . 69
- 5.6 Curve fitting . . . 72
- 5.7 Comparison with physical model tests . . . 80
- 5.8 Assumptions for predicting P . . . 81
- 5.9 Predictability . . . 84

6 CONCLUSIONS & RECOMMENDATIONS 85
- 6.1 Conclusions . . . 85
- 6.2 Discussion & Recommendations . . . 87

A SELECTION OF HYPOTHESES 93

B MODEL REFERENCE 95

C REFLECTION DATA ANALYSIS 97

D DATA FROM KIK INVESTIGATED 101

E MATLAB SCRIPTS 105

F TEST PROGRAM FOR PHYSICAL MODEL TESTS 125

G RESULTS 131

LIST OF FIGURES

Figure 1 Permeability coefficient for various structures. [Van der Meer, 1988] 2
Figure 2 Influence of permeability stability, for $S = 3$ and $S = 8$. [Van der Meer, 1988] 7
Figure 3 Dissipation Q as a function of period and core stone diameter. [Van der Meer, 1988] 8
Figure 4 Dissipation Q as a function of core stone diameter, with lines for values of P. [Van der Meer, 1988] 8
Figure 5 Figure showing an example of calculating P for $D_{50} = 0.05$. [Van der Meer, 1988] 9
Figure 6 Third structure tested by Kik. [Kik, 2011] . . . 10
Figure 7 Notional permeability as a function of the reflection coefficient. For $\cot(\alpha) = 2$, based on (9). 16
Figure 8 Influence wave height, water depth and wave period on the reflected wave. From [Muttray et al., 2006]. 20
Figure 9 Flow regions from [Van Gent, 1995] 21
Figure 10 Contributions of each term on the oscillatory signal, from [Van Gent, 1995] 21
Figure 11 Extra resistance due to oscillatory wave motion, from [Van Gent, 1995] 22
Figure 12 Validity of wave theories, adapted from [LeMéhauté, 1976] [Schiereck, 2012] 24
Figure 13 Velocities in turbulent, non-stationary flow. . . 25
Figure 14 Volume averaging process. From [IH Cantabria, 2012]. 26
Figure 15 False breaking phenomenon. [IH Cantabria, 2012] 27
Figure 16 Stone quarry in Soignies, Hainaut (province), Belgium. Photo by Jean-Pol Grandmont 28
Figure 17 Depiction of the concept 33
Figure 18 Screen capture of the animation made with Matlab 35
Figure 19 Structure A 38
Figure 20 Structure B 38
Figure 21 Structure C 39
Figure 22 Structure D 39
Figure 23 Structure E 40
Figure 24 Structures F to L 41

Figure 25 Figure showing structure as modeled in IH-2VOF 50
Figure 26 Results of the reflection hypothesis for intermediate structure D. 52
Figure 27 Results of the reflection hypothesis for intermediate structure E. 52
Figure 28 Interpolation based on Q for structure D. . . . 53
Figure 29 Interpolation based on Q for structure E. . . . 53
Figure 30 K_r values found for varying core thickness. . . 55
Figure 31 Q values found for varying core thickness. . . 55
Figure 32 Figures showing results for structures (F-I) with varied core thickness. 56
Figure 33 Figures showing results for structures (J-L) with varied core thickness. 57
Figure 34 Plot showing the interpolated P-values based on K_r based on relative core thickness. 58
Figure 35 Plot showing the interpolated P-values based on Q based on relative core thickness. 58
Figure 36 Plot showing mean values found for P, together with the range found in outcomes 59
Figure 37 Results for K_r (a) and Q (b) as a function of n . 60
Figure 38 Results for K_r (a) and Q (b) as a function of α 60
Figure 39 Results for K_r (a) and Q (b) as a function of β 60
Figure 40 Results for K_r (a) and Q (b) as a function of γ 61
Figure 41 K_r-values for increasing D_{n50} of the core. . . . 61
Figure 42 Q-values for increasing D_{n50} of the core. . . . 62
Figure 43 Interpolation based on K_r for $D_{n50,c}/D_{n50,a} = 0.025[-]$ 62
Figure 44 Interpolation based on Q for $D_{n50,c}/D_{n50,a} = 0.025[-]$ 63
Figure 45 Interpolation based on K_r for $D_{n50,c}/D_{n50,a} = 0.175[-]$ 63
Figure 46 Interpolation based on Q for $D_{n50,c}/D_{n50,a} = 0.175[-]$ 64
Figure 47 Interpolation based on K_r for $D_{n50,c}/D_{n50,a} = 0.25[-]$ 64
Figure 48 Interpolation based on Q for $D_{n50,c}/D_{n50,a} = 0.25[-]$ 65
Figure 49 Interpolation based on K_r for $D_{n50,c}/D_{n50,a} = 0.325[-]$ 65
Figure 50 Interpolation based on Q for $D_{n50,c}/D_{n50,a} = 0.325[-]$ 66
Figure 51 Interpolation based on K_r for $D_{n50,c}/D_{n50,a} = 0.4[-]$ 66
Figure 52 Interpolation based on Q for $D_{n50,c}/D_{n50,a} = 0.4[-]$ 67
Figure 53 All the obtained P-values based on K_r. 67

Figure 54 All the obtained P-values based on Q. 68
Figure 55 Plot showing mean values found for P when $D_{n50,c}$ is varied, together with the range found in outcomes 68
Figure 56 Q versus t_{core} 71
Figure 57 Q versus $D_{n50,c}$ 71
Figure 58 Q vs. t_{core} made dimensionless 73
Figure 59 Q vs. $D_{n50,core}$ made dimensionless 73
Figure 60 Results of regression analysis for t_c, lines are shown for various wave periods 74
Figure 61 Results of regression analysis for $D_{n50,c}$, lines are shown for various wave periods 75
Figure 62 $K_r - \xi$ with its fitted curves 75
Figure 63 $K_r - t_c/D_{n50,a}$ with its fitted curves, lines are shown for various wave periods 76
Figure 64 $K_r - D_{n50,c}/D_{n50,a}$ with its fitted curves, lines are shown for various wave periods 76
Figure 65 Relation (32) vs. measurements 78
Figure 66 Relation (33) vs. measurements 78
Figure 67 Influence of wave period on predictions of P . 79
Figure 68 Simplified, general relation for P along with simulation results 80
Figure 69 Plot showing relative values of calculated flow into the core, for known-P cases, extended with physical model tests of [Kik, 2011; Kluwen, 2012] 82
Figure 70 Plot showing relative values of calculated reflection coefficient, for known-P cases, extended with physical model tests of [Kik, 2011; Kluwen, 2012] 82
Figure 71 Plot showing predicted P-values for structure G, along with data from [Kik, 2011] 84
Figure 72 Data from physical tests. Interpolation based on wave period. All slopes. 97
Figure 73 Data from physical tests. Interpolation based on the surf similarity parameter. All slopes. . . 98
Figure 74 Data from physical tests. Interpolation based on the wave period. Only slopes with $\cot\alpha = 2$. 99
Figure 75 Resulting plot of method used by [Kik, 2011]. . 101
Figure 76 Plot showing damage levels for S=3 102
Figure 77 Plot showing damage levels for S=8 102
Figure 78 Data points for P=0.1 & P=0.5. 103
Figure 79 Scheme showing proven and unproven relations 125

Figure 80 Plot showing mean values found for P, together with the range found in outcomes 126

Table 1	Test program from [Van der Meer, 1988]	6
Table 2	Test program from [Kik, 2011]	11
Table 3	Test program by [Kluwen, 2012]	12
Table 4	Overview of data where reflection was measured.	17
Table 5	Forchheimer coefficients found in several empirical studies. From [Troch, 2000].	23
Table 6	Armourstone grading width. [CETMEF, 2007]	29
Table 7	Overview of structures with core thickness t_c	42
Table 8	Standard wave conditions applied	42
Table 9	Test program with varying porosity n.	44
Table 10	Test program with varying porosity α.	45
Table 11	Test program with varying porosity β.	45
Table 12	Test program with varying porosity γ.	46
Table 13	Overview of $D_{n50,c}$-values simulated	47
Table 14	Test program for simulations with varied $D_{n50,c}$.	48
Table 15	Summarizing the results for P from the linear interpolation based on K_r and Q.	54
Table 16	Summarizing the results for P from the linear interpolation based on K_r and Q for structures F to I.	54
Table 17	Summarizing the results for P from the linear interpolation based on K_r and Q for structures J to L.	55
Table 18	Table summarizing the relations found above.	70
Table 19	Example of minimal test program	128
Table 20	Table showing damage that can be expected during tests.	128
Table 21	All results obtained in the numerical simulations	131

α	Slope angle [rad]
α	Linear friction coefficient [-]
β	Non-linear friction coefficient [-]
Δ	Relative mass density [-]
δx	Horizontal grid cell size [m]
δy	Vertical grid cell size [m]
D_{n50}	Nominal stone diameter [m]
e	Void ratio [-]
Fr	Froude number [-]
γ	Added mass coefficient [-]
g	Gravitational acceleration [m/s^2]
h	Water depth in front of structure [m]
H_s	Significant wave height [m]
I	Pressure gradient [-]
K_r	Reflection coefficient [-]
k	Wave number [rad/m]
KC	Keulegan-Carpenter number [-]
L	Wave length [m]
L'	Wave length inside core [m]
N	Number of waves during a storm [-]
n	Porosity [-]
n_v	Porosity of bulk-placed materials[-]
n_{RRD}	Uniformity coefficient [-]
ν	Kinematic viscosity of water [m^s/s]
P	Notional permeability parameter [-]
p	Pressure [Pa]
Q	Flow into the core [m^2/s]
Re	Reynolds number [-]
S	Damage level [-]
s	Wave steepness [-]
t	Layer thickness [m]
T	Wave period [s]
u	Velocity [m/s]
ξ	Iribarren number [-]
ω	Angular frequency [rad/s]

SUBSCRIPTS

c	Core material
a	Armour layer
f	Filter
p	Peak
m	Mean
$\perp$	Perpendicular to

1 INTRODUCTION

1.1 BACKGROUND INFORMATION

Breakwaters can be found near coasts all over the world. Their main function is to absorb wave energy in order to prevent waves from entering a harbour, or to protect the coast itself. Several types of breakwaters exist, and can use mass to withstand the wave forcing or a slope to dissipate wave energy. In this thesis, so-called *rubble mound breakwaters* will be investigated. These structures consist of loose rock, typically an armour layer with a filter layer under it, and a core made out of sand or quarry run.

To evaluate the stability of a rubble mound breakwater several methods have been developed. After extensive testing, Hudson proposed his formula in 1953 and it is still being used as of today. [Verhagen et al., 2012] A more widely used method however is the 'Van der Meer Formula' [Van der Meer, 1988]. In the latter more variables were taken into account during the tests to acquire a more detailed formula.

The Van der Meer formula consists of 2 formulas, the choice depending on the Iribarren number. [Van der Meer, 1988]

$$\frac{H_s}{\Delta D_{n50}} = C_{pl} P^{0.18} \left(\frac{S}{\sqrt{N}}\right)^{0.2} \xi_m^{-0.5} \qquad \text{for } \xi < \xi_{cr} \qquad (1)$$

$$\frac{H_s}{\Delta D_{n50}} = C_s P^{-0.13} \left(\frac{S}{\sqrt{N}}\right)^{0.2} \xi_m^{P} \sqrt{\cot\alpha} \qquad \text{for } \xi > \xi_{cr} \qquad (2)$$

In which ξ_{cr} is the critical Iribarren number that depends on slope and wave conditions. Usually $\xi_{cr} = 2.5 - 4$. The other parameters can be found in the nomenclature, see page xv.

In the formulas a so-called *notional permeability* P is used. This parameter is based on structural properties. The value of this parameter has empirically been found to be 0.1 for a structure with an impermeable core, 0.5 for a permeable core and 0.6 for a homogeneous structure. The value of 0.4 has been defined with the help of model calculations, based on the amount of water flowing in the structure. In figure 1 on the following page the values for each type of cross section are depicted.

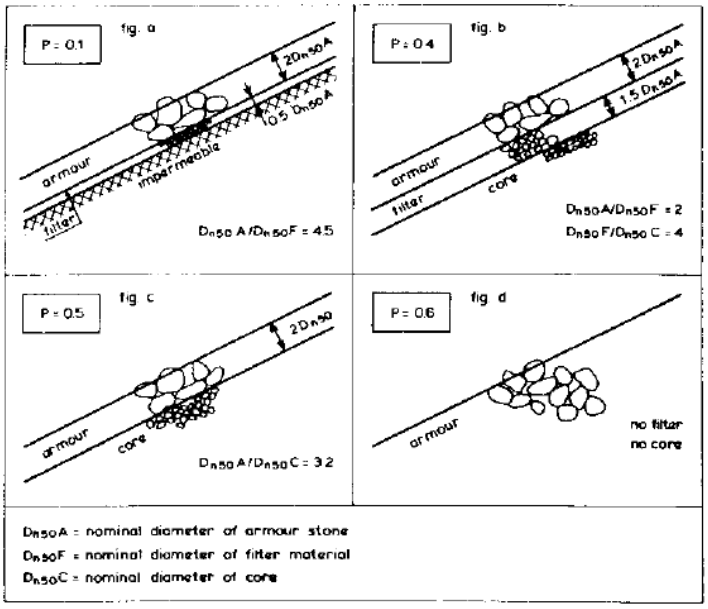

Figure 1: Permeability coefficient for various structures. [Van der Meer, 1988]

1.2 PROBLEM ANALYSIS

In practice however, the region of interest for designing rubble mound breakwaters is often between $P = 0.1$ and $P = 0.4$. Research with the goal to broaden the knowledge on this parameter is already available and tests have been executed to find a P value for other structures [Kik, 2011; Kluwen, 2012]. Moreover, studies were done to find a more physical basis for the parameter [Van der Neut, 2015; Jumelet, 2010; Van den Bos et al., 2015]. The issue of finding intermediate values for P is not so straightforward as it seems, as research pointed out that it does not only depend on structural parameters but on hydraulic conditions as well. At present, several hypotheses and methods to predict values for P have been proposed. None of the methods have been verified though, so the issue of finding an appropriate P when designing an arbitrary structure persists.

The problem for this study has been posed as follows:

PROBLEM DEFINITION In its current formulation, the *'Van der Meer formula'* is not versatile enough to calculate any given lay-out when designing a rubble mound breakwater, as P has only been validated for a few specific cross-sections. Methods to predict P for arbitrary rubble mound breakwaters exist, but have not been verified yet.

1.3 RESEARCH SCOPE

RESEARCH OBJECTIVE The ultimate goal is to find a method able to predict P-values for rubble mound breakwaters. For certain structures these values are known but for an important region between these values they are not. Several hypotheses exist to predict P for this intermediate region.

These hypotheses are based on different governing parameters. In this thesis the quality of prediction for various hypotheses is investigated.

RESEARCH QUESTIONS To fully comprehend and analyse the problem, it is subdivided into smaller research questions, formulated as follows:

- Which hypotheses are available to find values for P?
- What are the underlying processes in these methods?
- What is predicted by the various hypotheses?
- What is required to validate the method for the prediction of P?

1.4 METHODOLOGY

In short, the method to answer the research questions will be as follows:

- Investigate what hypotheses are available and make a selection for further analysis.
- Quantify parameters used by the hypotheses through numerical simulations.
- Predict P using these parameters.
- Vary hydraulic and structural parameters in order to evaluate accuracies.
- Select the most promising method.
- Define a physical test program for verification.

The methodology will be further elaborated in chapter 3 on page 31.

1.5 REPORT STRUCTURE

This report starts with a literature review (chapter 2). This section is split into a part covering research explicitly involving the notional permeability parameter, and a part covering general related research, to which references are made in following chapters. Thereafter, the report continues with the explanation of the methodology used in this research (chapter 3). The next chapters are used to explain the execution of this method (chapter 4), after which the results are presented (chapter 5) and finally what can be concluded from these results (chapter 6).

2

LITERATURE STUDY

In order to provide a basis for further research, past studies have been examined and a summary is provided in the first section. After that, other related research is summarized.

2.1 PREVIOUS STUDIES

Many studies have already been performed regarding the notional permeability parameter. This section provides an overview of previous research and highlights the important parts for this thesis.

2.1.1 *Research by Van der Meer*

In [Van der Meer, 1988] three structures with different permeabilities were tested: a revetment with impermeable core, a structure with permeable core and a homogeneous structure consisting only of armour stones, representing the upper boundary in terms of permeability. In figure 2 on page 7 the results for $\cot\alpha = 2$ are summarized. It shows a clear distinction for the different structures, where the more permeable ones are more stable. Van der Meer reasons the water motion on a permeable structure dissipates into the core and flow forces are thus less concentrated in the armour layer only, as is the case with impermeable structures.

In every test, the profile of the structure was measured before testing, after 1000 waves and after 3000 waves. With the data a certain damage level S could be determined, which could be plotted against test-parameters $H_s/\Delta D_{n50}$. This way so-called *wave height-damage curves* could be plotted, and a relation between S, N and $H_s/\Delta D_{n50}$ was found.

The test program for the physical model tests by Van der Meer was set up in such a way that the important parameters were varied in their applicable, practical range. The complete program can be found in table 1 on the next page.

DATA-FITTING PROCEDURE Using the results from the physical tests, relations were obtained by means of fitting power functions ($f = a * x^b$) through the data-points. Here, a and b were fitting

Table 1: Test program from [Van der Meer, 1988]

Slope angle $\cot\alpha$	Grading D_{85}/D_{15}	Spectral Shape	Core Permeability	Relative Mass Density	Number of Tests	Range $H_s/\Delta D_{n50}$	Range s_m
2	2.25	PM	none	1.63	19	0.8-1.6	0.005-0.016
3	2.25	PM	none	1.63	20	1.2-2.3	0.006-0.024
4	2.25	PM	none	1.63	21	1.2-3.3	0.005-0.059
6	2.25	PM	none	1.63	26	1.2-4.4	0.004-0.063
3	1.25	PM	none	1.62	21	1.4-2.9	0.006-0.038
4	1.25	PM	none	1.62	20	1.2-3.4	0.005-0.059
3	2.25	narrow	none	1.63	19	1.0-2.8	0.004-0.054
3	2.25	wide	none	1.63	20	1.0-2.4	0.004-0.043
3	1.25	PM	permeable	1.62	19	1.6-3.2	0.008-0.060
2	1.25	PM	permeable	1.62	20	1.5-2.8	0.007-0.056
1.5	1.25	PM	permeable	1.62	21	1.5-2.6	0.008-0.050
2	1.25	PM	homogeneous	1.62	16	1.8-3.2	0.008-0.059
2	1.25	PM	permeable	0.95	10	1.7-2.7	0.016-0.037
2	1.25	PM	permeable	2.05	10	1.6-2.5	0.014-0.032
2**	1.25	PM	permeable	1.62	16	1.6-2.5	0.010-0.031

** Foreshore of 1 : 30

coefficients. Reason to choose such a function was because the full applicable range was tested and the trend (increasing, decreasing or neutral) is described with one parameter, while the other describes the location of the line. The full procedure executed by Van der Meer started with above mentioned *wave height-damage curves*. Next step was to fit a relation for $H_s/\Delta D_{n_{50}} = \alpha\xi^b$, where $\alpha = f(S/\sqrt{N}, P)$. A clear change in trend was observed for $\xi < 2.5 - 4$ (depending on conditions), so a distinction was made between plunging and surging waves. For the plunging part ($\xi < 2.5 - 4$), $b = -0.5$ appeared to be consistent for every structure, damage level and storm duration. Now the relation could be written as $H_s/\Delta D_{n_{50}}\sqrt{\xi} = \alpha * (S/\sqrt{N})^b$ with $\alpha = f(P)$. Different values for α were found, results for b were quite constant around 0.2. A similar procedure was used for the surging part. From this analysis the b-values followed, called P.

FINDING OTHER P VALUES In the original thesis, Van der Meer proposes a method to calculate P for any given structure. This method was based on the idea that P could be linked to the amount of water entering the breakwater each wave. The HADEER model was used to calculate flow patterns in a breakwater under wave attack, which were used to compute the volume of water Q dissipating into the core per wave. Results are shown in figure 3. When the dissipated volume of water is now plotted as a function of the stone diameter D_{50}, lines for each permeability coefficient P can be added. The relative dissi-

pation into the structure as defined by [Van der Meer, 1988] is zero for a completely impermeable core, and 100% for a fully permeable core by definition, resulting in $P = 0.1$ and $P = 0.6$ respectively. In this context, a 'fully permeable core' refers to the situation where the structure consists only of armour stones and thus functions as an upper boundary concerning permeability. The result of this operation is shown in figure 4.

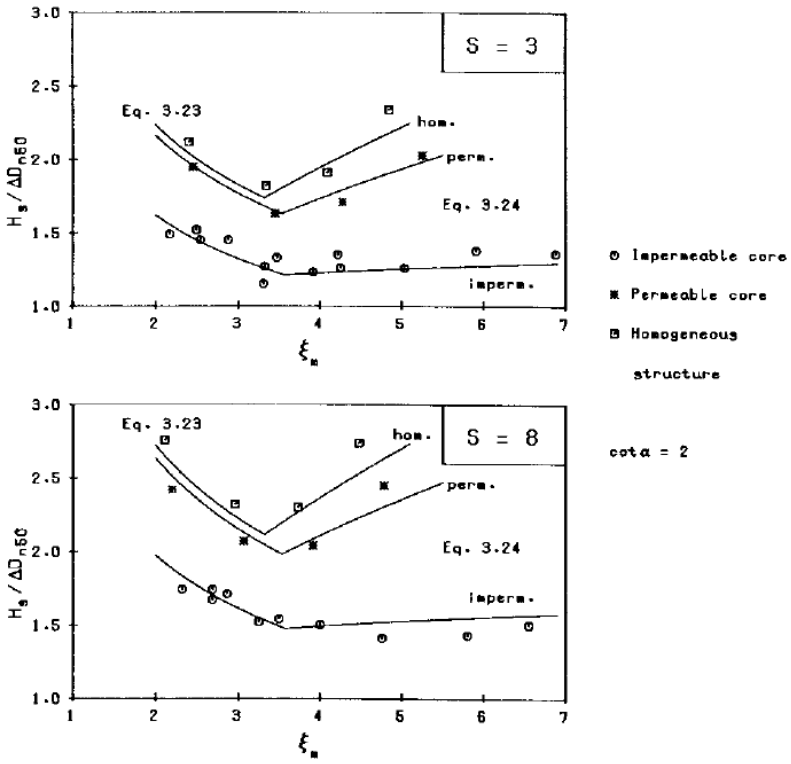

Figure 2: Influence of permeability stability, for $S = 3$ and $S = 8$. [Van der Meer, 1988]

The last step is to plot the relative dissipation versus the permeability coefficient, as shown in figure 5 for $D_{50} = 0.05$ m. The lines connecting the measurements in this graph have been assumed. For any specific structure the P value can now be estimated when the dissipation is calculated for a homogeneous and a permeable structure, and for the particular structure.

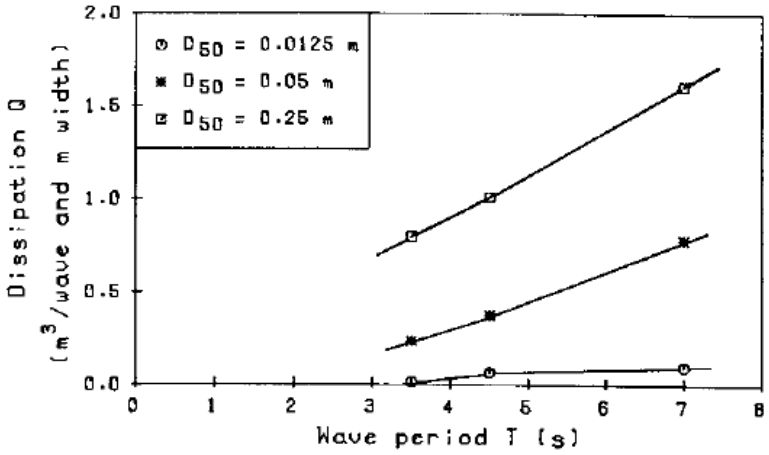

Figure 3: Dissipation Q as a function of period and core stone diameter. [Van der Meer, 1988]

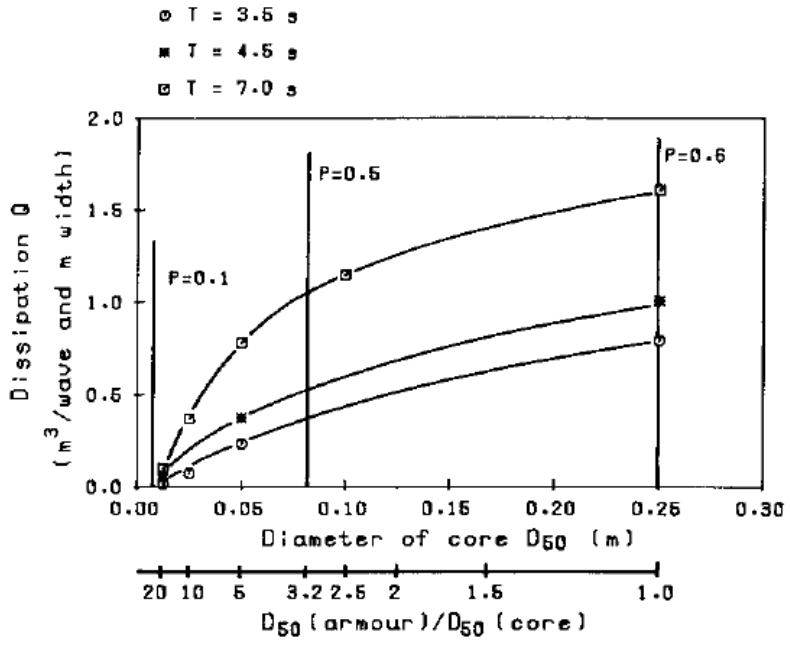

Figure 4: Dissipation Q as a function of core stone diameter, with lines for values of P. [Van der Meer, 1988]

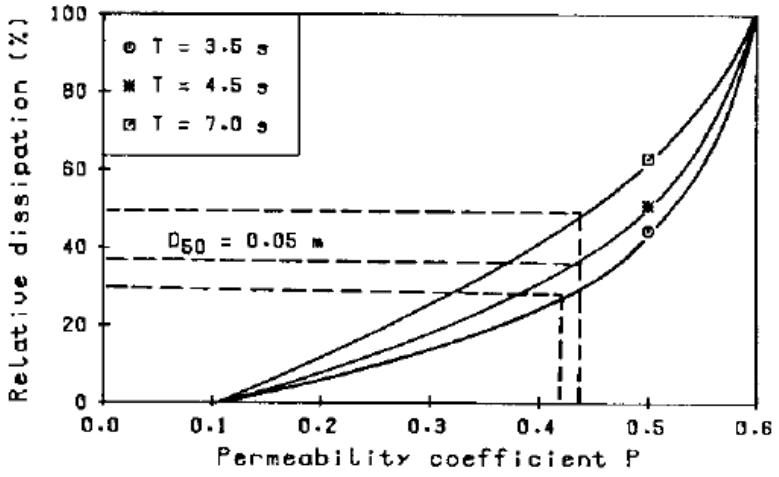

Figure 5: Figure showing an example of calculating P for $D_{50} = 0.05$. [Van der Meer, 1988]

2.1.2 *Research by Kik*

The research of Kik [2011] had the goal to broaden the available choices for P by testing a new structure. After two reference structures where similar results compared to the original thesis of [Van der Meer, 1988] were acquired, a new structure was tested. This new structure consisted of an impermeable core, followed by 2 filter layers as shown in figure 6.

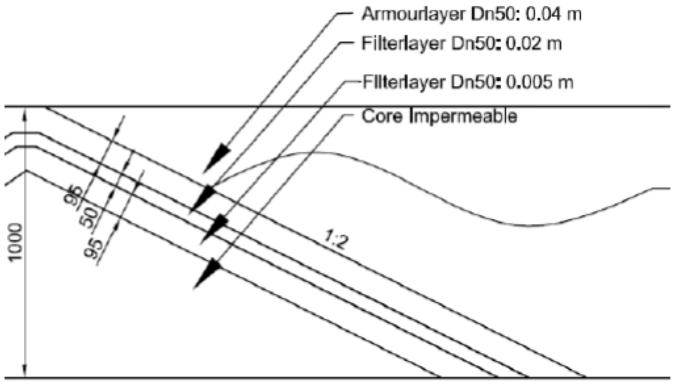

Figure 6: Third structure tested by Kik. [Kik, 2011]

TEST PROGRAM In table 2 on the facing page the test program as conducted by [Kik, 2011] can be found. The slope angle was not varied, and from the table it is directly clear that for every structure one wave height was accounted for. Reason for this decision were limitations of the flume (the wave reflection compensator) and time limits. Therefore in these tests Kik mainly focused on varying the Iribarren number, acquired by variation of the wave steepness through the wave period. The wave steepness was chosen such that it represents real-life situations (between 1% and 5%). To record the wave height, two sets of gauges were placed in the flume, one set just after the paddle and one set just in front of the structure. Using these gauges it is also possible to measure reflected waves, which have been calculated for the three structures. Kik found values that pointed (although marginal) in the opposite direction as expected, e.g. a higher reflection for a more permeable structure. He concludes therefore that reflection is not directly linked to the notional permeability. In appendix D his data is analyzed in more detail.

Table 2: Test program from [Kik, 2011]

Nr.	P	H_s	T_m(s)	T_p(s)	Steepness	Expected Damage
1	0.5	0.15	1.39	1.82	4.9	3.5
2	0.5	0.15	1.8	2.35	2.97	6.6
3	0.5	0.15	2.22	2.9	1.95	10.5
4	0.5	0.15	2.8	3.66	1.23	5.9
5	0.5	0.15	3.3	4.31	0.88	3.9
6	0.5	0.15	3.6	4.71	0.74	3.1
7	0.1	0.1	1.13	1.48	5.02	1.9
8	0.1	0.1	1.5	1.96	2.85	3.9
9	0.1	0.1	1.8	2.35	1.98	6.2
10	0.1	0.1	2.4	3.14	1.11	5.4
11	0.1	0.1	2.9	3.79	0.76	4.9
12	0.1	0.1	3.4	4.44	0.55	4.6
13	0.3?	0.13	1.3	1.7	4.93	2.7
14	0.3?	0.13	1.7	2.22	2.88	5.3
15	0.3?	0.13	2.3	3.01	1.57	11.3
16	0.3?	0.13	2.8	3.66	1.06	8.4
17	0.3?	0.13	3.2	4.18	0.81	6.9
18	0.3?	0.13	3.6	4.71	0.64	5.8

RESULTS Kik found a P value for his new construction of 0.35. However, he mentions that the slope angle was not varied and only surging waves were applied. Also the way of determining P was different than in the original work. Where Van der Meer [1988] used damage curves based on multiple measurements with equal wave period, Kik [2011] varied the Iribarren number directly and fitted the Van der Meer-formula to find a value for P.

2.1.3 *Research by Kluwen*

During her research, [Kluwen, 2012] performed model tests focusing on the influence of the layer thickness on the values of P. Concluded was that the thickness ratio of armour layer and second filter layer (t_a/t_f) determines the permeability. The value for P was calculated by fitting the Van der Meer formula to measured damage, so in a similar manner as in [Kik, 2011].

TEST PROGRAM The test program of Kluwen can be seen in table 3. She conducted more tests than Kik, and used the same method to vary the Iribarren number. Ranges are separated with a -, meaning multiple values in between were tested.

Table 3: Test program by [Kluwen, 2012]

Parameter	Test 3A	Test 4	Test 5
H_s	0.12	0.08-0.16	0.09-0.16
T_m	1.1-4.9	1.3, 1.7, 2.15, 3	1.3, 1.7, 2.15, 3
$\cot\alpha$	2	2	2
ξ_m	1.98-8.83	2.03-6.62	2.03-6.62
Δ	1.62	1.62	1.62
N	3000	3000	3000
D_{n50}	0.04	0.04	0.04
Core	Impermeable	Impermeable	Permeable

2.1.4 *Research by Neut*

While [Kik, 2011] and [Kluwen, 2012] executed physical model tests with the goal to increase the available options for choosing notional permeability parameter, [Van der Neut, 2015] focused more on describing the underlying processes. He used the original experiments by [Van der Meer, 1988] and the numerical model IH-2VOF. Output of this model consists of pressures and velocities inside the structure.

Van der Neut made a list of all relevant variables and he used the Buckingham Π theorem to determine dimensionless numbers. After a curve-fitting procedure the following formulas for predicting the

notional permeability were found:

$$P = 3.1 \cdot 10^2 \left|\frac{u_{\perp,min}}{ngT_{u\perp,min}}\right|^{1.6} \tag{3}$$

$$P = 4.1 \cdot 10^7 \left|\frac{n^2}{\rho}\left(\frac{\Delta p}{u^2}\right)_{\perp,min}\right|^{11.2} \tag{4}$$

$$P = 0.1 \left|\frac{u_{\perp,min} T_{u\perp}}{nD_{n50}}\right|^{0.9} \tag{5}$$

$$P = 7.2 \cdot 10^{-5} \left|\frac{u_{\perp,min} D_{n50}}{\nu(1-n)}\right|^{1.1} \tag{6}$$

In which:

$KC = \frac{uT}{nD}$	KC number
$Eu = \frac{n^2 \Delta p}{\rho u^2}$	Euler number
$Re = \frac{uD}{\nu(1-n)}$	Reynolds number
$Ac = \frac{u}{ngT}$	Acceleration parameter

The standard deviation for all relations separately for P is 0.18. This is quite significant. It is important to mention that this accuracy is likely to improve if more data points could be added. That means an extra intermediate structure would have to be physically tested to assess a P-value and the procedure in the thesis of [Van der Neut, 2015] would have to be repeated.

In his research, Van der Neut [2015] also explains the used model in detail. The formulas used, model performance, flaws in the software and pitfalls are elaborated. Also the parameters of the porous media, which have to be provided in the interface in which the structures are modeled, called CORAL, were calibrated to match measured pressures by [Kluwen, 2012]. For the Forchheimer coefficients, he found values of $\alpha = 0$, $\gamma = 0.51$ for all layers, $\beta = 5$ for armour layers and $\beta = 1.1$ for inner layers. See also section 2.2.3 for more information about these coefficients.

CONCLUSIONS In his conclusions, [Van der Neut, 2015] mentions that P should be used as a variable for optimal damage prediction. Furthermore, he stresses that the permeability has a large influence on the armour layer stability and that the flow inside a rubble mound breakwater can be described by the Forchheimer equation. It is also stated that the P value does not only depend on structural properties, but that P is variable and depends on external forcing (i.e. hydraulic conditions) as well. One of the recommendations is to keep hydraulic boundary conditions constant and to vary structural parameters, so the influences of the two can be distinguished.

2.1.5 *Research by Jumelet*

In his research, Jumelet [2010] looked into the physical processes governing armour layer stability and tried ways of describing them. He used a volume exchange model to investigate the influence of core permeability on the armour layer stability by calculating run-up levels. For surging waves, he found a correlation between the notional permeability factor and the so called *run-up reduction coefficient*, introduced in this study. These coefficients are used to replace P in the Van der Meer formula, resulting in:

$$\frac{H_s}{\Delta D_{n50}} = a_1 (c_r)^{n_1} \xi_m^{0.2} \sqrt{\cot\alpha} \left(\frac{S}{\sqrt{N}}\right)^{0.2} \text{ with } c_r = f(\alpha, H_s, T_0, b) \quad (7)$$

Where for homogeneous structures ($P = 0.6$): $\alpha_1 = 3.1$, $n_1 = 11$ and for permeable structures ($P = 0.5$): $\alpha_1 = 2.7$, $n_1 = 15$.

The dependencies of these α-values on the permeability of the structure causes an implicit description, as P is replaced with new values depending on P again.

An important limitation encountered using this model was that in case of a sloped water-structure interface, the volume exchange model could not compute the water inflow. The reason for this is the complexity of the phreatic surface inside the structure. Also the run-up coefficient could only be calculated for surging waves, as the wave breaking present in plunging waves was not incorporated. With the use of a model that calculates the free surface elevation these two problems could be solved.

Like [Van der Neut, 2015], Jumelet stresses that the notional permeability as it is described at the moment, does not incorporate hydraulic parameters and is based purely on structural geometry, while the tests show clearly the influence of wave period and wave height.

2.1.6 *Research by Broekhoven*

The research of Van Broekhoven [2011] can be seen as follow-up of the work of Jumelet [2010]. In his thesis, Broekhoven tried to gain insight in processes related to the influence of core permeability on armour layer stability. The wave run-up below the armour layer was the main governing parameter. He conducted several physical-model tests on sloped structures with different permeabilities, and measured the run-up with a video camera and resistance wires. The values measured by the resistance wires turned out to underestimate the run-up when compared to the images, most likely due to the spacing between stones and wires. Video seemed a better way of estimating

run-up using regular waves, as multiple points could be measured and averaged. For irregular waves measurements appeared to be difficult.

After analysis it was concluded that surface roughness seems to have little impact on armour stone stability and that the return flow causes the largest loads on the armour layer. The run-up is determined by the Iribarren number and stone diameters, and determines the flow into the structure. Contrary to the findings of [Jumelet, 2010], it is concluded that the permeability has little influence on the run-up.

2.1.7 *Research by Postma*

In the study of [Postma, 1989], wave reflection was analysed based on the data obtained in the physical model tests performed by [Van der Meer, 1988]. The focus of this study was to find a relation between structural properties of rubble mound breakwaters and the reflected wave. The relation found was:

$$K_r = 0.081 P^{-0.14} \cot\alpha^{-0.78} s^{-0.44} \tag{8}$$

Next to other parameters in this relation also P is present. The formula (8) can therefore be rewritten in (9).

$$P = 6.25 \cdot 10^{7}\ K_r^{-7.14}\ \cot\alpha^{-5.57}\ s^{-3.14} \tag{9}$$

SENSITIVITY OF THE RELATION From (9) it can be seen directly that the relation is sensitive to changing input, this is supported by conclusions from [Postma, 1989]. When looking at the formula it shows that K_r has the largest influence on P as it is raised to the power 7.14, followed by α (5.57) and the wave steepness (3.14). The latter is defined here using the deep water wave length and the peak period T_p.

In figure 7 the sensitivity of P is illustrated. It can be seen that P quickly increases for decreasing K_r. Here, the slope is set at 1:2 and P is plotted as a function of K_r for various values of the wave steepness s.

HYPOTHESIS TO CALCULATE P In [Van den Bos et al., 2015] a method is proposed to find values for P by interpolating the struc-

tures based on their reflection coefficient K_r. The basis for this hypothesis is the work of Postma [1989] mentioned above. However, as the formula might not be suited to calculate a value for P instantly, the reflection coefficient could be used when interpolated between structures with known-P.

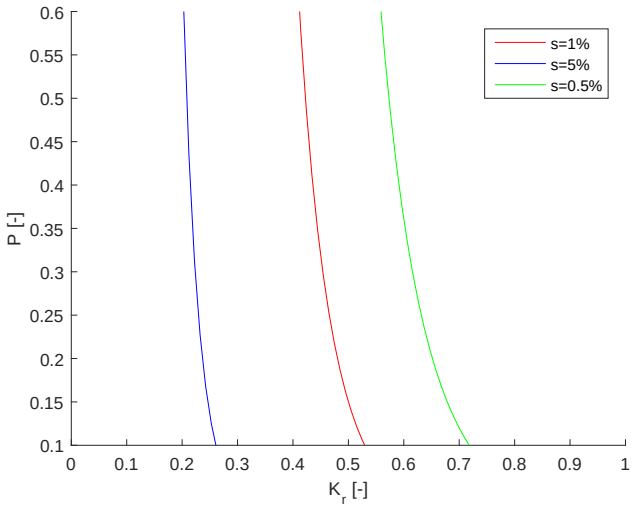

Figure 7: Notional permeability as a function of the reflection coefficient. For $\cot(\alpha) = 2$, based on (9).

PHYSICAL FOUNDATION The motivation for interpolating P-values based on the reflection coefficient for various wave periods T can be explained by the different processes governing reflection at the outer bounds. Reflection is mainly governed by wave steepness and breaking, slope angle of the structure and wave penetration into the structure [Postma, 1989]. For a certain slope angle, a fully impermeable structure ($P = 0.1$) offers the smallest space for wave penetration and thus dampening. At the other outer bound, a homogeneous structure made only out of armour stones ($P = 0.6$) causes the largest dampening and thus reflects less wave energy.

AVAILABLE DATA In table 4 an overview is presented of studies in which the reflection coefficient was measured on structures built according to a certain P-value lay-out.

As it might be useful to map existing data using the method described above, the data from [Postma, 1989; Kik, 2011; Van Broekhoven, 2011] are combined in K_r-P plots. The data is searched for measurements on different structures using similar wave periods. The reflection coefficients of those measurements are then linearly interpolated

Table 4: Overview of data where reflection was measured.

Research	Wave type	P-lay-out?
Vd Meer, Postma	Irregular	0.1, 0.5, 0.6
Kik	Irregular	0.1, 0.5, 0.35
Broekhoven	Regular	0.5
Kluwen	Regular	0.35, 0.4

and the point for the intermediate structure is plotted at its expected-P - K_r coordinate. It appears that in some cases, the measurements for the intermediate structure ($P = 0.35$) from [Kik, 2011] lie close to the expected value based on linear interpolation. Unfortunately, no consistent results were obtained, see appendix C on page 97.

2.2 GENERAL RELATED LITERATURE

Not all relevant literature is directly related to the notional permeability parameter, these are covered in this section.

2.2.1 *Scaling*

[Frostick et al., 2011] gives a good overview of how to organise a physical model experiment. Chapter 3 focuses on breakwater modeling. A summary of concepts important for this research is presented here.

SCALING Attention should be paid to scaling effects, as they can have a large influence on model behavior. The scale is determined by geometric, dynamic and kinematic similarity, and is often limited by dimensions of the flume. Various scaling numbers exist, and should be used depending on the most important forces in the model. However, due to fluid properties not all the scaling conditions can be met in practice. [Frostick et al., 2011, p. 52] provides recommendations for testing rubble mound breakwaters:

- Overall structural dimensions are scaled geometrically.
- Flow hydrodynamics (waves) need to conform the Froude criterion.
- Turbulent flow conditions have to exist throughout the primary armour layer.
- It is best to operate at larger scales when possible.

The most important scaling numbers are the *Froude (Fr)* and *Reynolds (Re)* numbers:

$$Fr = \frac{u}{\sqrt{g \cdot L}} \tag{10}$$

$$Re = \frac{u \cdot L}{\nu_k} \quad \text{or} \quad Re_D = \frac{\sqrt{gH_s \cdot D_n}}{\nu_k} \tag{11}$$

Where Re_D describes the flow conditions in the armour layer, and in which:

u = particle velocity

g = gravitational acceleration

ν_k = kinematic viscosity of water

L = characteristic length

H_s = significant wave height

D_n = nominal diameter of the armour units

SCALING OF THE CORE Geometric scaling of the core material may lead to unwanted effects. The most important being:

- Differences in permeability of the core layer, causing resistance for waves entering the structure. This causes wave forces to concentrate in the armour layer leading to a conservative estimate of stone size.
- Changes in energy dissipated, leading to unrealistic values for the reflection parameter K_r.
- Laminar flow in the core, dominated by viscous forces.

Several studies have been performed to find proper ways of scaling the core material. An often mentioned method is the one from [Andersen and Burcharth, 1995]. The core velocities are calculated at six specific locations and averaged afterwards, after which a different scaling factor can be derived. This research focused on maintaining turbulent flow and thus minimizing viscous forces. The pressure gradient in a rubble mound breakwater is given by:

$$p_{max}(x) = p_{0,max} e^{-\delta \frac{2\pi}{L'}} \tag{12}$$

In which x is the horizontal coordinate and L' the wave length in the core ($L' = L/D^{0.5}$) where $D \approx 1.4$. The reference pressure $p_{0,max}$ is related to the wave height in front of the structure and can be estimated with $p_{0,max} = \rho_w g \frac{H_s}{2}$. δ is a damping coefficient and

was found empirically to be $\delta = 0.0141 \frac{n^{0.5} L^2}{H_s b}$, in which n is the porosity of the core and b is the width of the structure.

In [Kik, 2011] this method is elaborated further, resulting in an expression for the pressure gradient under oscillating flow:

$$I_x = -\frac{\pi H_s}{L'} e^{-\delta \frac{2\pi}{L'} x} (\delta cos(\frac{2\pi}{L'} x + \frac{2\pi}{T_p} t) + cos(\frac{2\pi}{L'} x + \frac{2\pi}{T_p} t)) \quad (13)$$

2.2.2 *Reflection*

A propagating harmonic wave can be written as:

$$\eta(x,t) = a \sin(wt - kx) \quad (14)$$

Where η is the surface elevation, $a = \frac{H}{2}$ the wave amplitude, $w = \frac{2\pi}{T}$ the radian frequency and $k = \frac{2\pi}{L}$ the wave number. When this wave reaches the coast or a structure, part of the wave energy will be reflected. This reflection can be 100% in case of a vertical wall and can often be ignored on flat, sandy coasts. The reflected wave can also be expressed by equation (14), only is it propagating in opposite direction. The resulting wave profile is obtained when the *incoming* and *reflected* waves are summed:

$$\eta(x,t) = a_i \sin(wt - kx) + a_r \sin(wt + kx) \quad (15)$$

The reflection coefficient is written as $K_r = a_r/a_i$ and can, in the case of regular waves, be obtained by measuring the maximum and minimum amplitude heights. In practice, waves are random and short-crested. This complicates the determination of K_r, as it smooths the wave profile. [Holthuijsen, 2009]

There are methods to discern between the incoming and reflected wave in physical model tests. One of them is described by [Funke and Mansard, 1980]. This method finds an incoming and reflected wave spectra using a least squares analysis. Three simultaneous wave measurements are required.

The research of [Muttray et al., 2006] showed that wave reflection is mainly governed by the wave period T and that the wave height itself has a much smaller influence, see figure 8.

2.2.3 *Porous flow*

To describe flow in porous media, the most typical starting point is *Darcy's law*. It was found empirically but has later been verified

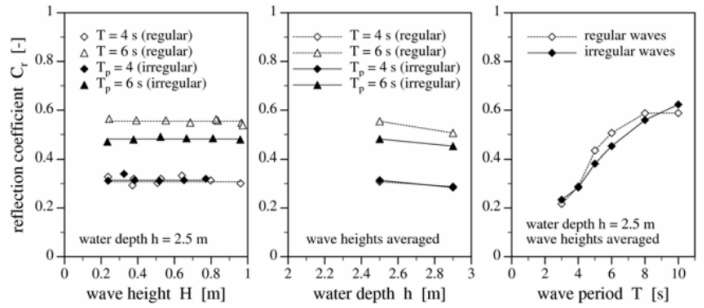

Figure 8: Influence wave height, water depth and wave period on the reflected wave. From [Muttray et al., 2006].

analytically. This was done by modifying the *Navier-Stokes equations*, under the assumption of stationary, incompressible flow and ignoring inertia. Darcy's law reads: [Fitts, 2013]

$$q = \frac{-k}{\mu}\nabla p \tag{16}$$

This method is not suited for turbulent flow, as inertia starts to play a role and *Darcy's law* can only be used in the case of laminar flow. *Forchheimer* proposed a method of adapting equation (16) to account for the turbulence contribution. Later, Van Gent extended this formula to account for non-stationary situations by adding an inertia term. This way the formula can be used for porous flow through rubble structures, at the transition between laminar and turbulent. After rewriting the formula and adding a term accounting for turbulence and non-stationary contributions, the *Forchheimer equation* becomes: [Van Gent, 1992]

$$I = au_f(t) + bu_f(t)\,|u(t)| + c\frac{\delta u_f}{\delta t} \tag{17}$$

In figure 9 the flow regions with their respective dominant resistance term are shown. The area marked with the black square is the region in which Van Gent performed tests to quantify each resistance term. These tests were done in an U-shaped water tunnel in order to simulate flow combined with oscillating water motion. The vertical axis shows the *Reynolds number*, $Re = \frac{uD}{\nu}$, and is a dimensionless quantity dividing inertial forces by viscous forces. It is used as a measure for describing turbulent (high Re) or laminar (low Re) flow regimes. At the horizontal axis the *Keulegan-Carpenter number* is plotted. This dimensionless quantity describes the relation between drag forces over inertia forces for objects in oscillatory water motion.

Using six samples, five made out of rocks and one containing wooden spheres, flow velocity fields were measured with a laser-Doppler velocity (LDV) meter. With these measurements the coefficients from

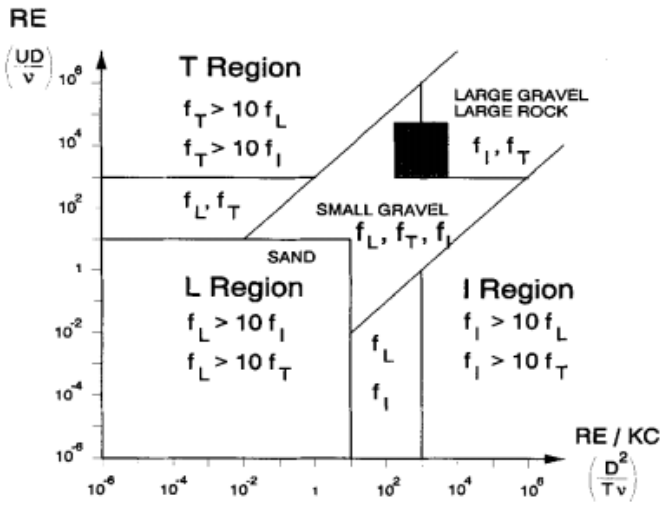

Figure 9: Flow regions from [Van Gent, 1995]

equation (17) could be fitted.

Starting point of the fitting procedure were the measurements using stationary flow. With the measured hydraulic gradient I and the calculated filter velocity u the coefficients a and b could now be fitted. The oscillating flow tests were used to fit the c coefficient. In figure 10 the contributions of each term on the total oscillatory signal is presented. It can be seen clearly that the contribution of c is maximum at the zero crossing of the signal, when $\frac{du}{dt}$ is largest. Still, its contribution is small.

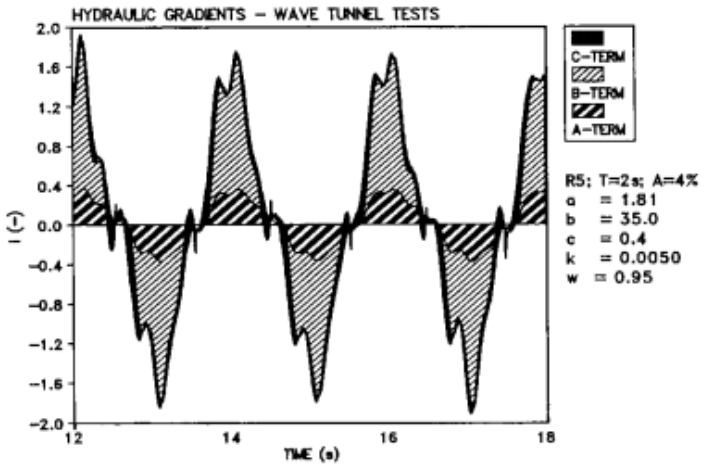

Figure 10: Contributions of each term on the oscillatory signal, from [Van Gent, 1995]

From measurements it appeared that the friction coefficient b is larger for oscillatory wave motion than for stationary flow, especially

for low KC-numbers. The non-dimensional coefficient β (used to calculate b) was split into a stationary and a non-stationary part, β_c and β' respectively. In figure 11 this extra resistance due to oscillatory wave motion is plotted against $KC = \frac{\hat{U}T}{nD_{n50}}$. This behavior is attributed to the formation of boundary layers and small eddies. As the flow direction changes these perturbations are destroyed, which costs energy. This process has a larger influence for low-KC numbers. It is because of this process that the KC number is incorporated in the expression for c. The final set of equations can be used with coefficients α and β of respectively 1000 and 1.1.

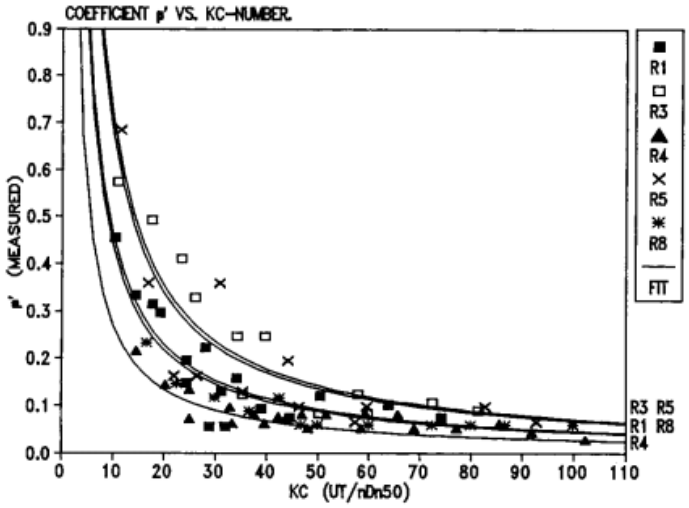

Figure 11: Extra resistance due to oscillatory wave motion, from [Van Gent, 1995]

$$a = \alpha\frac{(1-n)^2}{n^2}\frac{\nu}{gD_{n50}^2}$$

$$b = \beta(1+\frac{7.5}{KC})\frac{1-n}{n^3}\frac{1}{gD_{n50}} \qquad \textit{where} \quad KC = \frac{\hat{U}T}{nD_{n50}}$$

$$c = [1+\frac{1-n}{n}(0.85-\frac{0.015}{Ac})]/ng \qquad \textit{with}$$

$$AC = \frac{\hat{U}}{ngT} > 0.015/(\frac{n}{1-n}+0.85)$$

In [Sidiropoulou et al., 2007; Troch, 2000], overviews are provided of research done determining α, β and γ. The variety of research indicates that the precise values are still unknown. For turbulent flow, [Troch, 2000] summarized several of the values for α and β, see table 5.

Table 5: Forchheimer coefficients found in several empirical studies. From [Troch, 2000].

Material	Packing	d_{85}/d_{15}	Re	α	β	Source
Irregular rock	Random	1.4-1.8	600-10300	1400	2.4-3.0	B
		1.6	400-8200	13000	4.1-11	D
		-	-	270-1400	3.0-3.7	H
		1.3-1.4	300-5700	90-540	2.5-2.9	Sh
		1.3	750-7500	980-2100	3.7	W

Sources:
B: Burcharth and Christensen (1991); D: Dudgeon (1966); F: Fand et al. (1987); H: Hannoura and McCorquodale (1978); Sh: Shih (1990); W: Williams (1992).

In [Troch, 2000] it is stated that flow in the core of a breakwater structure is always in the turbulent region ($Re > 400$), and the Forchheimer equation simplifies to (18).

$$I = b'u^2 \tag{18}$$

In which $b' = \beta' \frac{1-n}{n^3} \frac{1}{gd}$.

2.2.4 *Wave Theories*

Waves can exist in a variety of situations. The *Navier-Stokes* equations can be adapted by neglecting specific terms to describe these waves, resulting in a different set of equations for that type of situation. Examples are open channel flow where friction is important, or long waves in deep water where friction can often be neglected..

Obviously, many parameters exist to describe these waves. Important variables when choosing a wave theory are the water depth, and the height and period of the wave, determining the wave steepness. For long waves in deep water with relatively small height and thus with limited steepness, the linear theory is often used. In this linear or first-order theory the wave is represented as a sine-wave. When steepness (H/gT^2) increases, a single sine wave can no longer represent the wave and multiple sine components have to be summed in order to obtain the desired wave-shape, resulting in 2^{nd} to 4^{th} order theories. In shallow water, steep waves should be described using the cnoidal wave theory. Different theories are depicted in figure 12 on the next page. In this graph the vertical axis represents the dimension-

less wave height, while the horizontal axis shows the dimensionless water level.

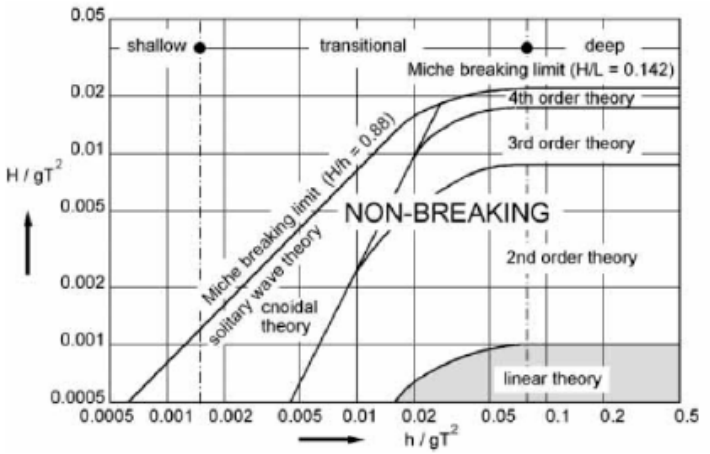

Figure 12: Validity of wave theories, adapted from [LeMéhauté, 1976] [Schiereck, 2012]

2.2.5 *The IH-2VOF model*

The model used in this study is the IH-2VOF model. Important background information as well as requirements on the input and output is provided here.

GOVERNING EQUATIONS To describe the fluid motion, the Reynolds Averaged Navier Stokes equations (RANS) are solved by the model. These formulas will be derived here. Starting point is the momentum equation for a 2-dimensional flow. The resulting force in x-direction is:

$$F_x = -\frac{\delta p}{\delta x} dx(dy\ dz) + \frac{\delta \tau}{\delta z} dz(dx\ dy) + F_{ext,x} \tag{19}$$

The second term in (19) is the rato of change of viscous shear stress and is for a Newtonian fluid:

$$\tau = \mu \frac{\delta u}{\delta z}, \rightarrow \frac{\delta \tau}{\delta z} = \mu(\frac{\delta^2 u}{\delta z^2}) \tag{20}$$

In which μ is the dynamic viscosity, a measure of resistance in a fluid to deformation by shear stress τ.

Acceleration in x-direction can be written as:

$$a_x = \frac{Du}{Dt} = \frac{\delta u}{\delta t} + \frac{\delta u}{\delta x}\frac{dx}{dt} + \frac{\delta u}{\delta z}\frac{dz}{dt} = \frac{\delta u}{\delta t} + u\frac{\delta u}{\delta x} + w\frac{\delta u}{\delta z} \tag{21}$$

In which $\frac{dx}{t} = u$, $\frac{dz}{dt} = w$. Substituting $ma_x = \rho(dxdydz)$ in (21):

$$(\frac{\delta u}{\delta t} + u\frac{\delta u}{\delta x} + w\frac{\delta u}{\delta z}) = -\frac{\delta p}{\delta x}dx(dydz) + \mu\frac{\delta^2 u}{\delta z^2}dz(dxdy) = F_x \tag{22}$$

When (22) is divided by $(dxdydz)$, the Navier-Stokes equation for the x-direction is obtained:

$$\rho(\frac{\delta u}{\delta t} + u\frac{\delta u}{\delta x} + w\frac{\delta u}{\delta z}) = -\frac{\delta p}{\delta x} + \mu\frac{\delta^2 u}{\delta z^2} \tag{23}$$

When turbulence is to be included in the equations, several steps are necessary. A turbulent velocity signal is depicted in figure 13. Using *Reynolds decomposition*, the flow velocity u can be split into a time-averaged and a fluctuating part, e.g. $u = \overline{u} + u'$. In which the overline denotes averaging and $'$ the fluctuating, turbulent part.

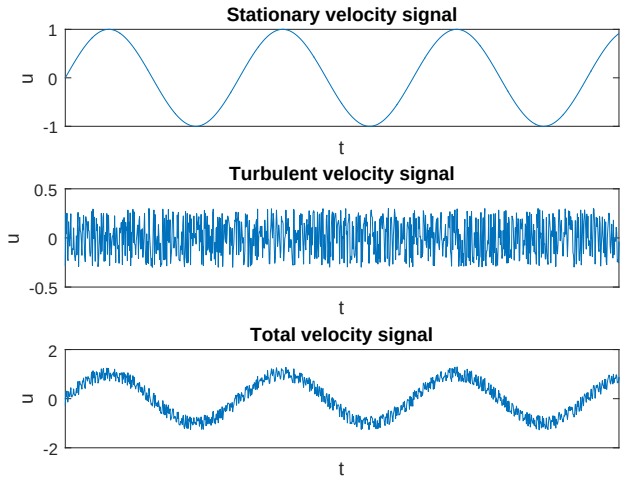

Figure 13: Velocities in turbulent, non-stationary flow.

When a period T is chosen such that turbulence fluctuations are smoothed while longer flow variations remain, the linear terms in equation (23) can be averaged. For example:

$$\begin{aligned}\overline{\frac{\delta u}{\delta t}} &= \frac{1}{T}\int_0^T \frac{\delta u}{\delta t}dt = \frac{\delta}{\delta t}\frac{1}{T}\int_0^T (\overline{u} + u')dt \\ &= \frac{\delta}{\delta t}\frac{1}{T}\int_0^T (\overline{u})dt + \frac{\delta}{\delta t}\frac{1}{T}\int_0^T (u')dt = \frac{\delta \overline{u}}{\delta t} + 0 = \frac{\delta \overline{u}}{\delta t}\end{aligned} \tag{24}$$

For w and p the same process applies. This way equation (23) can be rewritten into (25):

$$\rho(\frac{\delta\overline{u}}{\delta t}+\overline{u}\frac{\delta\overline{u}}{\delta x}+\overline{w}\frac{\delta\overline{u}}{\delta z}+\overline{u'\frac{\delta u'}{\delta x}}+\overline{w'\frac{\delta u'}{\delta z}})=-\frac{\delta\overline{p}}{\delta x}+\mu\frac{\delta^2\overline{u}}{\delta z^2} \tag{25}$$

Using the continuity equation (26):

$$\frac{\delta u}{\delta x}+\frac{\delta w}{\delta z}=0 \tag{26}$$

relation (25) can be rewritten into the so-called *Reynolds equation* (27)

$$\rho(\frac{\delta\overline{u}}{\delta t}+\overline{u}\frac{\delta\overline{u}}{\delta x}+\overline{w}\frac{\delta\overline{u}}{\delta z})=-\frac{\delta\overline{p}}{\delta x}+\mu\frac{\delta^2\overline{u}}{\delta z^2}-\rho(\frac{\delta\overline{u'^2}}{\delta x}+\frac{\delta\overline{u'w'}}{\delta z}) \tag{27}$$

In this latter equation, the last two non-linear terms are called the Reynolds-stresses, being the forces that result from working with time-averaged values. The left-hand terms are the inertia terms, i.e. the transport of mass. The first right hand side term is the pressure term followed by the viscous stress term, resulting from the deformation of the fluid.

In the IH-2VOF model, this *Reynolds Averaged Navier Stokes*-equation (RANS) is coupled with a turbulence model to solve the Reynolds stress term, and hence solve the fluid motion for the whole domain. Flow in porous media however is too complex to solve directly at pore-scale. Therefore the RANS-equations is averaged over a volume larger than characteristic pore scale but smaller than length scale of the flow. This process is shown schematically in figure 14.

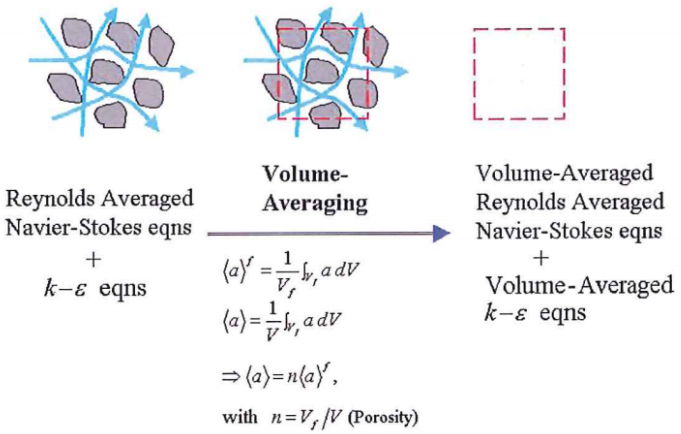

Figure 14: Volume averaging process. From [IH Cantabria, 2012].

The specific quantities in each cell are averaged over the volume with $\langle a \rangle = \frac{1}{V_f} \int_{V_f} a dV$, in which $\langle\rangle$ denotes volume averaging and a is the considered quantity. When applying this process to equation (27), two additional terms arise: a term describing momentum transfer between fluid phase and porous media, and a residual stress term resulting from the volume averaging, similar to the *Reynolds-stress* term found earlier. These two extra terms are modeled using the *Forchheimer coefficients* described in section 2.2.3 on page 19.

2.2.6 *How to set-up the model*

In [IH Cantabria, 2012] an extensive description is provided on how to set-up model calculations. In this section the most important parts are presented for later reference.

DOMAIN SIZE In order to have sufficient length for the waves to propagate before the structure, the recommended length of the numerical domain should be a minimum of twice the wavelength plus the length of the structure. For the height of the domain the run-up at the structure is governing.

GRID RESOLUTION In [IH Cantabria, 2012] two prerequisites are mentioned to prevent the so-called *false breaking effect*. This phenomena occurs when the wave steepness becomes too high so that full fluid cells are adjacent to empty cells. Figure 15 illustrates this problem. The recommendations are to use a minimum vertical resolution so that at least 10 cells per wave height are available. Next, it is advised to maintain $\Delta x < 2.5\Delta y$ to be able to correctly handle steep waves. Another recommendation can be found in [Van den Bos et al., 2014], in which with the earlier mentioned values still a large error was experienced and thus a $L/\Delta x = 150$ is recommended as a minimum of horizontal grid points.

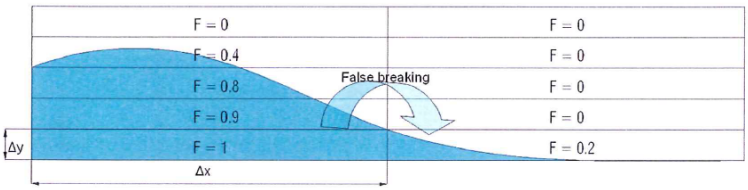

Figure 15: False breaking phenomenon. [IH Cantabria, 2012]

SIMULATION PERIOD In the original physical model tests, the simulation period was an important parameter, as the measured damage was dependent on the number of waves. With the IH-2VOF model however, damage is not evaluated so the only criterion is that the full wave-spectrum is represented. Research by [Van der Neut, 2015] showed that in the case of irregular waves, with comparable wave periods, a simulation length of 300 seconds is a good balance between calculation time and representation of the spectrum, i.e. further increasing the simulated duration does not increase accuracy. For the wave generation the *static paddle* option is selected, as suggested in the same thesis. The time step Δt is automatically chosen by the software through the *Courant number*.

2.2.7 *Stone properties*

This thesis focuses on rubble mound breakwaters, structures made out of bulk placed rock material. In this chapter some basic information on rock properties important for this research is provided.

Figure 16: Stone quarry in Soignies, Hainaut (province), Belgium. Photo by Jean-Pol Grandmont

STONE DIMENSIONS Stone dimensions obtained from a quarry cover a wide range of dimensions. A sieve curve can be used to derive certain parameters for practical use. This sieve curve is obtained by sieving the sample using increasing sieve diameters. A cumulative size distribution then provides the values D_x, e.g. the stone diameter of which x percent passes the sieve. Using these values a grading width can be calculated. High values indicate a wide grading and low values mean a uniformly graded sample, see table 6.

Another representation of stone dimension parameter is the *nominal diameter*, written as D_{nx}, this value is the size of a cube with equivalent weight. Again the x means percentage of stones that would pass the sieve.

Table 6: Armourstone grading width. [CETMEF, 2007]

Grading width	D_{85}/D_{15}	M_{85}/M_{15}
Narrow or single-sized gradation	Less than 1.5	1.7-2.7
Wide gradation	1.5-2.5	2.7-16
Very wide or quarry run gradation	2.5-5.0	16-125+

In table 3.6 in [CETMEF, 2007] an overview is given of several standard gradings, as specified in EN13383. This table can be used for design purposes, especially the expected M_{50}, the median sample weight is important when designing a breakwater.

POROSITY The porosity of a certain sample indicates how much space is taken by the stones. It is calculated by dividing the volume of pore space by the total volume of the sample, $n = V_p/V_t$. Grading width and placement method are the main factors influencing the in-situ porosity, or bulk porosity. A wide graded sample has a low porosity, as relatively fine material fills the pores between the relatively larger stones.

The porosity can be estimated using formula (28), see [CETMEF, 2007, p.121]. In this formula e_0 is a void ratio obtained from experiments. Values range from $e_0 \approx 0.55$ for steel balls to $e_0 \approx 1$ flat rock fragments. The parameter n_{RRD} is the uniformity coefficient. It can be calculated using a Ros-Ram curve and increases for heavier stones. For standard gradings, its value can be found in table 3.6 from [CETMEF, 2007]. Porosity is especially important for calculating the amount of core material needed for filling the structure.

$$e = \frac{1}{90}(e_0)\arctan(0.645\, n_{RRD}) \quad with \quad n_v = \frac{e}{1+e} \tag{28}$$

3

METHODOLOGY

In this chapter the approach to answer the research questions is presented, a start is made by expanding the research goal from chapter 1.

3.1 RESEARCH OBJECTIVE

PROBLEM DEFINITION In its current formulation, the *'Van der Meer formula'* is not versatile enough to calculate any given lay-out when designing a rubble mound breakwater, as P has only been validated for a few specific cross-sections. Methods to predict P for arbitrary rubble mound breakwaters exist, but have not been verified yet.

RESEARCH QUESTIONS The research questions from the introduction, see section 1.3, are repeated below:

- Which hypotheses are available to find values for P?
- What are the underlying processes in these methods?
- What is the influence of structural and hydraulic parameters on predictions of P?
- What would an appropriate physical test program look like?

RESEARCH GOAL The goal of this research is to investigate predictability of the notional permeability parameter based on several existing hypotheses.

3.2 SELECTION OF HYPOTHESES

In chapter 2, four methods were mentioned to predict the notional permeability parameter. All the hypotheses make use of certain *governing parameters*, being:

- Numerically obtained dimensionless numbers
- Run-up below the armour layer
- Reflected wave K_r
- Flow into the core Q

A division is made between *direct* and *indirect* methods. With a *direct* approach a P-value can be found by directly substituting relevant parameters into a formula. The hypotheses of [Van Broekhoven, 2011] and [Van der Neut, 2015], using run-up and dimensionless numbers respectively, fall in this category. The *indirect* methods make use of a parameter that is calculated for both known- and unknown-P structures, and subsequently interpolating this parameter between known-P structures to find an intermediate value. This category entails both the 'flow into the core'-method by [Van der Meer, 1988] as well as the reflection hypothesis by [Van den Bos et al., 2015].

In this thesis, the choice was made to only investigate the indirect methods. The direct methods appear to be very sensitive to varying input with greater complexity. These drawbacks in combination with time constraints were the most important considerations. In appendix A, the choice of continuing with the indirect methods is explained further.

3.3 RESEARCH SET-UP

The goal of this research is to investigate the predictability of the notional permeability parameter based on different hypotheses. The selected indirect methods aim to relate both structural and hydraulic parameters (e.g. wave conditions) to P. At this point only the type of structure determines this parameter. Thus, to see whether a method can predict outcomes for P, a range of simulations are executed in which parameters are varied and P is calculated for comparison. However, wave conditions and structural properties can be varied in many ways. Thus, for this research a more specific set of variables needs to be defined.

In [Van der Meer, 1988] the method using a flow into the core Q is explained, here the groundwater-flow model HADEER is used to calculate flow velocities inside the structure. This is done for various wave periods, while keeping the wave height fixed. This way a range of Iribarren numbers $\xi = \frac{\tan\alpha}{\sqrt{2\pi H/gT^2}}$ could be simulated in a practical way.

The hypothesis posed in [Van den Bos et al., 2015] elaborates on this idea by replacing the flow into the core by the reflection coefficient and interpolate in the same way. As research of [Postma, 1989] showed, the reflection coefficient is dependent on ξ. Research of [Muttray et al., 2006] showed that wave height is of minor importance for K_r and that it is the wave period T (which is also present in ξ) governing reflection on rubble mound structures. Supported by these

conclusions and in order to limit the scope of simulations, in this thesis the wave period is chosen as the main hydraulic parameter. Figure 17 depicts the relation that is investigated. The region enclosed by the lines marks the possible influence of various wave periods.

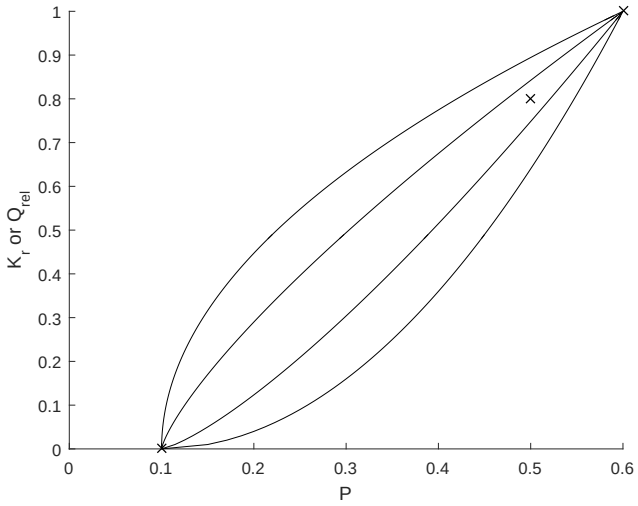

Figure 17: Depiction of the concept

3.4 NUMERICAL TESTING

A numerical model is used to simulate varying structural parameters in combination with various wave periods. The IH-2VOF model is selected because of its ability to calculate flow velocities in porous media and its availability at the TU Delft. The model is explained more in depth in chapters 2 and 4.

Regarding varying structural parameters, the focus will be on properties of the core layer. This way a few parameters can be chosen such that a range can be simulated including a known-P structure, similar as in [Van der Meer, 1988; Van den Bos et al., 2015].

The simulations are subdivided into 4 *sets*. The first series includes the structures of which the notional permeability is known to provide a framework for interpolation. In set 2 & 4 structural parameters (core thickness and core stone diameter) are varied. In test series 3 sensitivities of porous media parameters (n, α, β, γ) are evaluated.

- Set 1: Framework testing method.
- Set 2: Varying thickness of core layer.

- Set 3: Investigating sensitivities to model parameters.
- Set 4: Altering the D_{n50} of the core material.

Details on the test programs, test set-up and the tested structures can be found in chapter 4.

3.4.1 *Note on used wave period*

Preferably, a wave spectrum is used during simulations, as in reality also irregular waves are present. However, during the first test series it appeared that calculating Q from these type of simulations was difficult. Therefore it was decided to perform every simulation with regular waves as well so Q could be calculated. An important note regarding the wave period should be mentioned here. In the tests with irregular waves, the peak wave period T_p, being the frequency with the highest energy, was used as main statistical parameter instead of the mean wave period T_m. With regular waves these are the same. In the following chapters, T therefore indicates T_p.

3.5 CALCULATING THE GOVERNING PARAMETERS

Estimating P either using K_r or Q is done by interpolation, the necessary steps are explained below.

3.5.1 *Flow into the core*

The simulations with regular wave series were analyzed and a flow into the core Q was calculated for each scenario using MATLAB. The script is provided in appendix E on page 105. Q has been defined as the inward directed flow per wave through a cross-section just on top of the core. In figure 18 this flow is shown for an arbitrary time step. At every time step a new velocity field at the interface is calculated and interpolated to find Q. The way of presenting the results is done in a similar way as in [Van den Bos et al., 2015].

REFLECTION The reflection coefficients for the simulations using irregular wave series were calculated with the MATLAB-based tool *decomp*, by Henk Jan Bakkenes. This software uses a fourier transformation (see section 2.2.2) to discern between incident and reflected wave.

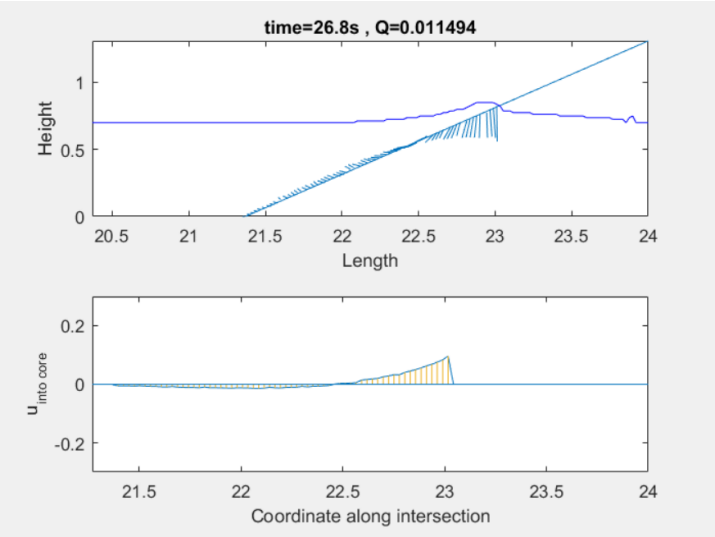

Figure 18: Screen capture of the animation made with Matlab

3.5.2 *Estimating P*

A prediction of the notional permeability parameter using the indirect methods is done using the following steps:

1. Determine Q and K_r for known structures (i.e. as defined by [Van der Meer, 1988], with $P = 0.1/0.5/0.6$)
2. Calculate Q and K_r for the unknown structure
3. Interpolate values of Q and K_r to predict P

4

NUMERICAL MODEL TESTING

4.1 INTRODUCTION

The model that will be used in this thesis is the IH-2VOF model, it is specifically designed to act as a *numerical flume*. Velocities, pressures and water levels can be calculated for the whole domain. As explained in chapter 3, the numerical simulations are subdivided into separate sets of tests:

- Set 1: Framework testing method.
- Set 2: Varying thickness of core layer.
- Set 3: Investigating sensitivities to model parameters.
- Set 4: Altering the D_{n50} of the core material.

This chapter consists of multiple sections. First, the constructions that will be tested in the various sets are shown in section 4.2. Next, the wave conditions are presented in section 4.3. Finally, using information found in section 2.2.5, the model set-up is explained.

4.2 OVERVIEW OF TESTED STRUCTURES

The cross-sections that will be tested are grouped per simulation set below. In total 12 different lay-outs have been made, named A to L.

4.2.1 *Structures for the first test series*

For the first test round, structures A to E were used. The first three (A-C) correspond to the cross-sections described by Van der Meer [1988], with P-values of 0.1, 0.5 & 0.6 respectively. Structures D and E are cross-sections for which no P-value has been established yet. These structures serve to explore the methods and are part of the first test round and are presented in figures 22 and 23.

STRUCTURES D AND E The two intermediate structures for the first simulation set can be found in figures 22 and 23. They differ slightly from the three tested structures by Van der Meer [1988] (A-C).

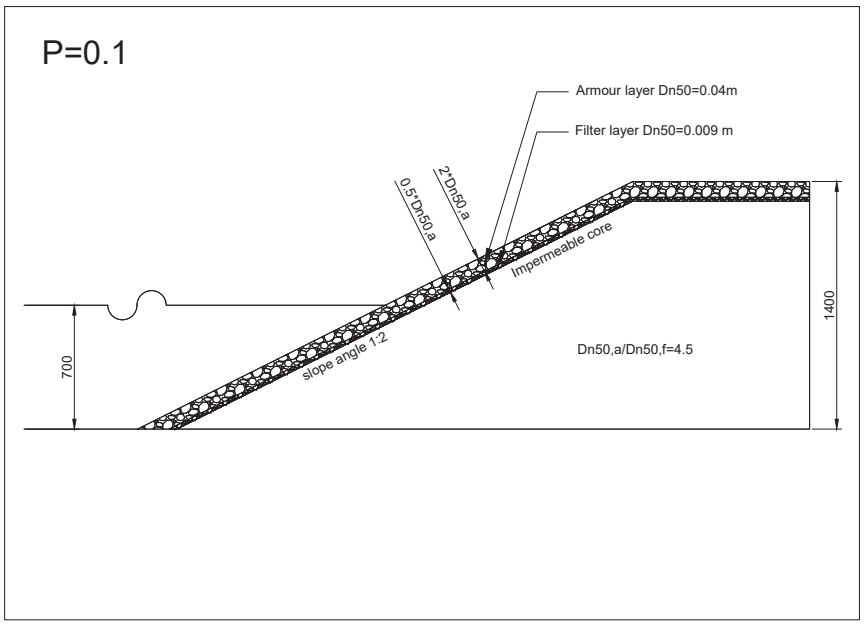

Figure 19: Structure A

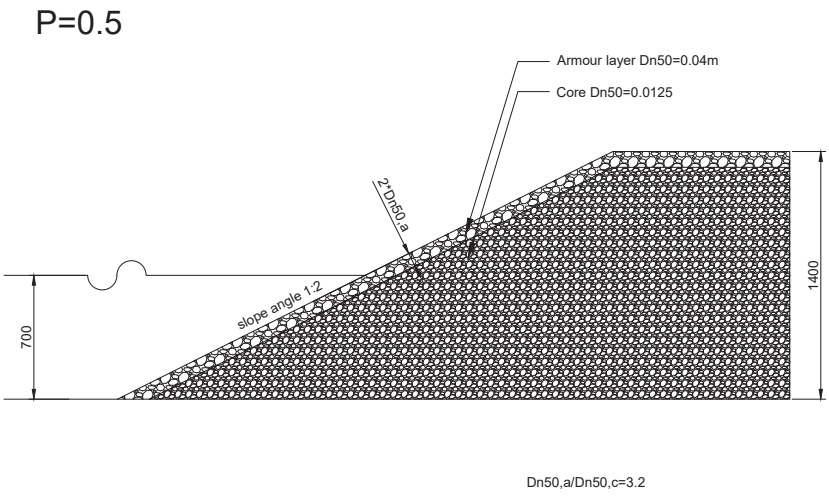

Figure 20: Structure B

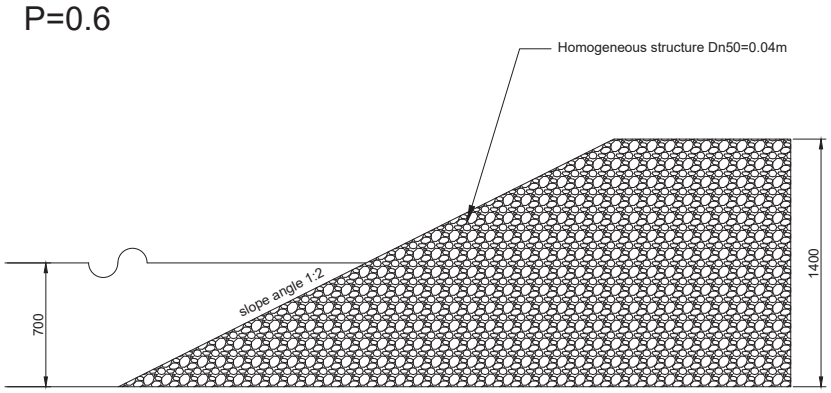

Figure 21: Structure C

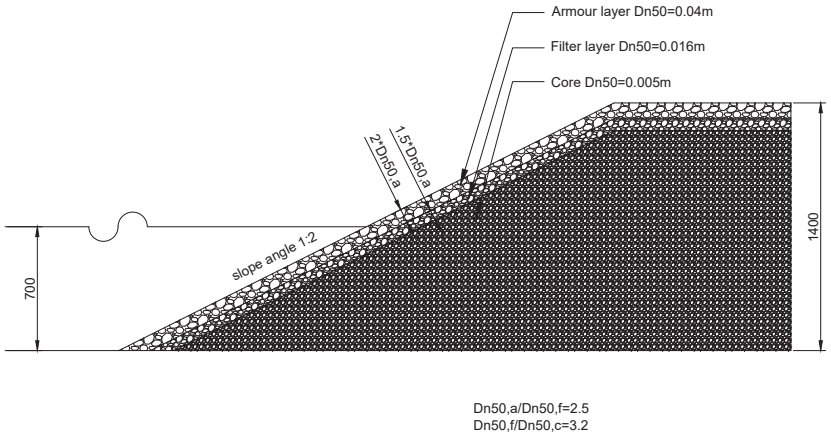

Figure 22: Structure D

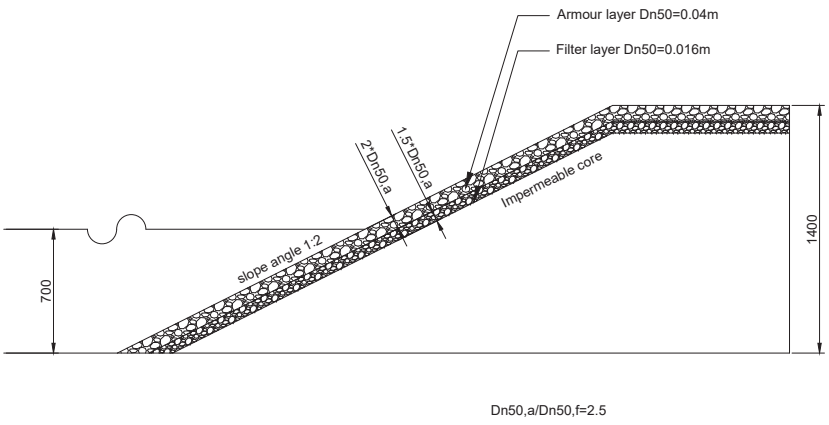

Figure 23: Structure E

D is somewhat similar to a fourth structure as defined by Van der Meer [1988] as it contains a filter layer with a thickness of $1.5 \cdot D_{n50,A}$ placed upon a permeable core. The main difference are the stone sizes. The ratio $D_{n50,A}/D_{n50,F}$ is 2.5 in structure D compared to 2 in the original $P = 0.4$ structure. Also the core material is somewhat finer as $D_{n50,A}/D_{n50,C}$ increases from 5 to 8.

As both the materials are finer than in the $P = 0.4$ case, the expectation is that permeability is smaller compared to that cross-section. However, as this structure has not been tested in physical model tests the actual results under different wave periods are not known and thus no conclusions regarding P for a *somewhat* different structure can be drawn. When compared to structure B representing the $P = 0.5$ cross-section, it is safe to expect a P-value smaller than this.

The second intermediate structure consists of an armour layer placed upon a filter layer and an impermeable core. Compared to A, which is built according to the $P = 0.1$ structure from [Van der Meer, 1988], it has a thicker filter layer made out of larger stones. The ratio $D_{n50,A}/D_{n50,F}$ decreases from 4.5 to 2.5. Therefore it is expected that $P > 0.1$.

4.2.2 *Structures with varying core thickness*

In the structures from the second simulation round, named F to L, the core thickness is varied, i.e. the distance between filter layer and solid boundary. In figure 24 these structures are depicted. The goal of these tests is to investigate outcomes of the two methods for a varying core thickness. In these simulations, the nominal diameter of the core material is 0.005 m.

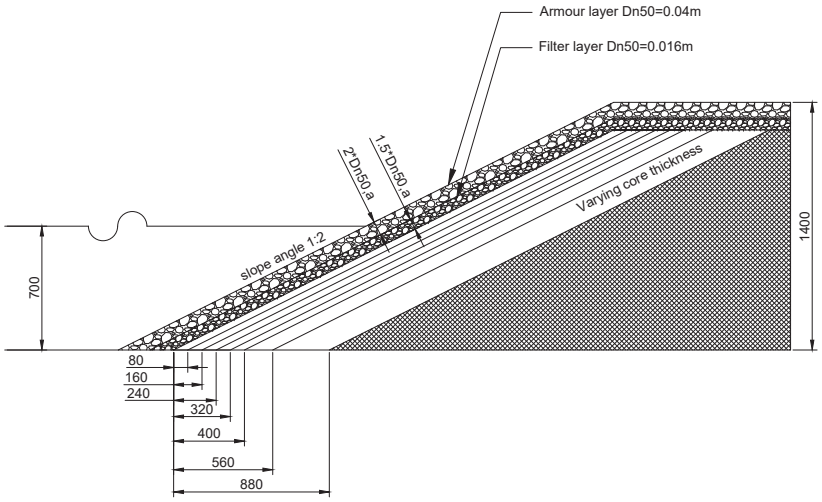

Figure 24: Structures F to L

The core thickness was varied by shifting the slope horizontally. However, core thickness t_c is measured perpendicular to the slope. Table 7 shows both the horizontal displacement as well as t_c for every structure.

4.2.3 *Sensitivities of core parameters*

The structure used in the third set of tests is cross-section F. This structure was chosen because the results obtained in the second set of simulations showed the largest difference between both hypotheses, see chapter 5.

Table 7: Overview of structures with core thickness t_c

Structure	dx [mm]	t_c [mm]	$t_c/D_{n50,a}$ [-]
F	80	35.8	0.9
G	160	71.6	1.8
H	240	107.3	2.7
I	320	143.1	3.6
J	400	178.9	4.5
K	560	250.4	6.3
L	880	393.5	9.8

4.2.4 *Varying nominal diameter of the core layer*

In the fourth simulation round the core stone diameter was varied. Structure K was chosen as a basis. The stone dimensions used can be found in section 4.3.

4.3 TEST PROGRAMS

In the test programs provided below all the tests performed are summarized. In order to keep the results comparable the same wave conditions are applied each test. These consist of regular and irregular waves at different wave periods. The wave height is kept equal. The wave conditions are described in table 8 and are basically applied to all structures described in section 4.2.

Table 8: Standard wave conditions applied

Wave Type	Wave Period	Wave Height	Water depth	Wave Steepness
Regular	1.5	0.12	0.7	3.1%
	2.0	0.12	0.7	2.4%
	3.0	0.12	0.7	1.5%
	4.0	0.12	0.7	1.1%
Irregular	1.5	0.12	0.7	3.1%
	2.0	0.12	0.7	2.4%
	3.0	0.12	0.7	1.5%
	4.0	0.12	0.7	1.1%

MOTIVATION FOR WAVE CONDITIONS The standard wave conditions used were set-up using following considerations:

WAVE TYPE Regular as well as irregular waves were used in the tests. This has been done in order to calculate K_r for a complete irregular-wave spectrum, as this is found in reality. The regular waves were used for the calculation of Q, this could not be realized using irregular waves.

WAVE PERIOD This is the most important variable in this research. In both the hypotheses under investigation the wave period is thought to have a significant influence in governing processes. The periods were chosen such that a realistic range of wave steepness-values were simulated. As mentioned in chapter 3, the peak wave period T_p is used for both wave types.

WAVE HEIGHT Wave height is kept constant for two reasons. The first is that its effect on the reflected wave proved to be negligible, see [Muttray et al., 2006]. The second reason is that in the original simulations by [Van der Meer, 1988] using the HADEER-model to calculate Q, the wave height was kept constant as well. The height of the waves was defined using an overview of wave theories, see section 2.2.4 on page 23. Waves of 0.12 are the highest waves that, in combination with chosen periods, can be described using *Stokes 2nd-order theory*.

WATER DEPTH The water depth is assumed to have negligible influence on results, and is kept constant for the same reasons described above. The height is chosen such that it can be used in physical model tests at the TU Delft facility as well.

4.3.1 *First simulation round*

In the first set of simulations the standard structures with known-P (A to C) were simulated along with two slightly deviating structures (D and E), see section 4.2. The standard wave conditions as presented in table 8 were applied to each of these structures, resulting in a total of 40 simulations.

4.3.2 *Varying core thickness*

The second set of simulations can be seen as an extension of the first part. In these tests the thickness of the core layer was varied, as depicted in figure 24 on page 41. To be able to compare the results with the standard structures, the same wave conditions were applied, resulting in a total of 56 simulations.

4.3.3 *Investigating sensitivities*

In this set of numerical model tests, specific model parameters regarding the core layer were altered. All the executed tests are shown in tables 9 to 12, grouped per varied parameter. These parameters can be split into the *Forchheimer*-coefficients and the layer porosity, n. The values for n are chosen such that a practical range is modeled ($n = 0.36 - 0.42$), see [CETMEF, 2007].

The *Forchheimer*-coefficients, explained in section 2.2.3, are the result of curve fitting experimental data. The exact values are still unknown [IH Cantabria, 2012]. However, many studies have been performed to find these values. In table 5, values are presented from various studies. In this study, α is varied between 0-4000, β between 0-4 and γ between 0-4. For both β and γ, these ranges contain outer values that are unrealistically high, these are included to see whether large effects are noticeable.

Table 9: Test program with varying porosity n.

Structure	Wave Type	Wave Period	Porosity n
F	Regular	1.5	0.36
			0.38
			0.40
			0.42
		3.0	0.36
			0.38
			0.40
			0.42
	Irregular	1.5	0.36
			0.38
			0.40
			0.42
		3.0	0.36
			0.38
			0.40
			0.42

Table 10: Test program with varying porosity α.

Structure	Wave Type	Wave Period	Linear friction coefficient α
F	Regular	1.5	0
			200
			1000
			4000
		3.0	0
			200
			1000
			4000
	Irregular	1.5	0
			200
			1000
			4000
		3.0	0
			200
			1000
			4000

Table 11: Test program with varying porosity β.

Structure	Wave Type	Wave Period	Non-linear friction coefficient β
F	Regular	1.5	0
			1.1
			4
		3.0	0
			1.1
			4
	Irregular	1.5	0
			1.1
			4
		3.0	0
			1.1
			4

Table 12: Test program with varying porosity γ.

Structure	Wave Type	Wave Period	Added mass coefficient γ
F	Regular	1.5	0
			0.51
			1
			4
		3.0	0
			0.51
			1
			4
	Irregular	1.5	0
			0.51
			1
			4
		3.0	0
			0.51
			1
			4

4.3.4 *Varying nominal diameter of the core layer*

The D_{n50} of the core material is varied in the final set of simulations. To maintain a physically correct representation of reality the flow should be turbulent, i.e. $Re = uD/\mu > 450$ [Troch, 2000]. Using formulas found in section 2.2.1 and 2.2.3 a wave height can be linked to a pressure gradient in the porous structure, and velocities can be estimated. It is found that $D_{n50,c}$ should be 0.001 m minimally to assure turbulent flow under all wave conditions. The larger diameters were increased in steps, and the largest case was specifically set at a similar value as the filter layer for two reasons: first, increasing the stone diameter would make little sense physically and secondly, this way results could be compared to the $P = 0.5$ case, defined as an armour layer on a permeable core.

The structure that served as a base case is cross-section K, with $t_c/D_{n50,a} = 6.3$, in order to have a core large enough to show an influence. All the values of $D_{n50,c}$ simulated are summarized in table 13. For all these stone diameters, the standard wave conditions from 8 were applied. All tests performed are shown in table 14.

Table 13: Overview of $D_{n50,c}$-values simulated

$D_{n50,c}$ [m]	$D_{n50,c}/D_{n50,a}$	Remark
0.001	0.025	Minimal diameter to guarantee turbulence
0.005	0.125	Already simulated
0.007	0.175	
0.01	0.25	
0.013	0.325	
0.016	0.4	Diameter of filter layer

Table 14: Test program for simulations with varied $D_{n50,c}$.

Structure	Wave Type	Wave Period [s]	$D_{n50,c}$ [m]
K	Regular	1.5	0.001
			0.007
			0.01
			0.013
			0.016
		2	0.001
			0.007
			0.01
			0.013
			0.016
		3	0.001
			0.007
			0.01
			0.013
			0.016
		4	0.001
			0.007
			0.01
			0.013
			0.016
K	Irregular	1.5	0.001
			0.007
			0.01
			0.013
			0.016
		2	0.001
			0.007
			0.01
			0.013
			0.016
		3	0.001
			0.007
			0.01
			0.013
			0.016
		4	0.001
			0.007
			0.01
			0.013
			0.016

4.4 MODEL SET-UP

Setting up the model simulations was done using [IH Cantabria, 2012; Van der Neut, 2015], see also section 2.2.5. Scaling has been done such that the scaled structures can be tested at TU Delft in a later stage. This last consideration is done with validation by physical scale models in mind.

DOMAIN SIZE Using a water height of 0.7 m and the maximum wave period of 4 s, the wave celerity becomes 2.62 m/s and thus the wave length becomes 10.48 m. [IH Cantabria, 2012] recommends a minimum of $1.5 - 2 \cdot L$ in front of the structure. When space for the structure is accounted for as well, the domain length should be 26 m. The height of the domain is set at 2.0 m, this way the structure can be 1.4 m high so no overtopping of the structure is expected.

GRID RESOLUTION A large grid is beneficial in terms of computing time, but increasing the size of the grid cells too much will negatively affect accuracy of the computations. In [IH Cantabria, 2012; Van den Bos et al., 2014] recommendations are given:

Δx Minimum size of horizontal grid cells should be $L/150$ [Van den Bos et al., 2014].

Δy The false breaking criterion (see 2.2.5) states that the vertical grid cell size is dependent on Δx and should be $\Delta x < 2.5\Delta y$. [IH Cantabria, 2012]

Here, the smallest wave length of 3.93 m is governing. The horizontal grid size becomes $3.93/150 \approx 0.026m$ and with the false breaking criterion $\Delta y \approx 0.012$.

POROUS MEDIA INPUT The layers of the structures, described as *porous media*, require further specifications, mainly for describing turbulent flow. The required input is:

1. A linear friction coefficient α
2. A non-linear friction coefficient β
3. An added mass coefficient γ
4. Porosity n
5. The nominal diameter of the material D_{n50}

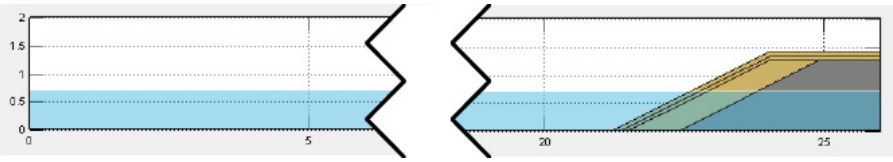

Figure 25: Figure showing structure as modeled in IH-2VOF

The first three items mentioned above are the *Forchheimer coefficients*, see 2.2.3 on page 19. In his thesis, Van der Neut [2015] investigated the influence of these parameters and calibrated them with physical model tests. These values will be used in all the simulation rounds except for set 3, in which the sensitivity of these parameters is investigated. For armour layers the following settings were used: $\alpha = 0$, $\beta = 5.0$, $\gamma = 0.51$. For filter and core layers $\alpha = 0$, $\beta = 1.1$, $\gamma = 0.51$ was used. The high value for β for the armour layer was chosen in order to account for turbulence present at the fluid-structure interface, see [Van der Neut, 2015]. Porosity was set at $n = 0.4$ in all cases.

5 RESULTS

In this chapter the results of the numerical model testing will be presented and evaluated. The goal is to evaluate predictability of P based on different methods. The chapter is divided in 4 parts, representing the different simulation rounds, as explained in chapter 3. All results can be found in appendix G.

5.1 FRAMEWORK TESTS

In this first set of simulations the governing parameters Q and K_r are determined for the structures with known P (structures A-C). These are required to form the basis for the interpolation, see chapter 3 for further details. Two cross-sections (D-E), see section 4.2 on page 37 are added, so that plots for these structures can be made.

5.1.1 *Reflection*

In figures 26 and 27, the results for the two intermediate structures are plotted when interpolated for K_r. For structure D it can be seen that, according to this hypothesis, the P-value varies between 0.42 and 0.47 depending on the wave period T. For structure E the spread is larger and P varies between 0.13 and 0.23.

5.1.2 *Flow into the core*

In figure 28 the result is presented when the intermediate structure D is interpolated based on Q. As with the results based on reflection above, this linear line is an assumption and serves only for a first estimation of P. For structure E, with an impermeable core, the flow into the core is zero by definition and thus a P-value of 0.1 is calculated, see figure 29.

According to this hypothesis, the P-value for structure D thus lies between 0.45-0.48.

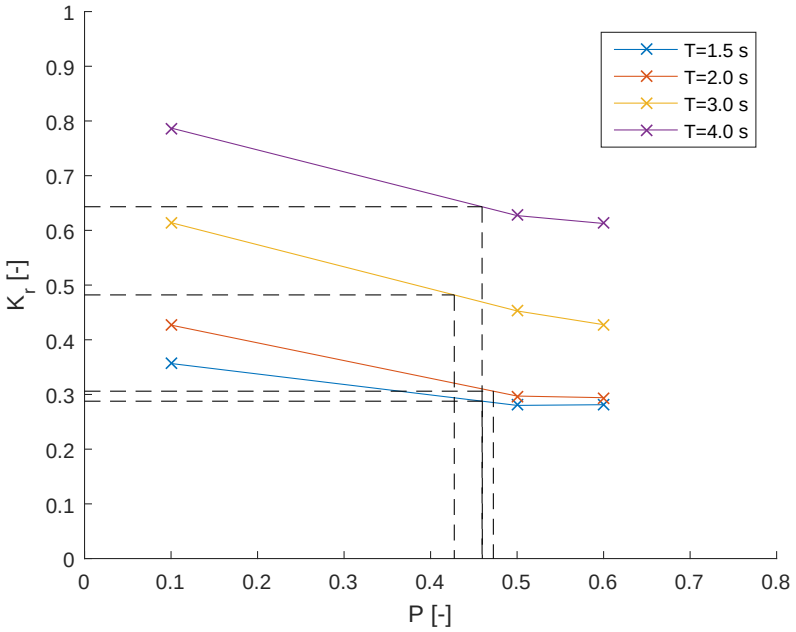

Figure 26: Results of the reflection hypothesis for intermediate structure D.

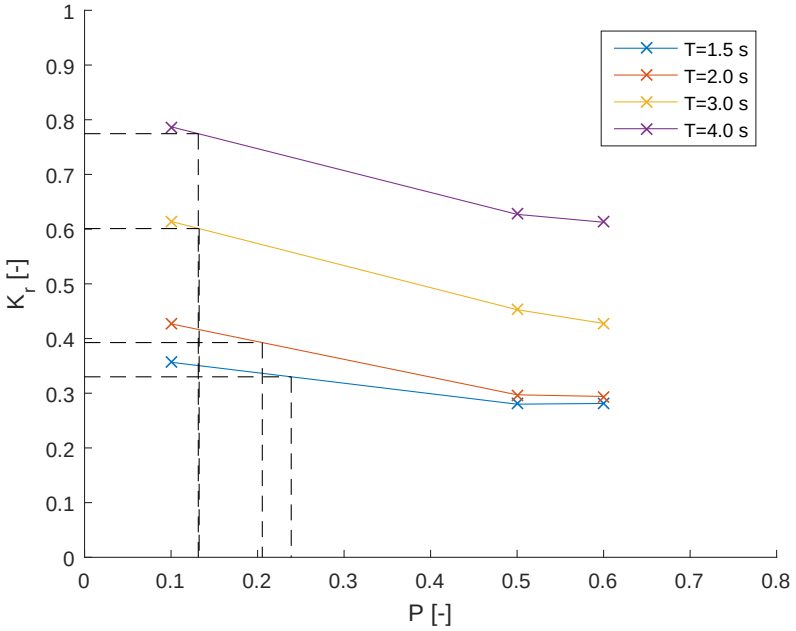

Figure 27: Results of the reflection hypothesis for intermediate structure E.

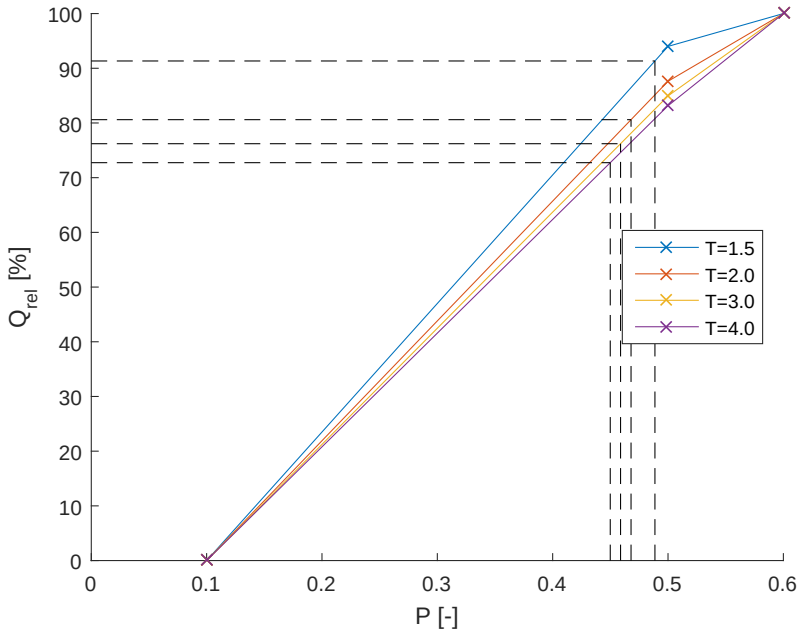

Figure 28: Interpolation based on Q for structure D.

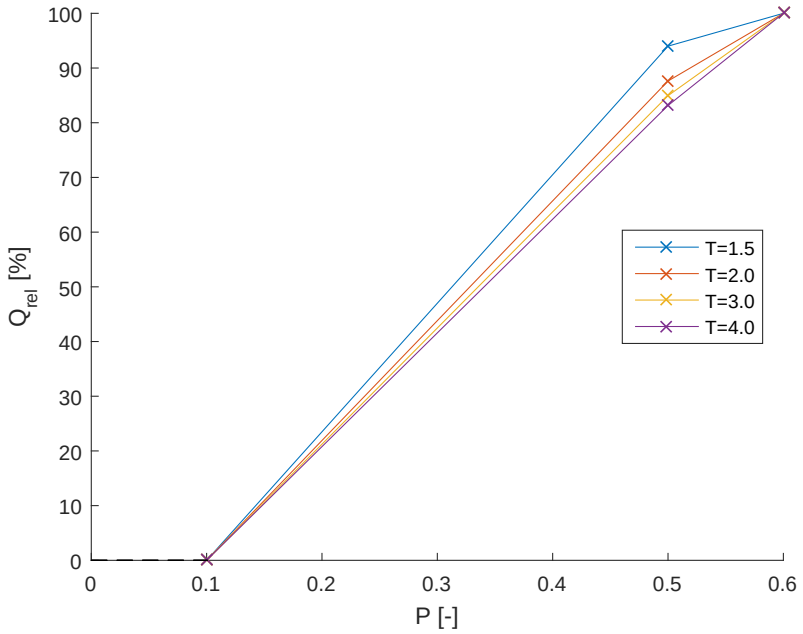

Figure 29: Interpolation based on Q for structure E.

5.1.3 *Comparison*

In table 15 the ranges for P found are summarized. The values seem to correspond quite well and are close to their expected values.

Table 15: Summarizing the results for P from the linear interpolation based on K_r and Q.

	Structure D		Structure E	
T	K_r	Q	K_r	Q
1.5	0.46	0.49	0.24	0.10
2	0.47	0.47	0.20	0.10
3	0.42	0.46	0.13	0.10
4	0.46	0.45	0.13	0.10

5.2 VARYING CORE THICKNESS

As explained in chapter 3, predictions for P are made for an *intermediate* region. The results from the first exploratory test series, see table 15, provide a first estimate for structures close to known P-structures. Next, a range of structures is simulated with varying core thickness, as explained in section 4.2.

All the resulting values found for the governing parameters K_r and Q are plotted in figures 30 and 31. The intermediate structures are interpolated based on these values. This process is shown in figures 32 and 33. The P-values resulting from this process are presented in figures 34 and 35. Finally, these values are averaged and plotted along with the range found in the outcomes in figure 36.

Table 16: Summarizing the results for P from the linear interpolation based on K_r and Q for structures F to I.

	Structure F		Structure G		Structure H		Structure I	
Period	K_r	Q	K_r	Q	K_r	Q	K_r	Q
1.5	0.33	0.37	0.37	0.42	0.46	0.45	0.50	0.46
2	0.30	0.33	0.41	0.39	0.43	0.42	0.47	0.44
3	0.34	0.32	0.29	0.37	0.31	0.30	0.41	0.42
4	0.46	0.32	0.38	0.36	0.44	0.39	0.58	0.41

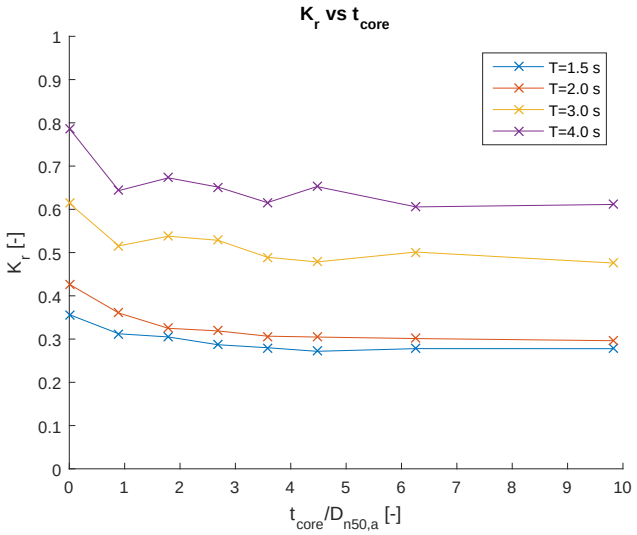

Figure 30: K_r values found for varying core thickness.

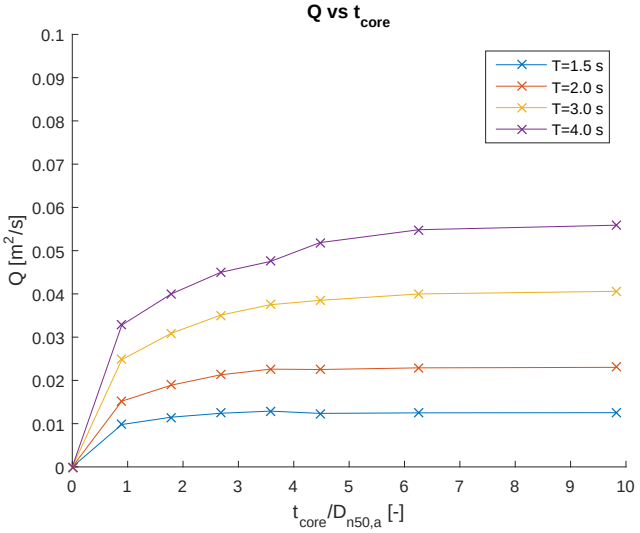

Figure 31: Q values found for varying core thickness.

Table 17: Summarizing the results for P from the linear interpolation based on K_r and Q for structures J to L.

	Structure J		Structure K		Structure L	
Period	K_r	Q	K_r	Q	K_r	Q
1.5	0*	0.45	0*	0.45	0*	0.45
2	0.47	0.44	0.48	0.45	0.53	0.45
3	0.43	0.44	0.38	0.45	0.44	0.45
4	0.43	0.44	0*	0.46	0*	0.47

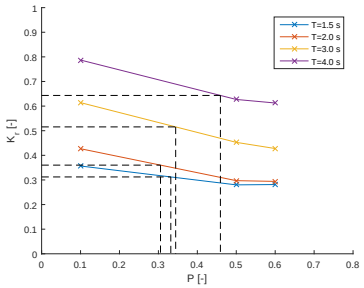

(a) Reflection,structure F

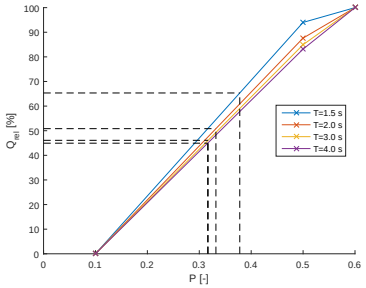

(b) Flow into the core, structure F

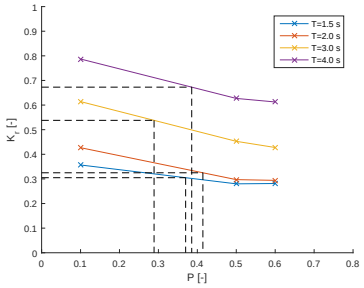

(c) Reflection, structure G

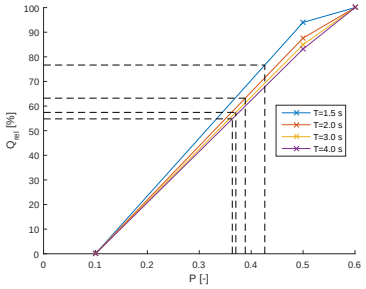

(d) Flow into the core, structure G

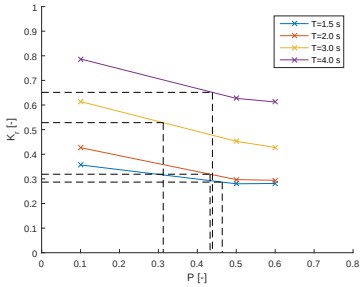

(e) Reflection, structure H

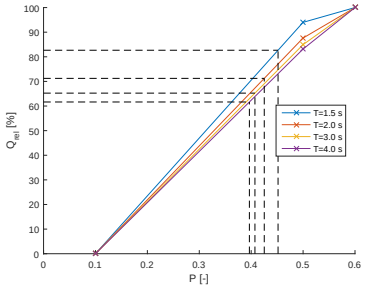

(f) Flow into the core, structure H

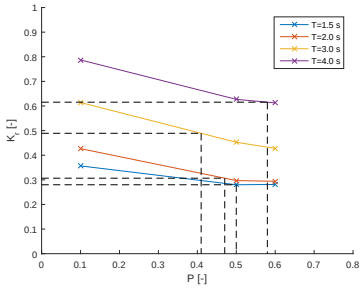

(g) Reflection, structure I

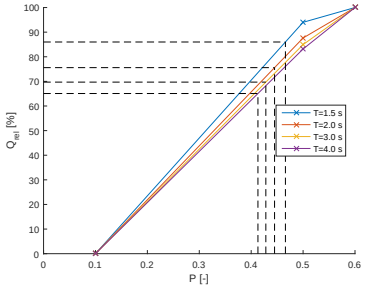

(h) Flow into the core, structure I

Figure 32: Figures showing results for structures (F-I) with varied core thickness.

In table 17, some values are marked with an (*). This indicates that the obtained values are outside the range of interpolation. In all cases the reflection coefficient found for the intermediate structure is lower

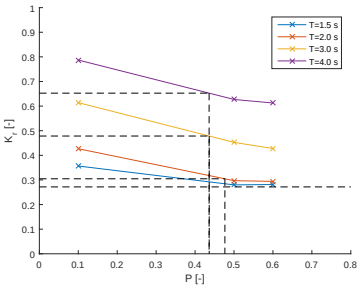

(a) Reflection, structure J

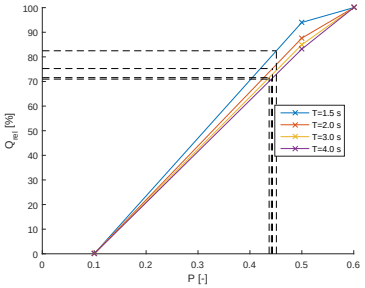

(b) Flow into the core, structure J

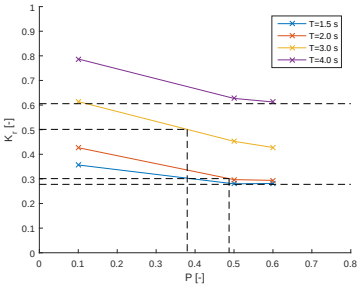

(c) Reflection, structure K

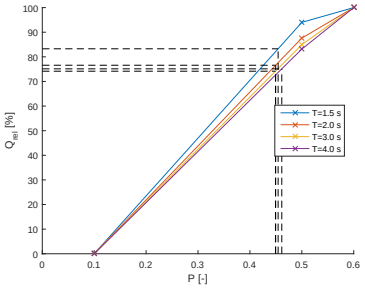

(d) Flow into the core, structure K

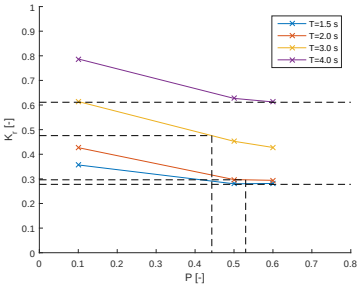

(e) Reflection, structure L

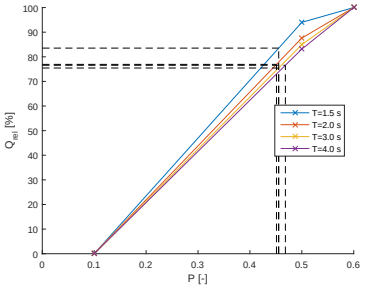

(f) Flow into the core, structure L

Figure 33: Figures showing results for structures (J-L) with varied core thickness.

than that of the $P = 0.6$ structure. As a minimum K_r value is expected for this latter structure, finding an even lower value indicates either uncertainty in the calculation of K_r or measurement errors.

The results for P are plotted in figures 34 and 35. A clear trend can be seen in the figure based on interpolation of Q. For P based on reflection this trend is not present and P-values seem to deviate much from an expected trend. Also overall spread is larger for K_r.

In figure 36, the values found for P are averaged and the range found in the results is marked. This provides a good overview of differences between the methods.

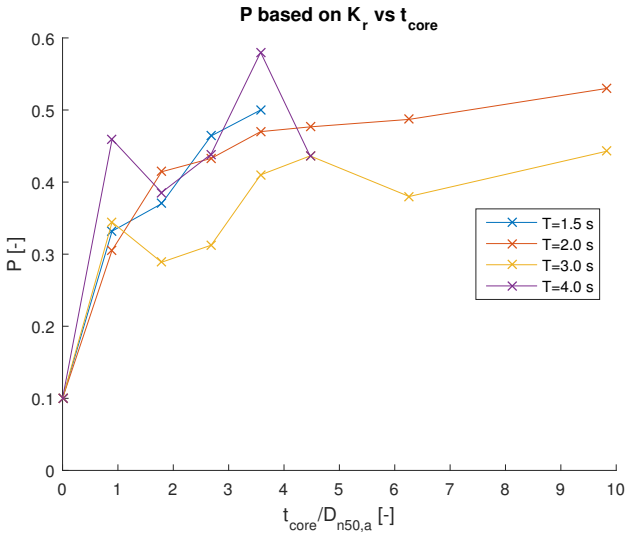

Figure 34: Plot showing the interpolated P-values based on K_r based on relative core thickness.

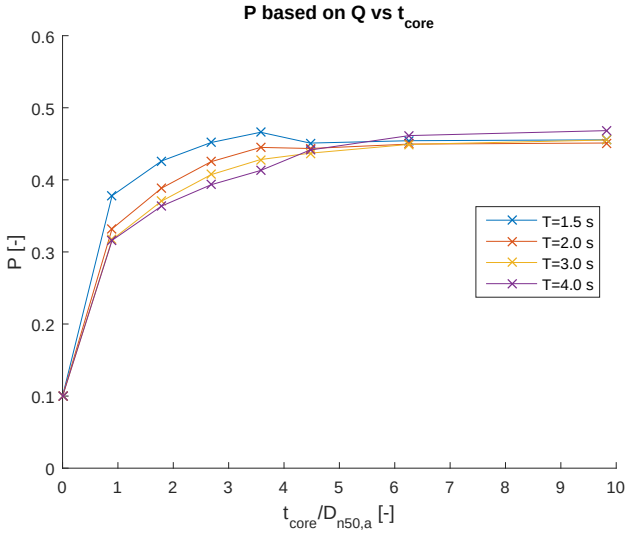

Figure 35: Plot showing the interpolated P-values based on Q based on relative core thickness.

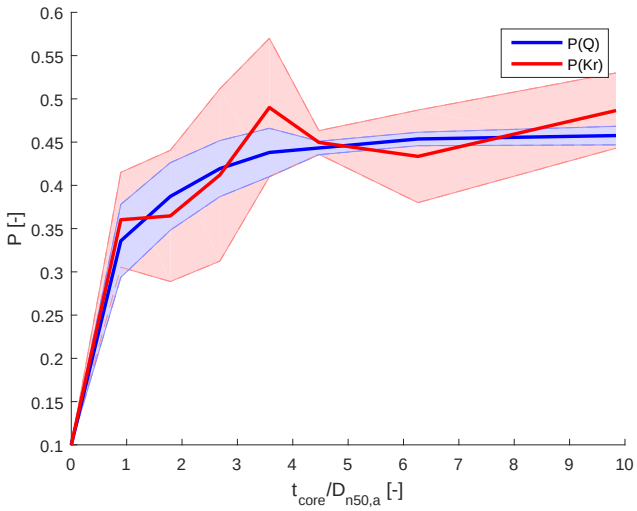

Figure 36: Plot showing mean values found for P, together with the range found in outcomes

5.3 SENSITIVITIES OF MODEL PARAMETERS

In the third set of model simulations, the porous media parameters (n, α, β, γ) in the numerical model have been varied. Only those of the core layer were adapted. This was done in order to gain insight into model sensitivities as well as governing processes in the structure. Results are treated per parameter below and outcomes are plotted in figures 37 to 40.

POROSITY The porosity of the core layer has been varied in 4 steps, see table 9. The effect on the reflected wave and the flow into the core are plotted in figure 37 respectively. It is clear that the impact on the governing parameters is limited, as deviations are in the order of 3%. Only for longer waves the reflection coefficient shows a somewhat larger deviation of order 7%.

LINEAR FRICTION COEFFICIENT The results of the sensitivity analysis for the α-parameter of the Forchheimer relation are plotted in figure 38. Increasing and decreasing trends can be noticed for the outer values of α, for K_r and Q respectively. Deviations are in the order of 10% when K_r is considered and around 30% for Q. However, the applicable range for α is around 200-1100, see [IH Cantabria, 2012], it can be concluded that the influence of this parameter is not that large.

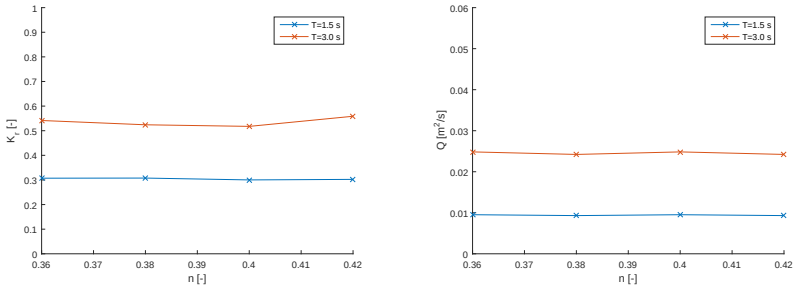

(a) (b)

Figure 37: Results for K_r (a) and Q (b) as a function of n

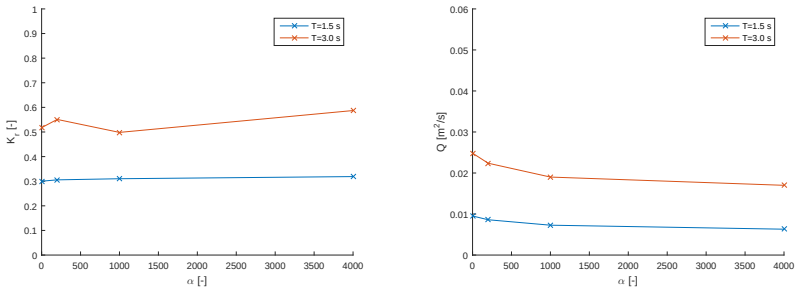

(a) (b)

Figure 38: Results for K_r (a) and Q (b) as a function of α

NON-LINEAR FRICTION COEFFICIENT In figure 39 the results for the two governing parameters are plotted when the non-linear friction coefficient from the Forchheimer-relation is varied. Here, the same holds as found above. The outer values dominate the variation, and in the applicable range of β hardly any variation is noticable.

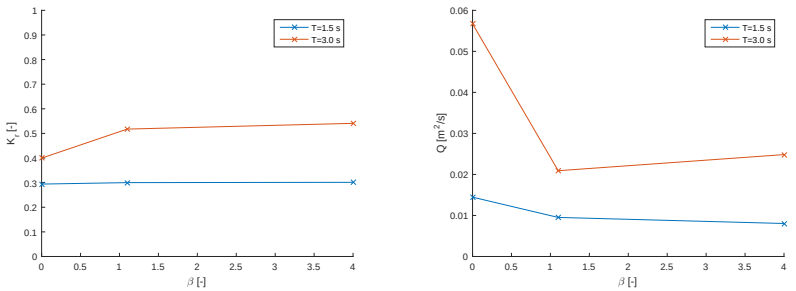

(a) (b)

Figure 39: Results for K_r (a) and Q (b) as a function of β

ADDED MASS COEFFICIENT As becomes clear from figure 40, the added mass coefficient from the Forchheimer-relation has very little

impact. The largest deviation in the modeled range can be found for K_r and is relatively small with 7%.

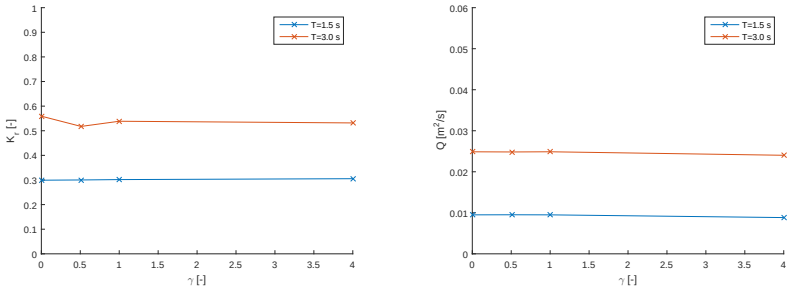

(a) (b)

Figure 40: Results for K_r (a) and Q (b) as a function of γ

5.4 VARYING NOMINAL DIAMETER OF THE CORE LAYER

In the final set of simulations, the nominal stone diameter of the core layer has been varied in order to investigate the effect on both the reflected wave and the flow into the core. The values found for both Q and K_r are plotted in figures 41 and 42. The diameter of core material is made dimensionless by dividing by the $D_{n50,a}$, which was not varied. All results are presented in appendix G.

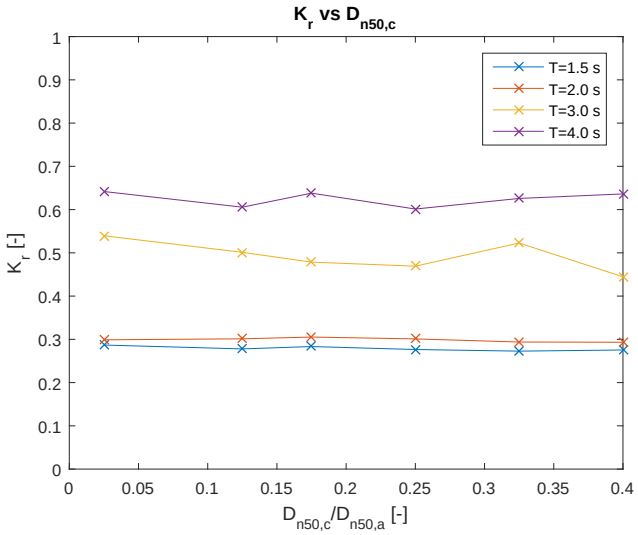

Figure 41: K_r-values for increasing D_{n50} of the core.

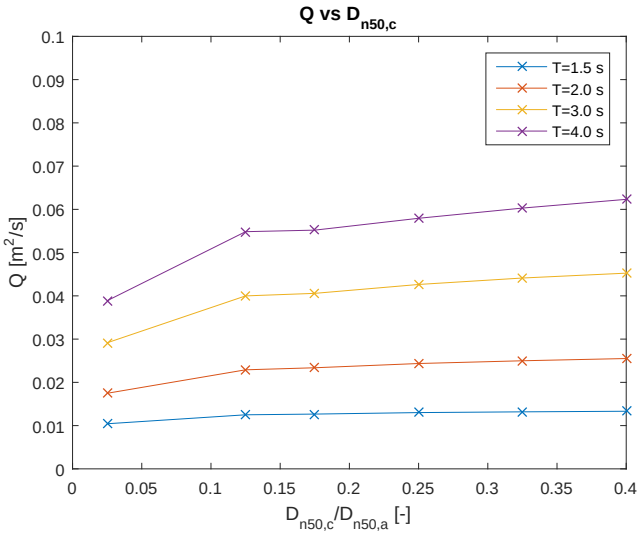

Figure 42: Q-values for increasing D_{n50} of the core.

5.4.1 *Estimating P-values*

First the P-values are estimated according to the two hypotheses by means of interpolating for Q and K_r. The results of this process are shown in figures 43 to 52.

While increasing the diameter of the core material, at a certain point the reflected wave measured is lower than in the 'reference' case with known P, resulting in a failure of finding a P-value, as was the case in some of the simulations with varying core.

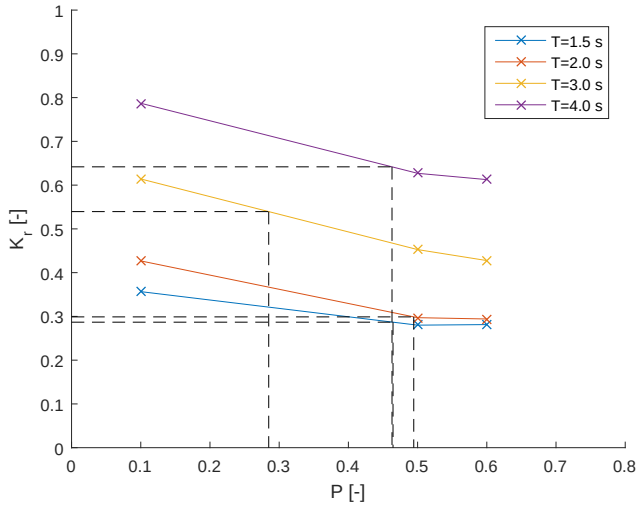

Figure 43: Interpolation based on K_r for $D_{n50,c}/D_{n50,a} = 0.025[-]$

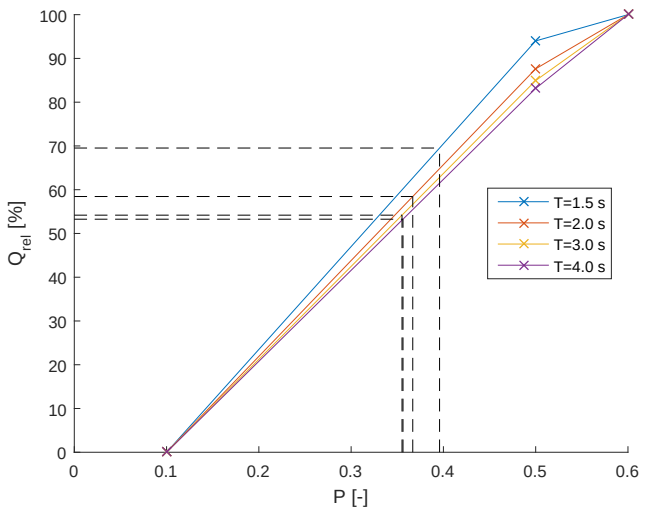

Figure 44: Interpolation based on Q for $D_{n50,c}/D_{n50,a} = 0.025[-]$

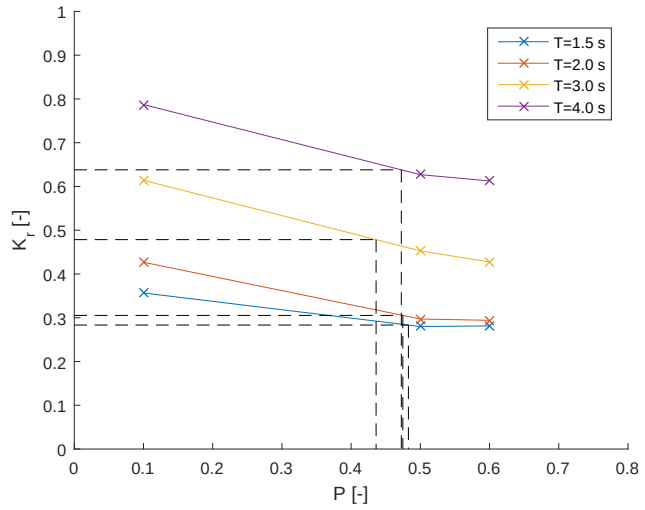

Figure 45: Interpolation based on K_r for $D_{n50,c}/D_{n50,a} = 0.175[-]$

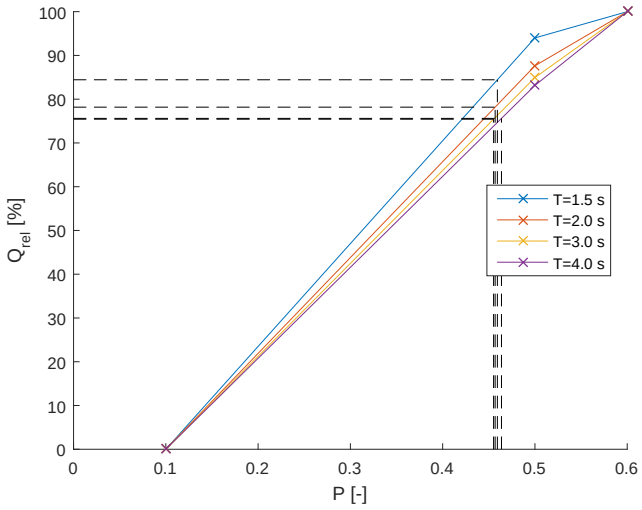

Figure 46: Interpolation based on Q for $D_{n50,c}/D_{n50,a} = 0.175[-]$

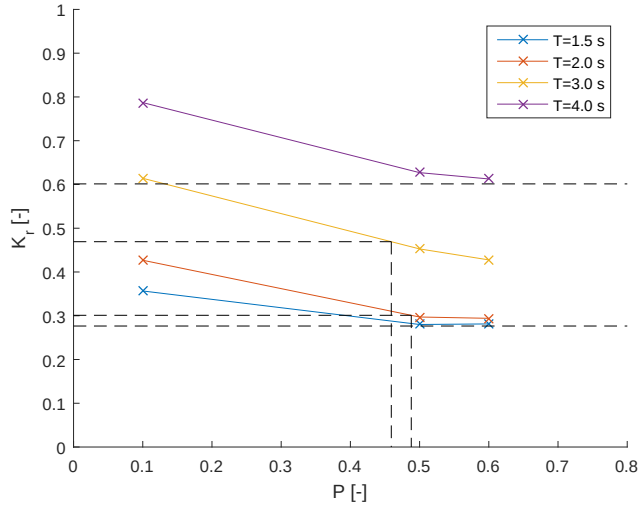

Figure 47: Interpolation based on K_r for $D_{n50,c}/D_{n50,a} = 0.25[-]$

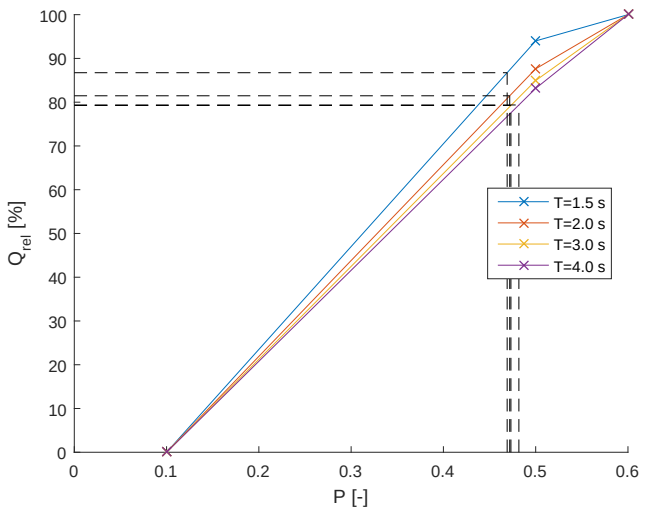

Figure 48: Interpolation based on Q for $D_{n50,c}/D_{n50,a} = 0.25[-]$

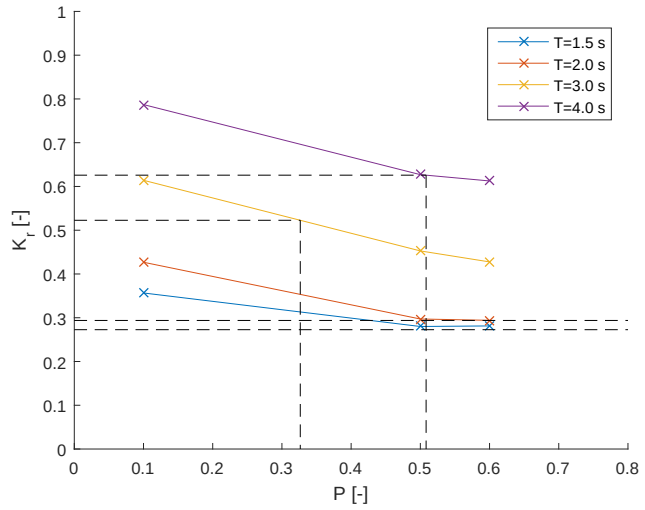

Figure 49: Interpolation based on K_r for $D_{n50,c}/D_{n50,a} = 0.325[-]$

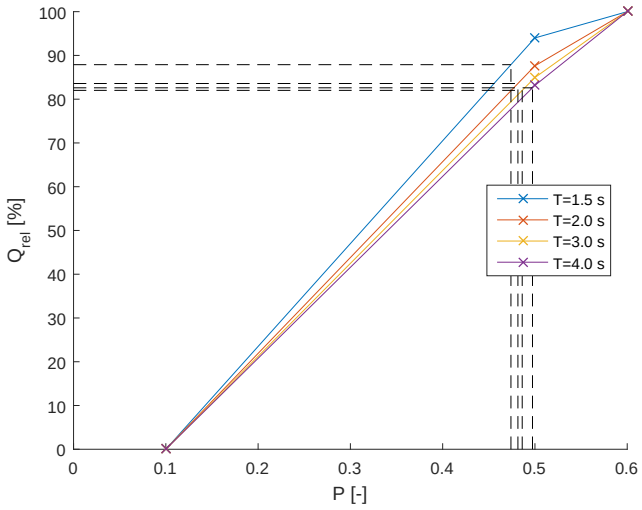

Figure 50: Interpolation based on Q for $D_{n50,c}/D_{n50,a} = 0.325[-]$

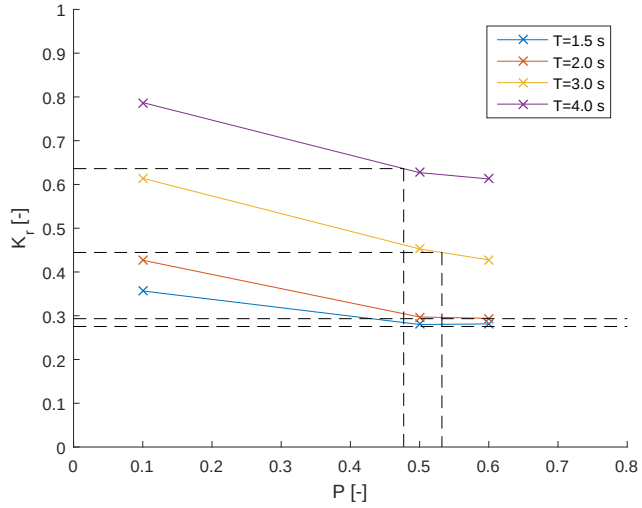

Figure 51: Interpolation based on K_r for $D_{n50,c}/D_{n50,a} = 0.4[-]$

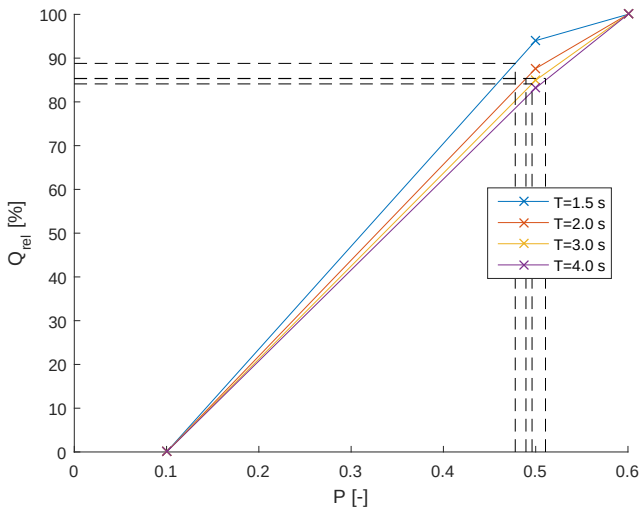

Figure 52: Interpolation based on Q for $D_{n50,c}/D_{n50,a} = 0.4[-]$

In figure 53 and 54 all the obtained P-values are summarized. Some points are missing in the $P - K_r$ plot because of failing interpolation, described above. Although less clear than in the case of varying core thickness, a similar trend can be seen in both figures, where obtained P-values diverge in the $0 < D_{n50,c}/D_{n50,a} < 0.15$ region. In figure 55 this effects is made clearer as the results are combined into one plot.

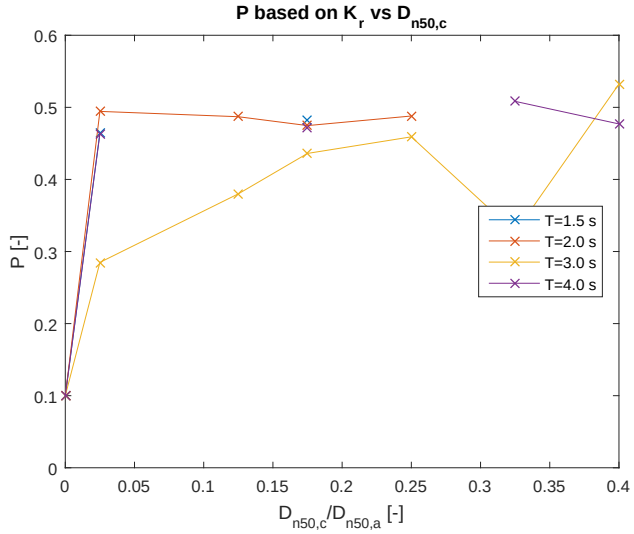

Figure 53: All the obtained P-values based on K_r.

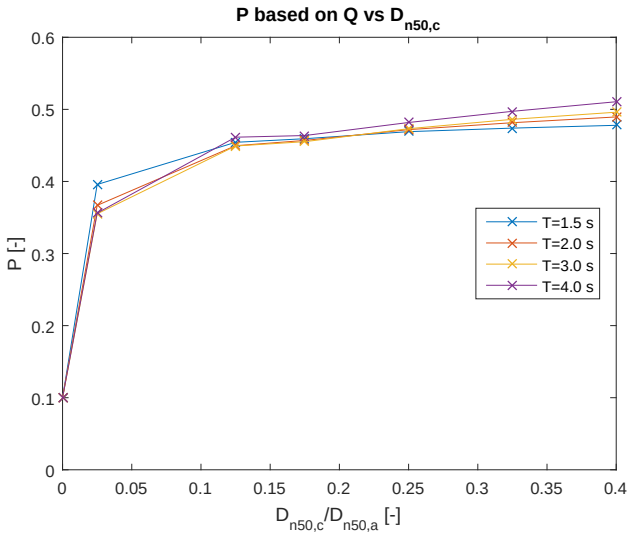

Figure 54: All the obtained P-values based on Q.

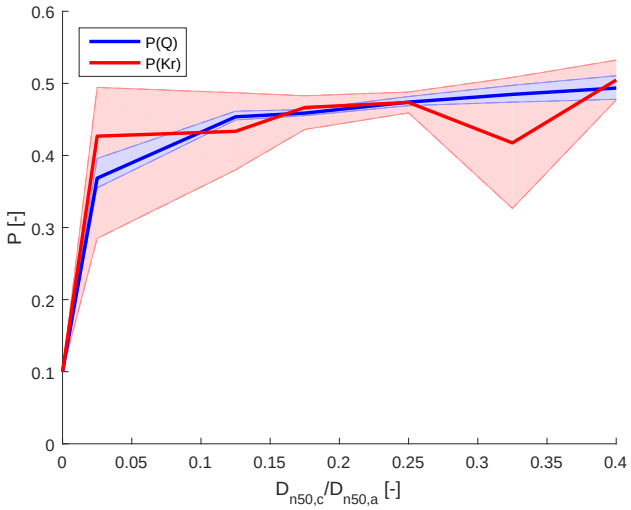

Figure 55: Plot showing mean values found for P when $D_{n50,c}$ is varied, together with the range found in outcomes

5.5 ANALYSIS OF RESULTS

In this part of the thesis, the results obtained in previous sections are analyzed. First, general trends found are described. Then, after making the variables dimensionless, curves are fitted through the results to find relations describing $Q = f(\xi, t_c, D_{n50,c})$ and $K_r = f(\xi, t_c, D_{n50,c})$.

5.5.1 *Trends in results*

To find trends in the results, first a recapitulation is made of what parameters have been varied:

- Thickness of the core layer
- D_{n50} of the core material
- Porous flow parameters of the core layer (n, α, β, γ)
- All tests for multiple wave periods

THICKNESS OF CORE LAYER When all parameters except for the core thickness are kept constant, as depicted in figure 24, P increases for larger thickness t_c as expected. There is more room for the wave force to dissipate, resulting in a lower reflected wave and thus a higher P-value. A thicker core also means less resistance for water to enter the layer, resulting in higher velocities and thus an increased Q, leading to higher P-values as well.

However, this effect is much more evident when P is obtained through interpolation of Q than via K_r, as shown in figures 34 and 35. It appears that although the same overall trend can be distinguished, results obtained from Q show a much smaller scatter.

DIAMETER OF THE CORE MATERIAL The effects of varying the $D_{n50,c}$ are less pronounced. When P is interpolated based on the flow into the core, a clear increasing trend can be seen, see figure 54. This is expected as an increase in stone diameter decreases the friction the flow entering the core encounters, increasing Q and thus P. For $D_{n50,c}/D_{n50,a} = 0.5$ the structure is theoretically similar to the permeable structure from [Van der Meer, 1988], with $P = 0.5$. This matches the results as well, as the average of the 4 wave periods ≈ 0.5. In case of interpolation based on K_r the results don't show a clear trend. This has to do with the large deviations in the values of the reflected wave, resulting in out of range K_r-values and thus miss-

ing P-values, see figure 53.

When the direct results of the two governing parameters are plotted (41 and 42), the effect of increasing Q for larger diameters becomes clear. For K_r the lines show a less clear trend.

POROUS FLOW PARAMETERS OF THE CORE LAYER A sensitivity analysis was performed by varying model parameters. In their applicable range, the parameters seem to have little effect on Q or K_r. However, this could be caused by the relatively small core layer thickness of the base case ($t_c/D_{n50,a} \approx 1$). This is discussed in chapter 6.

WAVE PERIOD As explained in chapter 3, the wave period has a large influence on the two governing parameters Q and K_r. The amount of water displaced per wave as well as the amount of energy reflected is dependent on the wave period. This is evident in the results as well. For both varied structural parameters, t_c and $D_{n50,c}$, the lines for various wave periods appear to follow similar trends, only shifted vertically. This effect is more apparent for Q rather than for K_r.

SUMMARY OF RELATIONS In table 18 all the relations found are summarized. When no clear relation is found, e.g. in case of interpolating out of range values, the relation is marked as 'undefined'. The relation between the interpolated $P(K_r)$-value and the simulated variables is mostly marked as undefined and a function describing the relation would not be very reliable. The relation $Q(T, D_{n50,c}, t_c)$ appears to be defined more clearly, so a start is made by finding a function to describe this relation.

Table 18: Table summarizing the relations found above.

Variable	Parameters			
(increasing)	Q	K_r	P(Q)	$P(K_r)$
T	Increasing	Increasing	Undefined	Undefined
$D_{n50,core}$	Increasing	Undefined/Decreasing	Increasing	Undefined
t_{core}	Increasing	Decreasing	Increasing	Undefined/Increasing

The plots of Q-t_c and Q-$D_{n50,c}$ are repeated in 56 and 57.

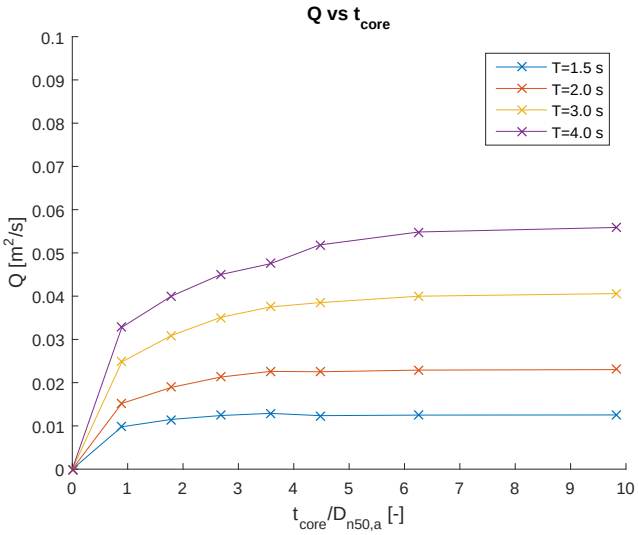

Figure 56: Q versus t_{core}

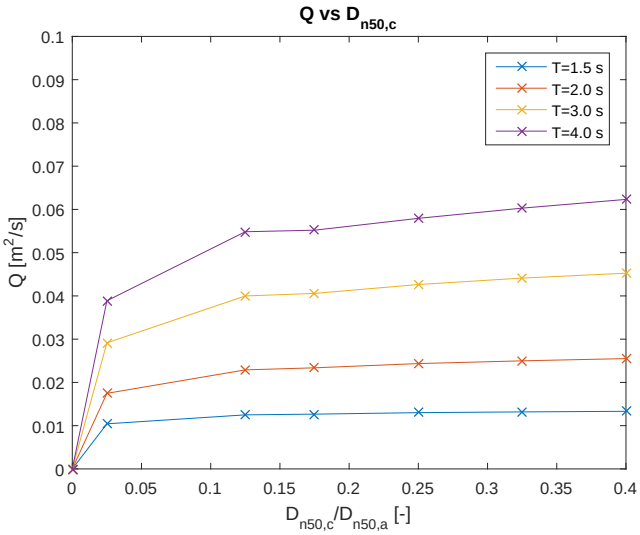

Figure 57: Q versus $D_{n50,c}$

5.6 CURVE FITTING

5.6.1 *Dimensionless quantities*

First both the axis are made dimensionless so that the quantity has no physical unit that affects its applicable range. In figure 56 and 57, the horizontal axis is already dimensionless. The vertical axis is not however, its dimension is $[m^2/s]$.

The flow into the core is the result of fluid velocities directed inwards on the core-filter interface. The amount of water moved per wave is governed mostly by the wave height H and wave period T. Water is 'piled up' on the slope from where it enters the porous medium. The phreatic line in the structure is lower, thus creating a pressure difference. As explained in section 2.2.3, velocities in porous media are determined by pressure gradients.

An analogy with the research of [Jumelet, 2010; Van Broekhoven, 2011] can be made, where run-up was coupled to the notional permeability of the structure, by means of calculating a volume inflow into the structure. As run-up has dimensions [m], it is usually made dimensionless by dividing by the wave height, see for example Hunt's formula in [Schiereck, 2012]. Run-up relates closely to wave overtopping, defined as the amount of water passing over the crest of a structure. Formula's quantifying wave overtopping are for example Bradbury et al. or Franco et al., see [Verhagen et al., 2012]. Here, Q is divided by $\sqrt{gH^3}$, resulting in a dimensionless number. The term can be seen as a certain velocity, multiplied by its height to come to a flow. In the following sections, Q is made dimensionless in a similar manner.

Changing Q to the dimensionless parameter $\frac{Q}{\sqrt{gH^3}}$ changes figures 56 and 57 to 58 and 59.

All terms except the wave period are now dimensionless. To match dimensions in the final formulas, T is rewritten into $\xi[-]$. The following phase is to fit curves through the dataset to find a relation for $\frac{Q}{\sqrt{gH^3}} = f(\xi, t_c, D_{n50,c})$. The fitting is done in 3 steps using non-linear regression analysis in MATLAB. The function that is used to fit the data to is called the model function and should be able to describe the trend. A start is made by fitting a curve through the data points for varying ξ. Here, a model function of the form $Y = \beta_1 X^{\beta_2}$ is used, in which Y represents $\frac{Q}{\sqrt{gH^3}}$ and $X = \xi$. For β_2 a value of 1.3 is found.

The following step is to fit curves for the varied core layer properties. Plotting the relations separately reveals that the lines cross zero.

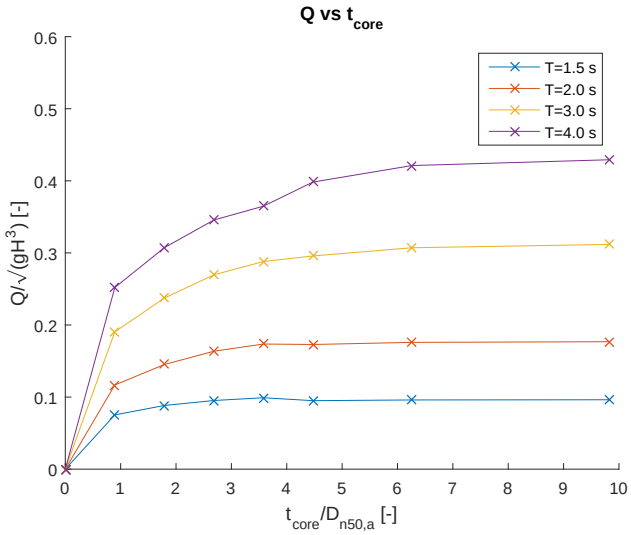

Figure 58: Q vs. t_{core} made dimensionless

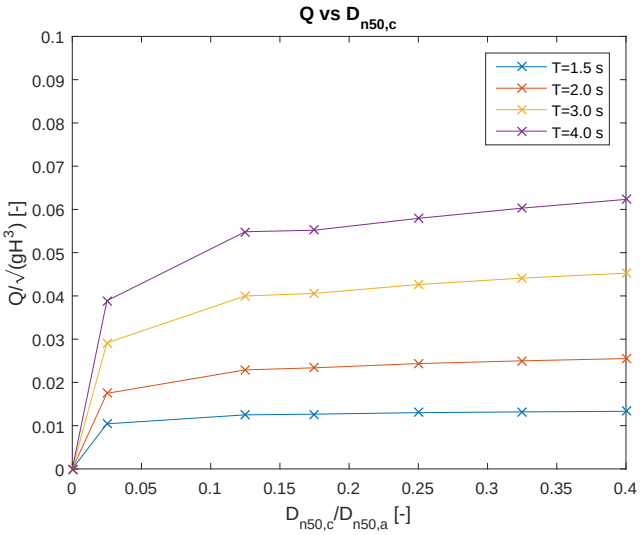

Figure 59: Q vs. $D_{n50,core}$ made dimensionless

When t_c approaches zero, no core layer is present and a flow into a non-existent layer is zero too. A $D_{n50,c}$ approaching zero could be seen as a structure with an impermeable core and thus a zero Q as well. In figure 58 an hyperbolic effect is noticeable: at some point, further increasing the core thickness does not increase Q. Therefore the model function $\xi^{1.3}\beta_1 * \log(X+1)^{\beta 2}$ is chosen. The extra $+1$ is added in order to maintain positive values. The result of this first step is plotted in figure 60, in which the various relations for varying wave periods are plotted. The relation found is:

$$\frac{Q}{\sqrt{gH^3}} = 0.022 * \xi^{1.3} \log(\frac{t_c}{D_{n50,a}} + 1)^{0.38} \tag{29}$$

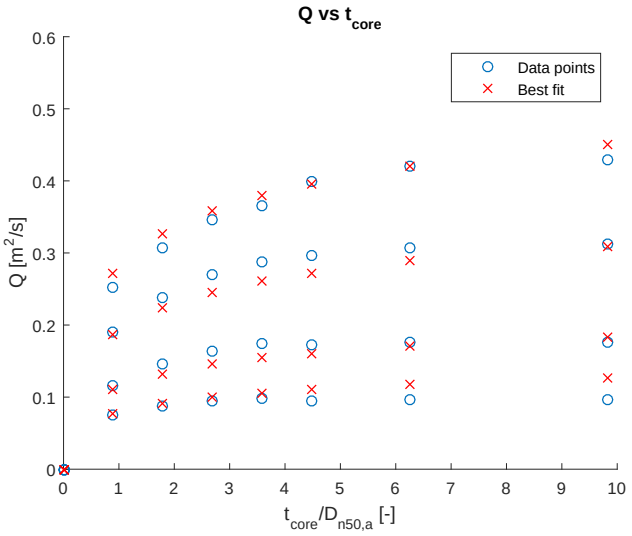

Figure 60: Results of regression analysis for t_c, lines are shown for various wave periods

Next, a curve is fitted through the points in figure 59, whilst taking the earlier found expression into account. These points all have the value $\frac{t_c}{D_{n50,a}} = 6.26$. A model function of the form $\xi^{1.3}\beta_1 * X^{\beta 2} * \log(6.26+1)^{0.38}$ is chosen, in which X now represents the term $\frac{D_{n50,c}}{D_{n50,a}}$. The result of this second step is shown in figure 61, presenting the fitted points with the actual measurements.

The final function describing $\frac{Q}{\sqrt{gH^3}} = f(\xi, t_c, D_{n50,c})$ is:

$$\frac{Q}{\sqrt{gH^3}} = 3 \cdot 10^{-2} \xi^{1.3} (\log(\frac{t_{core}}{D_{n50,a}} + 1))^{0.4} (\frac{D_{n50,c}}{D_{n50,a}})^{0.15} \tag{30}$$

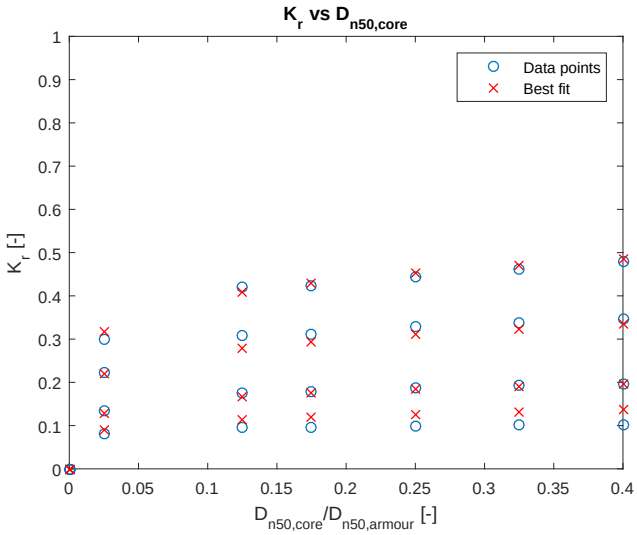

Figure 61: Results of regression analysis for $D_{n50,c}$, lines are shown for various wave periods

5.6.2 *Finding a relation for Kr*

The process described above can be repeated for K_r. This parameter is already dimensionless. Again, a relation in the form of $K_r = f(\xi, D_{n50,c}, t_c)$ is desired.

First a curve is fitted for $K_r - \xi$. As model function $\beta_1 X^{\beta_2}$ is used. The values found are $\beta_1 = 0.1$ and $\beta_2 = 0.89$ The result is shown in figure 62.

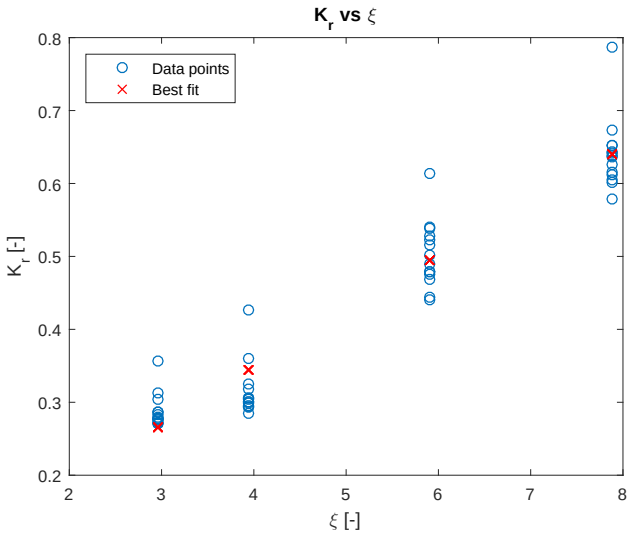

Figure 62: $K_r - \xi$ with its fitted curves

The following step involves fitting data for $K_r - t_c/D_{n50,a}$, where the values obtained in the previous step are taken into account. This results in figure 63.

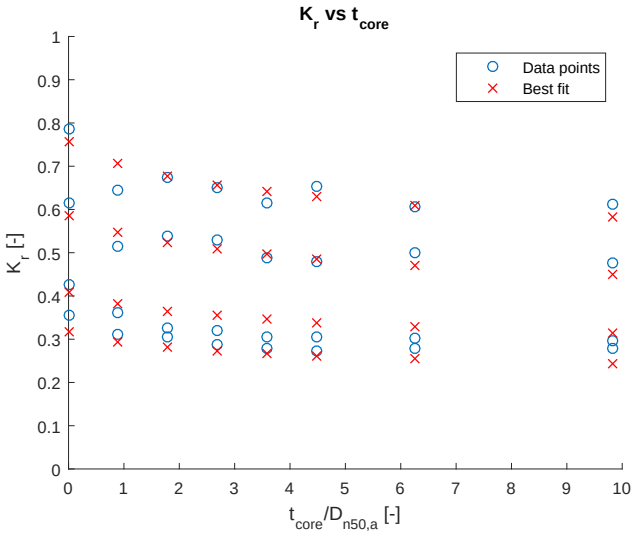

Figure 63: $K_r - t_c/D_{n50,a}$ with its fitted curves, lines are shown for various wave periods

Finally, a curve is fitted for $K_r - D_{n50,c}/D_{n50,a}$, yielding figure 64.

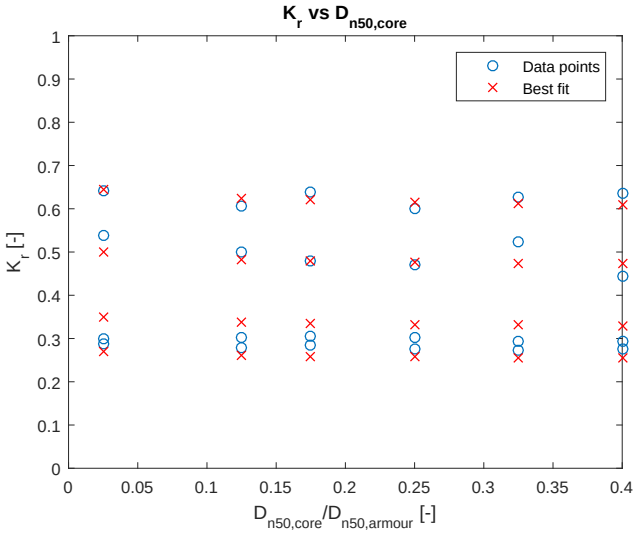

Figure 64: $K_r - D_{n50,c}/D_{n50,a}$ with its fitted curves, lines are shown for various wave periods

The relation $K_r = f(\xi, D_{n50,c}, t_c)$ can thus be described by the function:

$$K_r = 0.12\xi^{0.9}\left(\frac{D_{n50,c}}{D_{n50,a}}\right)^{-0.02}\left(\frac{t_c}{D_{n50,a}}\right)^{-0.11} \tag{31}$$

5.6.3 *Fitting P directly*

The process of fitting is repeated, but now directly for P. This way two relations are found: $P(Q) = f(\xi, D_{n50,c}, t_c)$ and $P(K_r) = f(\xi, D_{n50,c}, t_c)$, see below:

$$P(Q) = 0.1 + 0.3\xi^{-0.044}\left(\frac{D_{n50,c}}{D_{n50,a}}\right)^{0.15}\left(\log\left(\frac{t_c}{D_{n50,a}} + 1\right)\right)^{0.3} \quad (32)$$

$$P(K_r) = 0.1 + 0.24\xi^{0.04}\left(\frac{D_{n50,c}}{D_{n50,a}}\right)^{0.1}\left(\log\left(\frac{t_c}{D_{n50,a}} + 1\right)\right)^{0.33} \quad (33)$$

Observing equations (32) and (33), it is clear that the influence of ξ is small for the range considered, and the powers (-0.044 and 0.037) are of the same order. This suggests that although the influence of this parameter on both Q and K_r is large, interpolation of the outcomes diminishes its influence on P. Moreover, the wave period influences the flow into the core as well as the measured reflection to the same extent.

The other fitting coefficients are similar in both equations, showing that interpolated P-values are influenced by $\frac{t_c}{D_{n50,a}}$ and $\frac{D_{n50,c}}{D_{n50,a}}$ regardless of chosen interpolation parameter.

It must be noted that above relations are only able to assign influences of parameters that were varied, and are valid only for the simulated ranges.

Figures 65 and 66 show a plot of equations (32) and (33) together with all the results from the simulations.

5.6.4 *A general relation for P*

All resulting predictions of the notional permeability parameter obtained in the simulation round in which the core parameters were varied, are grouped per wave period and the range of outcomes is plotted, see figure 67. The large hatched area comes from the fact that all simulations are incorporated.

From the figure it is clear that for every wave period there exists a certain bandwidth of predicted P-values. In the case of $P(Q)$ this bandwidth is smaller and follows a more predictable trend, as seen by the more horizontal lines. Predictions based on K_r cover a wider range and follow a less clear trend.

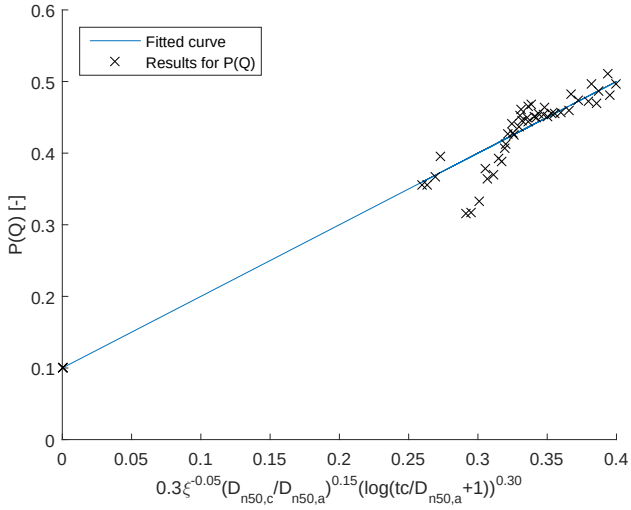

Figure 65: Relation (32) vs. measurements

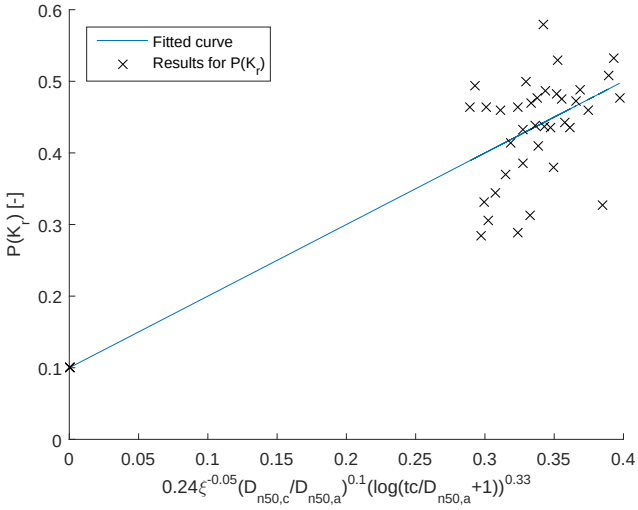

Figure 66: Relation (33) vs. measurements

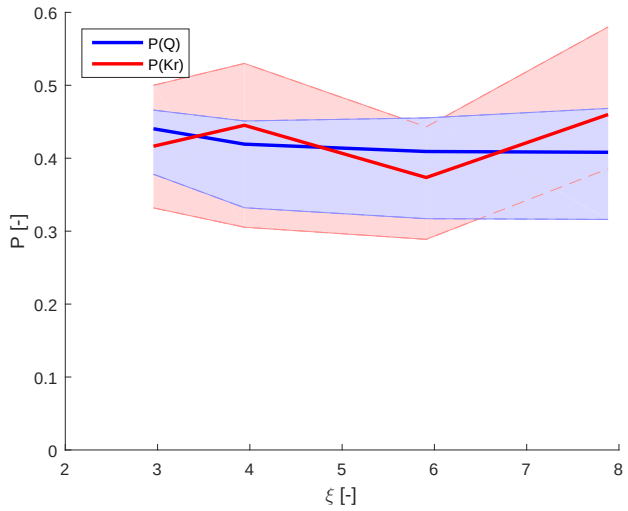

Figure 67: Influence of wave period on predictions of P

A single relation for $P = f(\xi, D_{n50,c}, t_c)$ is acquired when equations (32) and (33) are combined. This is justified as in the end the same trend is described. It should be mentioned that this relation describes *the predicted notional permeability based on interpolation*, therefore the ξ-term is left out as its influence on the interpolated results is small. The combined relation can be written as:

$$P = 0.1 + 0.3\left(\frac{D_{n50,c}}{D_{n50,a}}\right)^{0.15}\left(\log\left(\frac{t_c}{D_{n50,a}} + 1\right)\right)^{0.3} \tag{34}$$

Relation (34) is only a function of the two varied core layer properties, and should thus only be used to quantify the influence of both of these parameters. More research is required to find a relation including more parameters that are of importance, like properties of other layers.

This function is plotted together with all the original simulation results for both Q and K_r in figure 68.

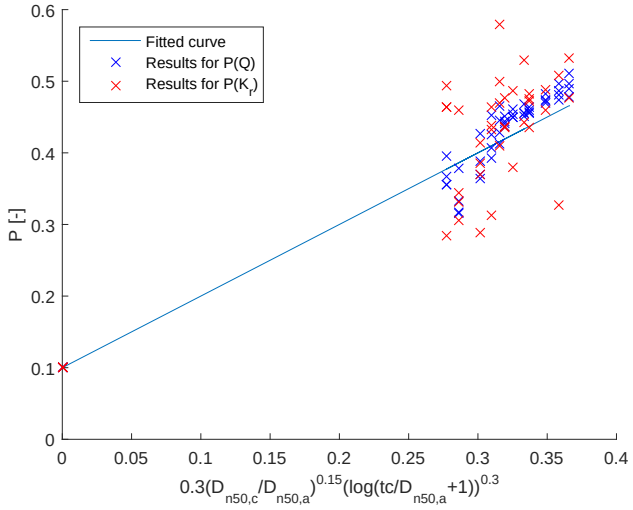

Figure 68: Simplified, general relation for P along with simulation results

5.7 COMPARISON WITH PHYSICAL MODEL TESTS

The results from this thesis are compared to earlier physical model tests executed by [Kik, 2011] and [Kluwen, 2012]. More information about these tests can be found in chapter 2.

5.7.1 *Results of Kik*

For the structure with unknown notional permeability coefficient of [Kik, 2011] (see section 2.1.2 on page 10) a P-value of 0.37 was found, rounded to 0.35 for practicality.

The lay-out of this so-called *test structure 3* is comparable to structure G from this thesis, defined in section 4.2. The structure from [Kik, 2011] features a filter layer with the same D_{n50} as the core layer in structure G. Thicknesses match quite well, with 95 mm for the lay-out from [Kik, 2011] vs 72 mm for structure G.

When the values found for the various wave periods are averaged, $P(K_r) = 0.36$ and $P(Q) = 0.38$ are obtained, which correspond well with measurements from [Kik, 2011].

5.7.2 *Results of Kluwen*

In the thesis of [Kluwen, 2012], 3 structures were tested and for 2 of them a value for the notional permeability parameter was obtained. A structure similar to the new structure in [Kik, 2011], now called

3A, was tested and a P-value of 0.38 was found, matching the value obtained by [Kik, 2011] and thus corresponding to the values found in this thesis as well.

The second structure is similar to the *fourth* structure from [Van der Meer, 1988]. Which was simulated using a numerical model, and for which $P = 0.4$ was defined, see section 2.1.1. [Kluwen, 2012] found a value for P of 0.45.

An exact copy of this lay-out has not been simulated, but structure D of this thesis is a close match, as only the thickness of the filter layer differs. See section 4.2 for details. For structure D, the values $P(K_r) = 0.45$ and $P(Q) = 0.47$ are obtained. This is a good match with the value found by [Kluwen, 2012]. For structure J, with a core thickness approaching a fully permeable structure (including filter layer), $P(K_r) = 0.45$ and $P(Q) = 0.44$ were obtained.

5.8 ASSUMPTIONS FOR PREDICTING P

The predictions of P were made with two assumptions in mind:

- Linear interpolation between structures with known-P.
- Averaging over various wave periods.

As appeared in the comparison with physical model tests above, obtaining a prediction for P works out well using these assumptions. With the results obtained in the simulations, a recap is made to investigate if these assumptions were correct.

5.8.1 *Linear interpolation*

When the notional permeability coefficients found in the physical tests of [Kik, 2011] and [Kluwen, 2012] are combined with the Q-values found in the simulations, figure 69 is obtained.

The trend in figure 69 seems to confirm that linear interpolation between the known-P cases (0.1 and 0.5) is allowed, as the points added for the tests of [Kik, 2011] and [Kluwen, 2012] lie in a straight line between these points. Only the line for $T = 1.5$ s seems to deviate, suggesting a more curved shape of the trend. Interestingly, this suggested trend is inverted from the lines drawn by [Van der Meer, 1988], see section 2.1.1 figure 5.

The process of adding the simulation results for the structures of [Kik, 2011] and [Kluwen, 2012], assuming a fixed and verified P of

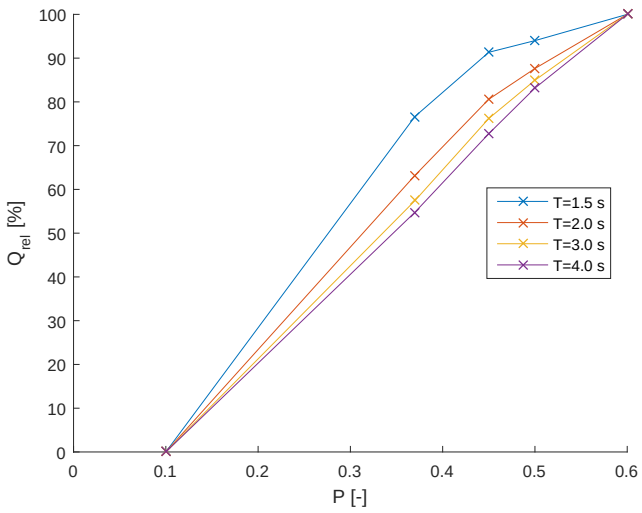

Figure 69: Plot showing relative values of calculated flow into the core, for known-P cases, extended with physical model tests of [Kik, 2011; Kluwen, 2012]

0.37 and 0.45 respectively, is repeated for K_r. This way figure 70 is obtained.

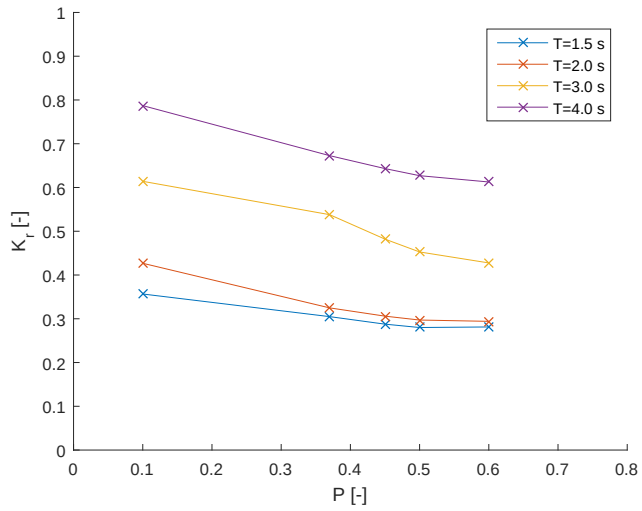

Figure 70: Plot showing relative values of calculated reflection coefficient, for known-P cases, extended with physical model tests of [Kik, 2011; Kluwen, 2012]

In this case again, the assumption of interpolation based on a linear line seems valid. A slightly curved trend can be noticed, especially for $T = 4.0$ s and $T = 2.0$ s. Compared to earlier results in which the reflection coefficients appeared to produce quite an amount of outliers or unexpected values, the results in figure 70 are remarkable.

5.8.2 *Averaging over wave periods*

Values of Q and K_r are to a large extent dependent on the wave period, as is clear from the relations obtained earlier:

$$\frac{Q}{\sqrt{gH^3}} = 3 \cdot 10^{-2} \xi^{1.3} (\log(\frac{t_{core}}{D_{n50,a}} + 1))^{0.4} (\frac{D_{n50,c}}{D_{n50,a}})^{0.15}$$

$$K_r = 0.12 \xi^{0.9} (\frac{D_{n50,c}}{D_{n50,a}})^{-0.02} (\frac{t_c}{D_{n50,a}})^{-0.11}$$

For predictability of P, the influence of wave period seems to be small, as is depicted in figure 67. More or less the same range for P is found, regardless of ξ. However, when looking at figure 35, in which predictions of P were plotted as a function of core thickness, it can be seen that (especially for the region $1 < t_c/D_{n50,a} < 4$) the wave period is of influence. Here, predictions based on $T = 4.0$ s are consistently lower than P based on $T = 1.5$ s. Thus, the prediction of P depends on the range of wave periods simulated.

Predictions for structure G are again compared with measurements from [Kik, 2011], see figure 71. The values shown as P_{Kik} require some explanation: [Kik, 2011] measured damage on the structure slope in his tests, and determined P by minimizing the error between measured and calculated damage levels. Hereby the assumption is made that P is fixed per structure. For comparison with results from this thesis, this assumption is discarded and P is calculated *per test*, again by fitting the Van der Meer formula. This way a P-value is obtained for a range of Iribarren numbers, shown as P_{Kik} in figure 71.

It should be mentioned here that this is not a sound method of calculating P-values as the large uncertainties in measured damage levels greatly influence the results. Nonetheless, a trend is observed of lower P for higher Iribarren numbers. This trend, although less clear, can also be seen in predictions based on Q and K_r.

It was already shown that the choice of the wave period influences the prediction of P. With figure 71 suggesting this trend is also apparent in physical model tests, that would mean certain processes are not accounted for.

As the reason of its influence is unknown at this point, it makes sense to choose a range of wave periods that can be expected in practice and average the results. After all, this is how it was done in [Van der Meer, 1988] originally.

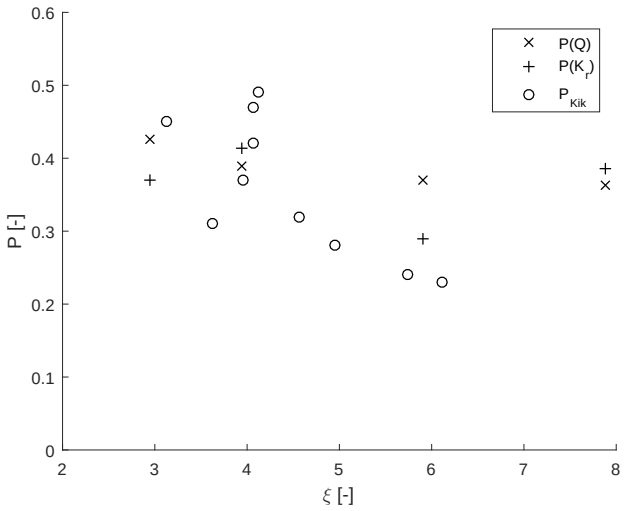

Figure 71: Plot showing predicted P-values for structure G, along with data from [Kik, 2011]

5.9 PREDICTABILITY

The term predictability of P is defined in this context as how well the selected method can provide an estimation of P. Thus, a clear trend in results and little scatter around this trend are factors defining this predictability.

For comparison, this predictability is quantified by calculating the root-mean-square error, being the average distance from the measurements to the trend in figures 65 and 66. The values found were $P \pm 0.016$ for predictions based on Q and $P \pm 0.046$ when based on K_r. This quantifies what can be seen from figure 68 directly: flow into core is a better way of predicting P than reflection coefficient.

The original description of P in [Van der Meer, 1988] does not provide error margins of P. However, the computations with the HADEER model (see section 2.1.1), calculated a P of 0.44 for an arbitrary structure, which later was adjusted to 0.4. This provides an indication for a reasonable order of magnitude ($P \pm 0.04$) and shows that performance of the methods as worked in this thesis are able to predict P with errors of the same order.

6 CONCLUSIONS & RECOMMENDATIONS

In this chapter the conclusions found in this thesis are summarized. After that some recommendations are provided to aid further research.

6.1 CONCLUSIONS

In its original description, the notional permeability parameter only depends on structural properties. However, for a region between the fixed outer bounds of P, hydraulic conditions seem to influence the parameter.

The variety of hypotheses that exist to predict P is an indication for the fact that the parameter is not fully understood. Four hypotheses are mentioned in this thesis, all based on other fundamental governing processes. These hypotheses either provide a relation, or interpolate for defined structures to calculate P, and can thus be subdivided into *direct* and *indirect* methods, respectively.

- Direct methods:
  - Dimensionless numbers found by numerical analysis by [Van der Neut, 2015]
  - Run-up reduction factor by [Jumelet, 2010; Van Broekhoven, 2011]
- Indirect methods:
  - Flow into the core Q by [Van der Meer, 1988]
  - Reflection coefficient K_r by [Van den Bos et al., 2015]

In this thesis the latter category was further investigated. These indirect methods need an interpolation-step to predict P.

Both these hypotheses are based on relating permeability to a form of energy dissipation. The flow into the core is governed by velocities at the core interface. In case of a relatively permeable structure, the flow enters the core layer with relative ease, resulting in a high Q and thus a high value for P. In case of the reflection coefficient, it is hypothesized in a similar way that the permeability of the structure determines the amount of energy dissipated, and that the reflected wave indicates how much energy was lost.

P is predicted using these methods by calculating either Q or K_r for the known-P structures (P=0.1, 0.5, 0.6), and for the unknown-P structure, and interpolating the values afterwards. This is done using the IH-2VOF numerical model, in which flow velocities and pressures can be simulated.

First, a test case is simulated to which the methods were applied. This way a framework is obtained that serves as a base case. Next, an intermediate-P region is defined by varying core layer properties: the thickness t_c and nominal diameter $D_{n50,c}$, thus creating a range of unknown-P structures between bounds for which P is known. When both t_c and $D_{n50,c}$ are increased, an increase in P is obtained regardless of chosen method.

This process is executed for multiple wave periods, resulting in a range of P-values. Predictions of P are made using linear interpolation between structures, while averaging for the various wave periods. The predictions based on Q and K_r are in good agreement.

The assumptions used for prediction were checked for validity by comparison of the results with physical model tests by [Kik, 2011; Kluwen, 2012]. Linearly interpolating between known-P structures yields similar results. The choice of wave periods has a small influence on predictions. It is thus recommended that a *realistic* range of wave steepnesses ($0.5 - 4\%$) is simulated. This is similar to the original method by [Van der Meer, 1988].

When varying structural properties of the core layer and predicting P using the reflection coefficient K_r, a spread in outcomes is noticed. Due to these outliers, interpolation of the results fails in some cases and thus no P-value can be predicted.

Interpolation using Q seems to yield more robust results, it shows a clearer trend and less scatter in outcomes.

Curves were fitted through the obtained datasets by means of non-linear regression analysis and relations for $Q/\sqrt{gH^3} = f(\xi, D_{n50,c}, t_c)$ and $K_r = f(\xi, D_{n50,c}, t_c)$ were found:

$$\frac{Q}{\sqrt{gH^3}} = 3 \cdot 10^{-2} \xi^{1.3} (\log(\frac{t_c}{D_{n50,a}} + 1))^{0.4} (\frac{D_{n50,c}}{D_{n50,a}})^{0.15}$$

$$K_r = 0.12 \xi^{0.9} (\frac{D_{n50,c}}{D_{n50,a}})^{-0.02} (\frac{t_c}{D_{n50,a}})^{-0.11}$$

For the parameters above, the influence of the wave period (included in ξ) is significant. However, after interpolation of the results for various wave periods, this influence is decreased dramati-

cally. Therefore, in a general relation describing *the predicted notional permeability based on interpolation*, the influence of ξ is omitted. The relation found reads:

$$P = 0.1 + 0.3\left(\frac{D_{n50,c}}{D_{n50,a}}\right)^{0.15}\left(\log\left(\frac{t_c}{D_{n50,a}} + 1\right)\right)^{0.3}$$

In practice, $P = 0.4$ can be used when designing a rubble mound breakwater with an armour layer ($t_a = 2 \cdot D_{n50,a}$), on top of a filter layer and porous core when $t_c/D_{n50,c} > 3$ and $D_{n50,c}/D_{n50,a} > 0.1$.

Predictability is defined as the ability to show a clear trend in results with little scatter around it. Average errors are calculated to quantify this predictability. The order of magnitude of the predictability based on K_r compares to values obtained by [Van der Meer, 1988] that were deemed acceptable. Results based on Q were better.

The porous media input parameters (n, α, β, γ), when varied for the core of the structure, have little influence on the flow into the core and the reflection coefficient.

6.2 DISCUSSION & RECOMMENDATIONS

6.2.1 *Physical tests*

The most important recommendation is to conduct physical model tests. The original method of deriving P is explained in section 2.1.1 on page 5. It included physical tests in which a certain damage S was measured and wave height-damage curves could be derived. Using these curves, P was established for various structures. That also means that P can only be derived for a 'new' structure by measuring damage in a physical model test.

Physical testing was not conducted in this thesis due to time constrains, but is the next logical step in the research process. A preliminary test program is described in appendix F. In this program, dimensions of the flume at the TU Delft are taken into account, as was done in this thesis as well. When tests are conducted in a different facility, the test program needs adaptation.

6.2.2 *Calculation of Kr*

As described above, the method based on K_r sometimes calculated outliers, making interpolation of results impossible. The cause of

these outliers and methods to improve accuracy of calculating K_r is recommended to be subject of further research. Predicting P using K_r has some advantages over the usage of Q. The fact that irregular waves can be simulated which are more realistic, and it omits the calculation of Q, a potential source of errors.

6.2.3 *Calculation of Q*

The script used to calculate Q is provided in appendix E on page 105. It requires the begin- and end-coordinates of the armour-core interface. Depending on the given resolution, it searches for the nearest cell for all these small sections of the interface and subsequently averages to calculate the flow field at the line. Integrating the positive values per wave period results in the desired output Q.

Over- or underestimation of Q can appear due to the selection of the nearest cells. The motivation was that cells above the interface were selected *on average* as much as cells below the interface. This way the sum of all the distances from each individual cell to its section of the interface approaches zero for a resolution high enough. However, as a small portion of the wave inside the structure reflects off the interface, the velocities above the interface are influenced by this effect and might influence the integrated velocity calculated.

This effect could be further investigated by only selecting cells below the interface, possibly together with decreasing grid cell size.

6.2.4 *Obtained relations*

The functions found in section 5.5 on page 69 relate P to Q and K_r on the one hand, to the thickness and nominal stone diameter of the core layer on the other hand. There are some important considerations regarding these relations however.

It should be noted that the P-values to which the curves were fitted, are only predictions based on hypotheses, and that these values should be treated as such.

The flow into the core Q $[m^2/s]$ has been made dimensionless using an analogy with formulas for overtopping. This implies that the flow is also dependent on the wave height. In this research only the wave period has been varied, it is therefore recommended to vary the wave height as well to validate the relation. It is expected that the flow Q increases for a larger wave height H. The effect on the inter-

polated P could be small however, as all values increase.

With the relation fitted, basically an indirect method has been transformed into a direct method. Another consideration is the fact that more parameters than the ones varied influence the predicted P. These are taken into account automatically when making predictions using an indirect approach, but taking the relation outside its context (e.g. with a different nominal diameter of the armour layer) could change its validity. Extending this research by adding more varied parameters could increase its applicability.

The general relation found for P is in its current form only able to predict values for P based on core layer properties, and should thus only be used when an indication is needed of changing core thickness or nominal stone diameter of the core layer on P. However, the armour and filter layer thicknesses are common so its applicability should be wide in practice.

In figure 68 on page 80 it can be seen that for a region between $0.2 < P < 0.3$, no data has been obtained. This is caused by the selection of simulated core properties. It is important to investigate the validity of the general formula for this region. This can be done for example by varying $D_{n50,c}$ for structures with smaller $t_c/D_{n50,a}$.

6.2.5 *Sensitivity analysis*

The sensitivity analysis, found in section 5.3 aimed at altering the porous flow parameters in order to assess their influence on the outcome. The results showed little variation, possibly indicating that the exact values of α, β, γ, n are not as important. Another possibility for small variations in results is that structure F, with a relatively small core layer thickness, was used as a base case from which the coefficients were altered. This small thickness provides little room for the flow to be influenced by a changing resistance, thus possibly leading to small variation in outcomes. Varying porous media coefficients on a layer with increased thickness should be investigated further in order to assess model sensitivity.

For new simulations, porous media settings of [Van der Neut, 2015] can be used for model set-up.

BIBLIOGRAPHY

Andersen, O. H. and Burcharth, H. F. (1995). On the one-dimensional steady and unsteady porous flow equation. *Coastal Engineering (24)*.

CETMEF, C. C. (2007). *The Rock Manual. The use of rock in hydraulic engineering*. C683, CIRIA, London.

Fitts, C. R. (2013). *Groundwater Science*. Elsevier.

Frostick, L. E., McLelland, S. J., and Mercer, T. G. (2011). *Users Guide to Physical Modelling and Experimentation*. CRC Press.

Funke, E. R. and Mansard, E. P. D. (1980). The measurement of incidient and reflected spectra using a least squares method. Paper presented at the 17th ICCE in Sidney, Australia, 1980.

Holthuijsen, L. H. (2009). *Waves in Oceanic and Coastal Waters*. Cambridge.

IH Cantabria (2012). Ih-2vof course manual.

Jumelet, H. D. (2010). The influence of core permeability on armour layer stability. Master's thesis, Delft University of Technology.

Kik, R. (2011). Notional permeability of breakwaters. Master's thesis, Delft University of Technology.

Kluwen, J. G. M. (2012). Physical model tests on the notional permeability of breakwaters. Master's thesis, Delft University of Technology.

Muttray, M., Oumeraci, H., and ten Oever, E. (2006). Wave reflection and wave run-up at rubble mound breakwaters. In *ICCE 2006*.

Postma, G. M. (1989). Wave reflection from rock slopes under random wave attack. Master's thesis, Delft University of Technology.

Schiereck, G. J. (2012). *Introduction to Bed, bank and shore protection*. VSSD, second edition by verhagen, h j edition.

Sidiropoulou, M. G., Moutsopoulos, K. N., and Tsihrintzis, V. A. (2007). Determination of forchheimer equation coefficients a and b. *Hydrological processes 21*.

Troch, P. (2000). *Experimentele studie en numerieke modellering van golfinteractie met stortsteengolfbrekers*. PhD thesis, Universiteit Gent.

Van Broekhoven, P. J. M. (2011). The influence of armour layer and core permeability on the wave run-up. Master's thesis, Delft University of Technology.

Van den Bos, J., Verhagen, H. J., Zijlema, M., and Mellink, B. (2014). Towards a practical application of numerical models to predict wave-structure interaction: An initial validation.

Van den Bos, J. P., Verhagen, H. J., and Kuiper, C. (2015). Numerical modelling of wave reflection and transmission in vertical porous structures.

Van der Meer, J. W. (1988). *Rock slopes and gravel beaches under wave attack*. PhD thesis, Delft University of Technology.

Van der Neut, E. M. (2015). Analysis of the notional permeability of rubble mound breakwaters by means of a vofmodel. Master's thesis, Delft University of Technology.

Van Gent, M. R. A. (1992). Formulae to describe porous flow. In *Communications on hydraulic and geotechnical engineering*, number 92-2. Faculty of Civil Engineering, Delft University of Technology.

Van Gent, M. R. A. (1995). Porous flow through rubble-mound material. *Journal of waterway, port, coastal and ocean engineering*.

Verhagen, H. J., d'Angremond, K., and van Roode, F. (2012). *Breakwaters and closure dams*. VSSD.

Verpoorten, S. P. K. (2015). Numerical evaluation of stability methods for rubble mound breakwater toes. Master's thesis, TU Delft.

Vilaplana Domingo, A. M. (2010). Evaluation of the volume-exchange model with van der meer laboratory tests results. Master's thesis, Delft University of Technology.

A

SELECTION OF HYPOTHESES

The four methods discussed in chapter 2 and summed in chapter 3 describe methods to find P-values for structures of which this parameter has not been defined by [Van der Meer, 1988]. A division is made into direct and indirect methods, see chapter 3. For this thesis, it is decided to continue investigating only the indirect methods.

A.1 DRAWBACKS OF THE DIRECT METHODS

Narrowing-down of the methods was necessary because of time constraints and to maintain a clear goal of the research. Considerations for the choice are explained below:

A.1.1 *Dimensionless parameters*

As Van der Neut [2015] suggests in his thesis, the *notional permeability* can be related to several parameters such as velocities at certain locations, stone dimensions and wave periods. The structures for which P is known (by definition), have been simulated in IH-2VOF and aforementioned parameters have been fitted to find relations for P.

However, the standard deviation of these relations is quite significant with $\sigma(P) = 0.18$, and the influence of simulated velocities is large. Moreover, the parameters are quite complex, and verification using physical model tests is impossible. This way, the method does not seem suited for engineering purposes. It should be noted that as physical testing leads to more knowledge of points to use for fitting these functions, the accuracy will most likely increase. Still, the complexity of the parameters remains.

A.1.2 *Run-up below the armour layer*

As [Jumelet, 2010; Van Broekhoven, 2011; Vilaplana Domingo, 2010] showed, there exists a correlation between the *notional permeability* and the run-up level on a permeable slope. The process is governed by both structural and hydraulic parameters. The downside of the approach

In [Vilaplana Domingo, 2010; Van Broekhoven, 2011; Jumelet, 2010] a theory was developed to find a value for P based on the run-up at the core. The basis of this hypothesis is founded in the research of Jumelet [2010]. He explains that the notional permeability parameter as explained by Van der Meer [1988] should depend on both structural and hydraulic parameters. For this reason, he used a so-called *run-up reduction coefficient* c_r, to describe the influence of core permeability on the external run-up process. The values were calculated using a volume exchange model and the results were coupled to P.

Later, the research of Van Broekhoven [2011] tried to validate the modeled outcomes with physical scale-model tests. This way he provided some adjustments to the existing theory and redefined the location where the run-up was measured from the maximum level on top of the armour layer towards just below this layer.

However, both versions of the hypothesis are extremely sensitive to the run-up reduction factor. The area for which sensible outcomes are obtained is small and a slight change results in large deviations of P. As calculating the exact water level surface height in a VOF-model is not possible (see [IH Cantabria, 2012]), estimating P using c_r obtained with such a model would not make sense.

A.1.3 *Indirect methods*

The other category are the indirect methods, thus assigning a P-value to a construction by interpolation between known structures for either reflection or flow into the core. Both these methods have an advantage that its defining processes, reflection K_r and flow into core Q are less complex than the former, that the IH-2VOF is able to predict both the parameters and that at least K_r can be verified at a later stage to improve on the method.

Moreover, by interpolating between known values, it is expected that model inconsistencies can be negated and thus an indirect method, in combination with a relatively simple process, could probably make a better engineering method.

Above considerations, in combination with time constraints, were enough reason to select the indirect methods for this thesis. Both hypotheses could be evaluated using the same numerical model, thus saving time.

B

MODEL REFERENCE

In this appendix some steps executed regarding the IH-2VOF are elaborated.

B.1 STORING DATA AT A CUSTOM LOCATION

Normally, the model will not save to an other location than the `C:` drive. This can cause difficulties when little storage is available. A work-around is to create a so-called *symbolic link*, basically causing the data to be written elsewhere. The standard save location is `C:\IH2VOF\CASES\`. To change the save folder to a custom location (e.g. an external drive), open up a command prompt window and enter:

```
mklink /D path_to_custom_folder C:\IH2VOF\CASES\
```

B.2 LIMITING OUTPUT

Output of the numerical model can be considerable. Limiting the output has the advantages of both reducing the model run time as well as reducing used disk space.

The input file, which is created when the model is set-up, can be adapted using a text editor such as *notepad++*. A few lines are of importance when limiting the output is desirable:

NUMBER_LINES This line is normally set at 1000. This is the amount of lines (time steps) after which a new .txt file is created. This results in large files that slow down post processing. In this thesis it was set to 100, resulting in files of $\approx$ 70 mb, which was manageable.

IBG A line with this header can be added under the '# OUTPUT' header. It represents the starting horizontal grid cell, from this point on data is written to the disk.

IEG As with ibg, only now it defines the end cell. This combination can be used to define an area of which data is written. Data outside this range is considered to be not important and is discarded, greatly reducing required storage space. Wave gauge data is written even when their locations lies outside this range.

B.3 ADAPTED EXECUTABLE

During his research, [Verpoorten, 2015] found some small flaws in the way the model worked. He made some improvements and recompiled the main executable. His version is a bit faster and shows the remaining time needed for computation, it also puts a *.lock* file in the working directory that is automatically deleted when the simulation ends, which is easy when batch-processing is used. The way the data is stored in the output text files has slightly changed, now each time step is written on a new row.

B.4 SAVING OUTPUT AS MATLAB-DATA

Storing the output files as .mat files saves storage space and improves time needed for post-processing. [Van der Neut, 2015] wrote a script to do so, it can be found in his thesis. When using the adapted executable described above, some small adaptations are needed to be able to read the data. This is done in the script presented in appendix E.

C

REFLECTION DATA ANALYSIS

As an experiment, acquired reflection coefficients from earlier tests is compared to see if K_r-values from intermediate structures matches interpolated values. Three datasets were used:

Dataset	Plot color
van der Meer & Stam	Black
Kik	Blue
Broekhoven	Red

First the period is used to discern between the various structures, the result can be seen in figure 72. The wave period used for the values of Stam (1.8, 2.2, 2.6 and 3.0) were scaled to ξ, from the HADEER of Van der Meer [1988] simulations.

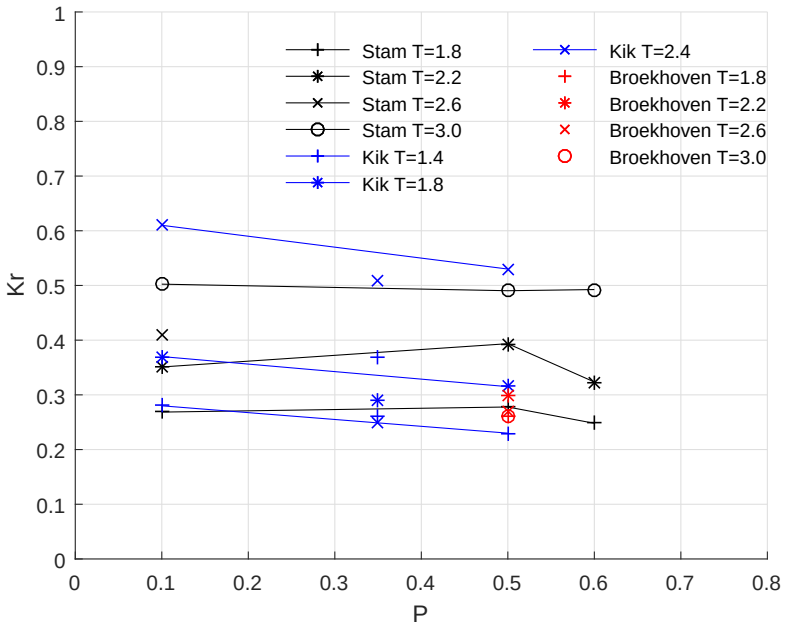

Figure 72: Data from physical tests. Interpolation based on wave period. All slopes.

It is clear that these results are not satisfactory, as:

1. There is no clear trend in the lines, as *Stam T=2.2 & Stam T=1.8* ascend while those of Kik descend.

2. The points for P = 0.35 of Kik do not match the interpolated lines. Only the lower of the two values for T = 1.4 is near its expected value.

3. The values of *Stam T=3* show no difference for the various structures.

4. The values obtained by [Van Broekhoven, 2011], in red, are much lower than those of the other two experiments, suggesting that experiments should not be compared against each other, or a physical process has not been accounted for.

To see whether inclusion of the slope by taking the *surf similarity parameter* ξ to interpolate the outcomes, figure 73 was made.

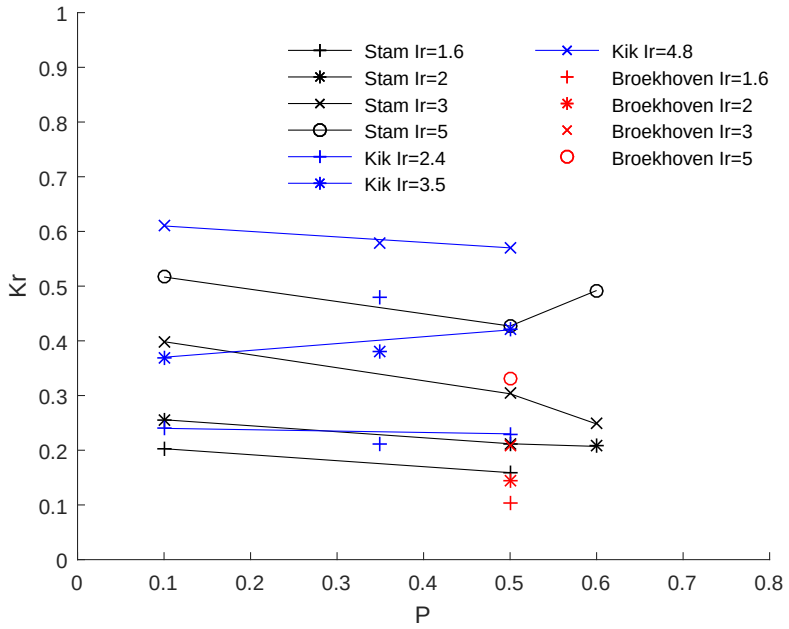

Figure 73: Data from physical tests. Interpolation based on the surf similarity parameter. All slopes.

Although not yet satisfactory, some improvements can be seen:

1. The trends, with exclusion of *Kik Ir=3.5*, seem to be more consistent.

2. While in figure 72 the dataset of Van Broekhoven [2011] showed similar values of K_r for all periods, inclusion of the slope seems to stretch this range. Still, the values seem rather low.

3. The data from Kik [2011] shows unexpected results. One reason for this could be the smaller size of the dataset. For the data points of *Stam*, multiple points with close ξ-values have

been averaged in order to reduce the influence of errors in measurements, while the data from Kik [2011] did not allow for this.

It can be concluded that inclusion of the slope results in better outcomes. Therefore interpolation based on period has been repeated, but now only using experiments executed on a slope of $\cot\alpha = 2$, resulting in figure 74. No selection in the dataset of Kik [2011] has been made, as all the experiments were done with $\cot\alpha = 2$.

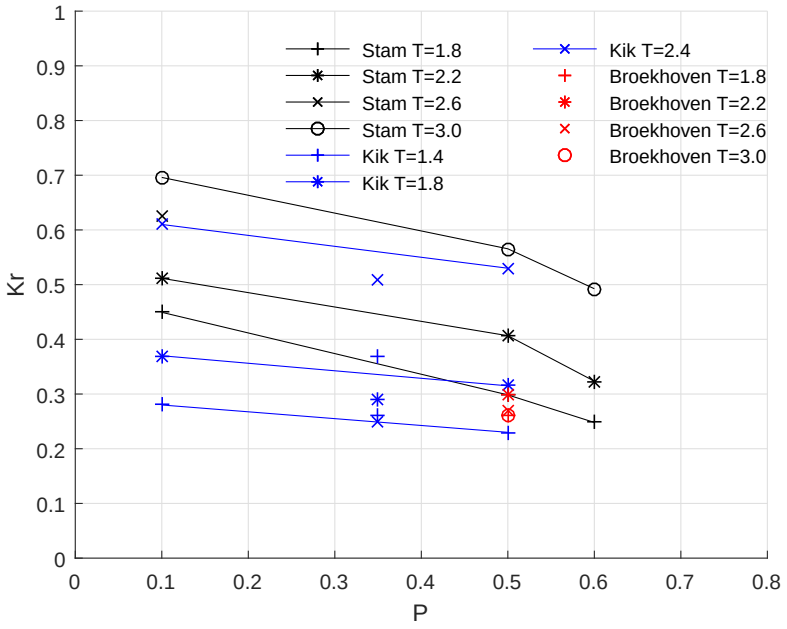

Figure 74: Data from physical tests. Interpolation based on the wave period. Only slopes with $\cot\alpha = 2$.

Selecting only one slope angle seems to improve the results. The following notions can be made:

1. Compared to figure 72, the lines have become steeper in general, discerning more between the various structures.
2. In all three cases, the reflected wave from a $P = 0.6$ structure is lower than from a $P = 0.5$ structure, as it should be.

The first notion above makes sense; the slope angle has a large influence on the amount of reflection, so a broad range of K_r-values is found for a structure when it is varied. Thus resulting in similar values for the two structures when averaged.

D

DATA FROM KIK INVESTIGATED

In his research, [Kik, 2011] ranged the Iribarren-number in order to make $\xi - H_s$-plots, and fit the *Van der Meer*-formula through the data points, as shown in 75. He thereby implicitly assumes a fixed P-value for the tested structure. For this research this assumption can't be made.

Ideally, we would like several wave heights to be tested at the same wave periods, in order to draw the damage curves as described in 2.1.1 on page 5. This data can not be found in the dataset. Below it is investigated if the dataset is still useful.

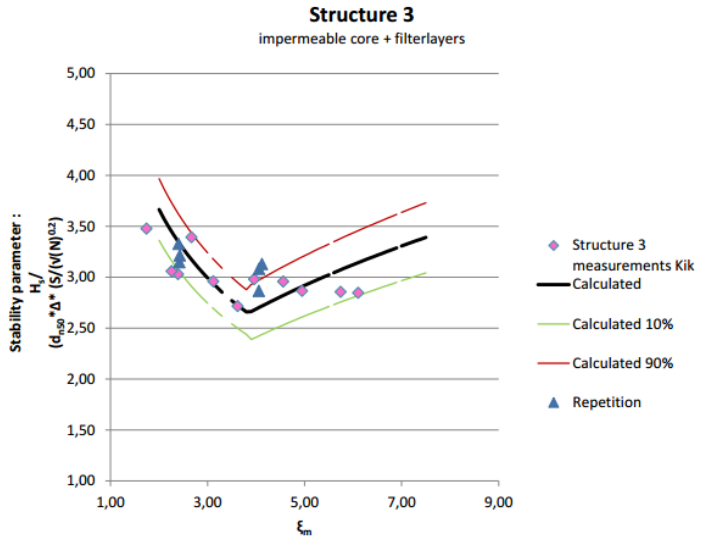

Figure 75: Resulting plot of method used by [Kik, 2011].

FIT PARAMETERS The lines drawn through measured damage points are fitted using a power function, αx^b, where $b = 5$. This can be seen when rewriting the *Van der Meer*-formula into a relation for H_s. The problem with having only one wave height measurement per wave period is that no line can be fitted through different points, and thus no wave heights for fixed damage levels can be read from the intersection. When assuming that for a zero wave height the damage is also zero, two points become available to fit a curve.

Now that the damage curves are available, the next step is to find the $H_s/\Delta D_{n50}$-values for fixed damage levels. This has been done for

$S = 3$ and $S = 8$, see 76 and 77

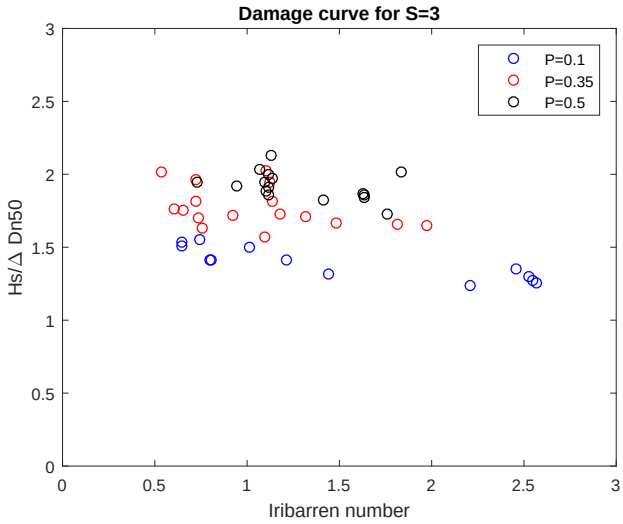

Figure 76: Plot showing damage levels for S=3

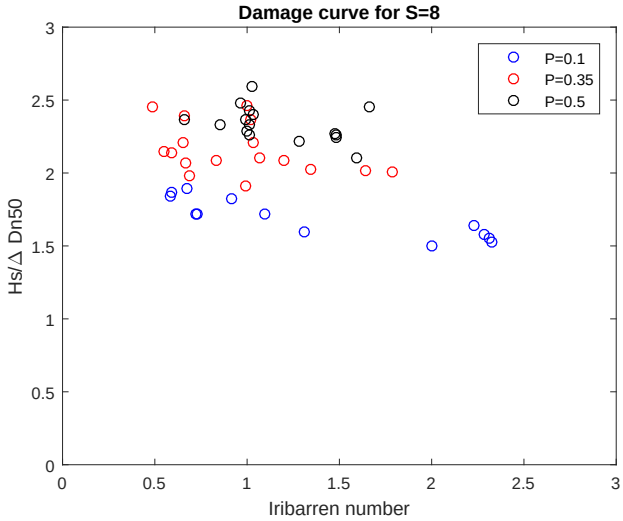

Figure 77: Plot showing damage levels for S=8

From these figures it becomes clear that although the difference in the tested structures can be seen clearly, the range of calculated Iribarren numbers is not wide enough to say anything about the plunging region ($\xi > 2.5 - 4$), this part is needed to estimate P. This way of fitting damage curves through (0,0) is not suitable for this dataset.

SECOND OPTION Instead of fitting damage curves through the data from [Kik, 2011], the idea can also be reversed: fit curves through the data from [Van der Meer, 1988] for damage levels obtained in tests

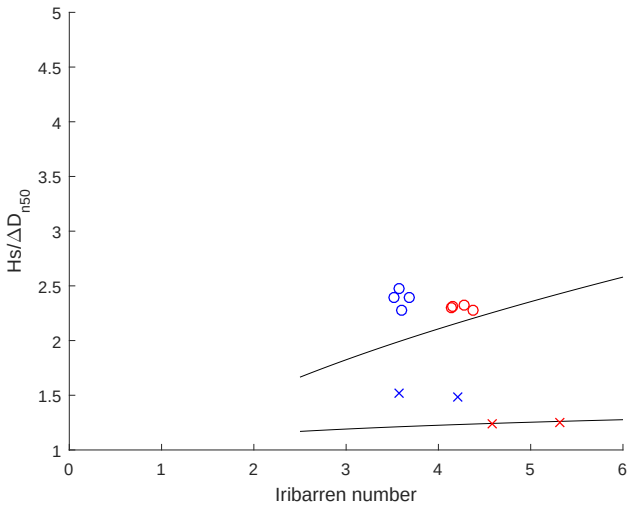

Figure 78: Data points for P=0.1 & P=0.5.

from [Kik, 2011]. This way no interpolation through limited data is done. This results in 78.

In figure 78, $Hs/\Delta D_{n50} - \xi$ is plotted for $P = 0.1$ and $P = 0.5$, including the *Van der Meer*-formula showed as a line for the surging region. From this figure it can be concluded that the way of interpolating the data performed here works when more data points are available. Conclusions about the influence of T on intermediate P-values can not be drawn, as these structures are at the outer bounds.

E

MATLAB SCRIPTS

Below the MATLAB scripts used in this thesis are presented.

E.1 CALCULATE FLOW INTO CORE

The script found below was used to calculate Q. It uses velocity data on the core layer interface based on simulations using regular waves. It assumes

```
lc;
clear all;
% Calculate Q over transection, above core layer
% Assumed 'postprocessing1_txttomat.m' is already run

%% settings:
% Enter coordinates start and endpoints:
xbts = 21.37;       % x begin trans section
xets = 24;       % x eind trans section
ybts = 0;
yets = 1.31;
dt = 0.1;           % model write frequency
res = 100;          % set desired resolution
run = 'reg_4_40';                                    % SET RUN
    NUMMER
ts = 20;                                    % start tijdsstap
h = 0.70; % water depth

%% Load data (cords, u, w)
mainfolder = ['path_to_folder' num2str(run) '\'];
load([mainfolder 'cords.mat']);             % load cords.mat
xc = (x_cords(:,1))';                       % only save 1
   row and transpose
clear x_cords                               % free up memory
yc = (y_cords(1,:));
clear y_cords
load([mainfolder 't.mat']);
vof = t;
tmax = length(t_t);
clear t t_t

c(1,:) = linspace(xbts, xets, res);
```

```
c(2,:) = linspace(ybts, yets, res);

%% find closest values
for i = 1:res
tmp = abs(xc-c(1,i));
[idx idx] = min(tmp);
c(5,i) = idx;
c(3,i) = xc(1, idx);
tmp = abs(yc-c(2,i));
[idx idx] = min(tmp);
c(6,i) = idx;                %rows with cellvalues
c(4,i) = yc(1, idx);         % of the coordinates
end

fig = figure();
Qsum=0;
Qpos=0;
Qneg=0;
load([mainfolder 'u.mat']);
load([mainfolder 'w.mat']);
clear w_t

%% find u for every point
run_time=tmax-ts;
un_pos=zeros(1,run_time);
qn_pos=zeros(1,run_time);
for t = 1:run_time        % start loop t
prog = ((t)/(run_time))*100;
clc
disp(['progress:' num2str(prog)]);

%clear u_t
ut = (u{1,t})';
%ut = flip(utt);             % ut are all velocities u on t
    in grid
clear utt
for i = 1:res
xtmp = c(5,i);
ytmp = c(6,i);
vl(1,i) = ut(ytmp,xtmp);
end
%clear ut
%clear u


wt = (w{1,t})';
```

```
% wt = flip(wtt);              % wt are all velocities w on t
    in grid
% clear wtt
for i = 1:res
xtmp = c(5,i);
ytmp = c(6,i);
vl(2,i) = wt(ytmp,xtmp);
end
% clear w
% clear wt


%% calculate normal-velocities
dx = xets - xbts;
dy = yets - ybts;
alpha = atan(dx/dy); % inverse slope angle
un=zeros(2,res);
L=sqrt(dx^2+dy^2); % length section

for i = 1:res
un(1,i) = cos(alpha)*vl(1,i) - (0.5*pi-cos(alpha))*vl(2,i);
   % velocity normal
if(un(1,i)>=0)
un_pos(1,t)=un_pos(1,t)+un(1,i);
qn_pos(1,t)=qn_pos(1,t)+un(1,i)*dt*L/res;
end
end

%% calc Q
dl=L/res; % length dsn per step
Qn=0;
Qpost=0;
Qnegt=0;
for i= 1:res
Qn=Qn+dl*un(1,i); %m2/s
if (Qn>0)
Qpost=Qpost+Qn*dt;
end
if (Qn<0)
Qnegt=Qnegt+Qn*dt;
end
end
Q=Qn;
Qt(1,t)=Q; % save Q per calculated step
Qpos(1,t)=Qpost;
Qneg(1,t)=Qnegt;
```

```
Qsum=Qsum+Q*dt; %sommatieum Q's x timestep


%% calc wave g on time t
voft = vof{1,t};
for i = 1:length(xc)
xtmp = xc(1,i);
[~,nvars] = size(voft);
hh=0;
ii=0;
while hh==0
tmp = nvars-ii;
if (voft(i,tmp)~=0)
hh=yc(1,tmp);
else
ii=ii+1;
end
end
gt(i,1)=xc(1,i);
gt(i,2)=hh;
end
%% plot results
subplot(2,1,1);
quiver(c(3,:),c(4,:),vl(1,:),vl(2,:),'.');
title(['time=' num2str(t*dt) 's , ' 'Q=' num2str(Q)]);
axis([xbts-1 xets ybts yets]);
hold on
line([xbts xets],[ybts yets]);
plot(gt(:,1),gt(:,2),'b');
ylabel('Height')
xlabel('Length')
hold off
subplot(2,1,2);
plot(c(1,:),un);
hold on
quiver(c(1,:),0,un(2,:),un(1,:),0,'.');
axis([xbts-0.1 xets -0.3 0.3]);
line([0 60], [0 0]);
ylabel('u_{into core}');
xlabel('Coordinate along intersection')
hold off

% maak gif
frame = getframe(fig);
im = frame2im(frame);
[imind,cm] = rgb2ind(im,256);
```

```
outfile = [mainfolder 'animation.gif'];

% On the first loop, create the file. In subsequent loops,
    append.
if t==1
imwrite(imind,cm,outfile,'gif','DelayTime',0,'loopcount',inf
    );
else
imwrite(imind,cm,outfile,'gif','DelayTime',0,'writemode','
    append');
end

end

%% PROCESS RESULTS FOR Q (versie 2)
T=str2num(run(end-1:end));
temp1=round((length(qn_pos)/2)-(length(qn_pos)*0.05));
temp2=round((length(qn_pos)/2)+(length(qn_pos)*0.05));
[~,t_start]=max(qn_pos(temp1:temp2));
t_start=t_start+temp1-1;

temp1=round((length(qn_pos))-(length(qn_pos)*0.05));
temp2=round((length(qn_pos)));
[~,t_end]=max(qn_pos(temp1:temp2));
t_end=t_end+temp1-1;

ap = round((t_end-t_start)/(T)); % aantal pieken totaal
Q_goed=sum(qn_pos(1,t_start:t_end))/ap

%% close
clearvars wn t tmpx tmpy Ri i Qpost Qnegt

save([mainfolder 'workspace.mat'],'Qt','qn_pos','Q_goed')
```

E.2 RUNNING SIMULATIONS PARALLEL IN BATCH-MODE

The following script is used when a large number of simulations are needed. Using a shared folder on a server containing predefined cases, multiple computers can run simulations simultaneously. To speed up the process of setting up cases, the adaptations to reduce output, see appendix B, are incorporated automatically. Also the locations of the wave gauges can be predetermined in the script and are incorporated as well.

This method consists of multiple scripts that need to be present in the same folder (active working directory in MATLAB) in order to work:

`batch_main.m` This is the main file that manages the other scripts. It is the file that is executed.

`alterinputfile1.m` This file opens the input file made by the model and changes some parameters.

`setup.m` Script used to make folders on the pc and copy the files from the server

`postproc_sv.m` Adaptation from [Van der Neut, 2015], used to rewrite .txt. files to .mat.

`importinputfile.m` A file used by script mentioned above.

E.2.1 *Preparation*

To successfully execute the scripts above some aspects should be taken care of. First of all the case files need to exist on a server that is accessible by the computer. A file named `log.xls` is needed. It contains the names of all the cases in column A and ends with the word 'end'. The executable file `IH_2VOF.exe` needs to be present in the main server folder as well.

The scripts presented below serve as a starting point from which a custom batch of simulations can be started. Customization and tweaking of these scripts is necessary.

E.2.2 *Batch_main.m*

```
%% batch script
% Assume server is mounted to Z:\
% Open log file
% read name of first non-executed entry
% mark as in progress
% copy case-files to local
% execute ih-2vof
% execute postprocessing1_txttomat
% copy files to server
% delete files from hdd

clc; clear all;
workfolder = 'C:\IH2VOF\CASES\batch\';
```

```
serverfolder = '\\server_path';
c_bezig={'0', '0', '0'};

%% Loop through case 1/2/3
while length(c_bezig) == 3
for c=1:3
casefolder = [workfolder 'case' num2str(c) '\'];
if exist([casefolder 'mesh.mes'], 'file') == 0 && exist([
    casefolder 'input'], 'file') == 0 && exist([casefolder '
    lock.lock'], 'file') == 0 %empty folder, set up new case
%% set up all files
[casenaam, eind] = setup(serverfolder, casefolder);
if eind==0
%% alter input file
alterinputfile1([casefolder 'input']);

%%RUN
%             dos(['start ' casefolder 'launcher.bat'])
cd(casefolder);
dos('start IH_2VOF.exe input noEnvelope');
cd('active_matlab_folder');
c_bezig{c}=casenaam; %set busy
pause(10);
else
disp('eind van log')
pause(180);
c_bezig{c}='klaar';
end
end
end

%% Check and compress/save
for c=1:3
casefolder = [workfolder 'case' num2str(c) '\'];
if exist([casefolder 'lock.lock'], 'file') == 0 && strcmp(
    c_bezig{c},'klaar')==0 %case klaar
%case folder
folder = [casefolder];

%create results folder
mkdir([folder 'files'])

%import simulation length, output-frequency, 'number_lines'
    per file
%and stored domain
input = importinputfile([folder 'input']);
```

```
idx = false(7,length(input));
for j = 1:length(input)
idx(:,j) = strcmp(input{j,1}, { ...
'twfin' ...
'freq_output' ...
'number_lines' ...
'ibg' ...
'ieg' ...
'jbg' ...
'jeg' ...
});
end
T = cell2mat(input(idx(1,:),2));
fs = 1/cell2mat(input(idx(2,:),2));
nr_lines = cell2mat(input(idx(3,:),2));
ibg = cell2mat(input(idx(4,:),2));
ieg = cell2mat(input(idx(5,:),2));
jbg = cell2mat(input(idx(6,:),2));
jeg = cell2mat(input(idx(7,:),2));

%load x-coordinates
x = load([folder 'xc_info.out']);
if (1 < ibg) & (ibg < ieg)
x = x(ibg:ieg);
end

%load y-coordinates
y = load([folder 'yc_info.out']);
if (1 < jbg) & (jbg < jeg)
y = y(jbg:jeg);
end

%generate meshgrid and save
[y_cords, x_cords] = meshgrid(y,x);
save([folder 'files\cords.mat'],'y_cords','x_cords')

%number of rows over which one 'y column' is distributed
nr_rows = 1;% ceil(length(y)/18);

%loop through folders filesPressure, filesU, filesVof and
    filesW
for j = 2:4
%initialise variables
B = cell(ceil(T/(nr_lines/fs)),nr_lines/fs);
timesteps = NaN(ceil(T/(nr_lines/fs)),nr_lines/fs);
```

```
%subfolder and variable names
if j == 1
subfolder = 'filesPressure\';
varname1 = 'p';
varname2 = 'p_t';
elseif j == 2
subfolder = 'filesU\';
varname1 = 'u';
varname2 = 'u_t';
elseif j == 3
subfolder = 'filesVof\';
varname1 = 't';
varname2 = 't_t';
elseif j == 4
subfolder = 'filesW\';
varname1 = 'w';
varname2 = 'w_t';
end

%loop through each text file
for k = 1:ceil(T/(nr_lines/fs))

%determine 'time-length' of current file
if k < ceil(T/(nr_lines/fs))
endT = nr_lines/fs;
elseif k == ceil(T/(nr_lines/fs))
endT = T - (k-1)*(nr_lines/fs);
end

%filename
filename = [folder subfolder varname1 sprintf('%03d',k) '.
    txt'];

%import text file
X = importfile1(filename, 1, (1+nr_rows*length(x))*fs*endT);

%loop through each time step in current text file
for l = 1:fs*endT

%determine start and end row of current timestep in X
startRow = l + (l-1)*length(x)*nr_rows;
endRow = l + l*length(x)*nr_rows;

%import into A
A = X(startRow:endRow,:);
[~,n]=size(A);
```

```
%initialise cell in B for current timestep
B{k,l} = NaN(length(x),n); %18*nr_rows);

%save timestep
timesteps(k,l) = A(1,1);

%reshape A and save in current cell of B
B{k,l} = (reshape(A(2:end,:)',n,length(x)))';

%delete NaN columns
B{k,l}(:,all(isnan(B{k,l}))) = [];
end
end

%reshape B and timesteps into rowvector
B = reshape(B',1,numel(B));
timesteps = reshape(timesteps',1,numel(timesteps));
B = B(~cellfun('isempty',B));
timesteps = timesteps(~isnan(timesteps));
timesteps(timesteps==0) = [];

%rename B and timesteps
assignin('base',varname1,B)
assignin('base',varname2,timesteps)

%save to .mat
save([folder 'files\' varname1 '.mat'],varname1,varname2,'-
    v7.3')
clear(varname1,varname2);

%delete folder
%rmdir([folder subfolder],'s')
end

pause(2)


dos(['robocopy ' casefolder 'files ' serverfolder '
    Cases_klaar\' c_bezig{c} ' /E']);
dos(['robocopy ' casefolder 'Sensor_freeSurface '
    serverfolder 'Cases_klaar\' c_bezig{c} ' /E']);
pause(5)
c_bezig{c}='0';
clear filename A B X x x_cords y y_cords nr_lines nr_rows
    ibg ieg varname1 varname2 subfolder
```

```
rmdir(casefolder,'s')
end
end
pause(10)
end
```

E.2.3 *alterinputfile1.m*

```
function [] = alterinputfile1(pathinputfile)

fid = fopen( pathinputfile );
cac = textscan( fid, '%s', 'Delimiter','\n', 'CollectOutput'
    ,true );
fclose( fid )
T = str2num(cac{1,1}{1,1}(end-1:end));
time = str2num(cac{1,1}{21,1}(end-2:end));
fid = fopen( pathinputfile, 'wt' );

ibg = 'ibg = start_i';
ieg = 'ieg = end_i';

switch T
case 15
xout = 'xout_fs = gauge_locations';
case 20
xout = 'xout_fs = gauge_locations';
case 30
xout = 'xout_fs = gauge_locations';
case 40
xout = 'xout_fs = gauge_locations';
end
timestring = ['tend_fs_sensor = ' num2str(time)];

insert={
'sensor_freesurfaceON = .true.';
'num_fs_sensor = 3';
xout;
'tinit_fs_sensor = 0';
timestring;
'freq_fs_sensor = 0.033333';
'/';
'&SENSOR_VELOCITY';
'sensor_velocityON = .true.';
'num_v_sensor = 3';
};

for jj = 1 : 18
```

```
fprintf( fid, '%s\n', cac{1,1}{jj} );
end
fprintf( fid, '%s\n', ibg );
fprintf( fid, '%s\n', ieg );
for jj = 19 : 24
fprintf( fid, '%s\n', cac{1,1}{jj} );
end
fprintf( fid, '%s\n', 'number_lines = 100' );
for jj = 26 : 34
fprintf( fid, '%s\n', cac{1,1}{jj} );
end
fprintf( fid, '%s\n', insert{:,1} );
for jj = 39 : length(cac{1,1})
fprintf( fid, '%s\n', cac{1,1}{jj} );
end
fclose( fid );
```

E.2.4 *setup.m*

```
function [casenaam, eind] = setup( serverfolder, casefolder
    )
%% Read log file
serverfolder = 'server_folder_path';
[num,txt,raw] = xlsread([serverfolder 'log']);
inprogress = num(:,1);
completed = num(:,2);
[row,col] = find(inprogress);
nr = length(col)+1;
eind = 0;
casenaam = txt{nr,1};
if strcmp(casenaam,'eind')==1; %eind bereikt, geen 1
    schrijven
eind = 1;
else
excelrange = ['B' num2str(nr)];
xlswrite([serverfolder 'log'],1,1,excelrange); %write 1 to
    row nr column B

%clear inprogress completed row col excelrange

%% Copy case files to local
command = ['if exist ' casefolder ' rmdir /Q /S ' casefolder
    ];
status = dos(command);
command = ['mkdir ' casefolder];
status = dos(command);
```

```
dos(['robocopy ' serverfolder ' ' casefolder ' IH_2VOF.exe'
    ]);
dos(['robocopy ' serverfolder 'Cases\' casenaam ' '
    casefolder ' /E']);

%% change .dat files to .in
dos(['rename "' casefolder 'eta_ext.dat"' ' "eta_ext.in"']);
dos(['rename "' casefolder 'info_ext.dat"' ' "info_ext.in"'
    ]);
dos(['rename "' casefolder 'u_ext.dat"' ' "u_ext.in"']);
dos(['rename "' casefolder 'v_ext.dat"' ' "v_ext.in"']);

% % create launcher.bat
% content = {['cd ' casefolder];
%     ['IH_2VOF.exe input noEnvelope']};
% fid2 = fopen([casefolder 'launcher.bat'],'w');
% fprintf(fid2, '%s \n',content{1,1});
% fprintf(fid2, '%s',content{2,1});

end
end
```

E.2.5 *postproc_SV.m*

```
function [] = postproc_SV( mainfolder, casefolders )
% mainfolder = 'folder_path'; %main folder
% casefolders = { ...  %cases
%     'case_name_1' 'case_name_2'};

%loop through each case folder
for i = 1:length(casefolders)
clearvars -except i mainfolder casefolders

%case folder
folder = [casefolders];

%create results folder
mkdir([folder 'files'])

%import simulation length, output-frequency, 'number_lines'
    per file
%and stored domain
input = importinputfile([folder 'input']);
idx = false(7,length(input));
for j = 1:length(input)
idx(:,j) = strcmp(input{j,1}, { ...
'twfin' ...
```

```
'freq_output' ...
'number_lines' ...
'ibg' ...
'ieg' ...
'jbg' ...
'jeg' ...
});
end
T = cell2mat(input(idx(1,:),2));
fs = 1/cell2mat(input(idx(2,:),2));
nr_lines = cell2mat(input(idx(3,:),2));
ibg = cell2mat(input(idx(4,:),2));
ieg = cell2mat(input(idx(5,:),2));
jbg = cell2mat(input(idx(6,:),2));
jeg = cell2mat(input(idx(7,:),2));

%load x-coordinates
x = load([folder 'xc_info.out']);
if (1 < ibg) & (ibg < ieg)
x = x(ibg:ieg);
end

%load y-coordinates
y = load([folder 'yc_info.out']);
if (1 < jbg) & (jbg < jeg)
y = y(jbg:jeg);
end

%generate meshgrid and save
[y_cords, x_cords] = meshgrid(y,x);
save([folder 'files\cords.mat'],'y_cords','x_cords')

%number of rows over which one 'y column' is distributed
nr_rows = 1;% ceil(length(y)/18);

%initialise waitbar
h = waitbar(0,'');
set(h,'Name',casefolders);

%loop through folders filesPressure, filesU, filesVof and
    filesW
for j = 2:4
%initialise variables
B = cell(ceil(T/(nr_lines/fs)),nr_lines/fs);
timesteps = NaN(ceil(T/(nr_lines/fs)),nr_lines/fs);
```

```
%subfolder and variable names
if j == 1
subfolder = 'filesPressure\';
varname1 = 'p';
varname2 = 'p_t';
elseif j == 2
subfolder = 'filesU\';
varname1 = 'u';
varname2 = 'u_t';
elseif j == 3
subfolder = 'filesVof\';
varname1 = 't';
varname2 = 't_t';
elseif j == 4
subfolder = 'filesW\';
varname1 = 'w';
varname2 = 'w_t';
end

%loop through each text file
for k = 1:ceil(T/(nr_lines/fs))
waitbar(((j-1)*ceil(T/(nr_lines/fs))+k)/ ...
(4*ceil(T/(nr_lines/fs))),h,'Reading text file')

%determine 'time-length' of current file
if k < ceil(T/(nr_lines/fs))
endT = nr_lines/fs;
elseif k == ceil(T/(nr_lines/fs))
endT = T - (k-1)*(nr_lines/fs);
end

%filename
filename = [folder subfolder varname1 sprintf('%03d',k) '.
    txt'];

%import text file
X = importfile1(filename, 1, (1+nr_rows*length(x))*fs*endT);

%loop through each time step in current text file
for l = 1:fs*endT
waitbar(l/(fs*endT),h,'Processing text file')

%determine start and end row of current timestep in X
startRow = l + (l-1)*length(x)*nr_rows;
endRow = l + l*length(x)*nr_rows;
```

```
%import into A
A = X(startRow:endRow,:);
[~,n]=size(A);

%initialise cell in B for current timestep
B{k,l} = NaN(length(x),n); %18*nr_rows);

%save timestep
timesteps(k,l) = A(1,1);

%reshape A and save in current cell of B
B{k,l} = (reshape(A(2:end,:)',n,length(x)))';

%delete NaN columns
B{k,l}(:,all(isnan(B{k,l}))) = [];
end
end
waitbar(1,h,'Saving to .mat file')

%reshape B and timesteps into rowvector
B = reshape(B',1,numel(B));
timesteps = reshape(timesteps',1,numel(timesteps));
B = B(~cellfun('isempty',B));
timesteps = timesteps(~isnan(timesteps));
timesteps(timesteps==0) = [];

%rename B and timesteps
waitbar(1,h,sprintf('Saving results...'))
assignin('base',varname1,B)
assignin('base',varname2,timesteps)

%save to .mat
save([folder 'files\' varname1 '.mat'],varname1,varname2,'-
    v7.3')
clear(varname1,varname2);

%delete folder
rmdir([folder subfolder],'s')
end

close(h)
end
end
```

E.2.6 *importinputfile.m*

```
function input = importinputfile(filename)
```

```
%IMPORTFILE1 Import numeric data from a text file as a
    matrix.
%   INPUT = IMPORTFILE1(FILENAME) Reads data from text file
    FILENAME for
%   the default selection.
%
%   INPUT = IMPORTFILE1(FILENAME, STARTROW, ENDROW) Reads
    data from rows
%   STARTROW through ENDROW of text file FILENAME.
%
% Example:
%   input = importfile1('input', 1, 60);
%
%    See also TEXTSCAN.

% Auto-generated by MATLAB on 2014/09/15 12:34:56

%% Initialize variables.
delimiter = ' ';
startRow = 1;
endRow = inf;

%% Read columns of data as strings:
% For more information, see the TEXTSCAN documentation.
formatSpec = '%s%*s%s%[^\n\r]';

%% Open the text file.
fileID = fopen(filename,'r');

%% Read columns of data according to format string.
% This call is based on the structure of the file used to
    generate this
% code. If an error occurs for a different file, try
    regenerating the code
% from the Import Tool.
textscan(fileID, '%[^\n\r]', startRow(1)-1, 'ReturnOnError',
     false);
dataArray = textscan(fileID, formatSpec, endRow(1)-startRow
    (1)+1, 'Delimiter', delimiter, 'MultipleDelimsAsOne',
    true, 'ReturnOnError', false);
for block=2:length(startRow)
frewind(fileID);
textscan(fileID, '%[^\n\r]', startRow(block)-1, '
    ReturnOnError', false);
```

```
dataArrayBlock = textscan(fileID, formatSpec, endRow(block)-
    startRow(block)+1, 'Delimiter', delimiter, '
    MultipleDelimsAsOne', true, 'ReturnOnError', false);
for col=1:length(dataArray)
dataArray{col} = [dataArray{col};dataArrayBlock{col}];
end
end

%% Close the text file.
fclose(fileID);

%% Convert the contents of columns containing numeric
    strings to numbers.
% Replace non-numeric strings with NaN.
raw = repmat({''},length(dataArray{1}),length(dataArray)-1);
for col=1:length(dataArray)-1
raw(1:length(dataArray{col}),col) = dataArray{col};
end
numericData = NaN(size(dataArray{1},1),size(dataArray,2));

% Converts strings in the input cell array to numbers.
    Replaced non-numeric
% strings with NaN.
rawData = dataArray{2};
for row=1:size(rawData, 1);
% Create a regular expression to detect and remove non-
    numeric prefixes and
% suffixes.
regexstr = '(?<prefix>.*?)(?<numbers>([-]*(\d+[\,]*)
    +[\.]{0,1}\d*[eEdD]{0,1}[-+]*\d*[i]{0,1})|([-]*(\d
    +[\,]*)*[\.]{1,1}\d+[eEdD]{0,1}[-+]*\d*[i]{0,1}))(?<
    suffix>.*)';
try
result = regexp(rawData{row}, regexstr, 'names');
numbers = result.numbers;

% Detected commas in non-thousand locations.
invalidThousandsSeparator = false;
if any(numbers==',');
thousandsRegExp = '^\d+?(\,\d{3})*\.{0,1}\d*$';
if isempty(regexp(thousandsRegExp, ',', 'once'));
numbers = NaN;
invalidThousandsSeparator = true;
end
end
% Convert numeric strings to numbers.
```

```
if ~invalidThousandsSeparator;
numbers = textscan(strrep(numbers, ',', ''), '%f');
numericData(row, 2) = numbers{1};
raw{row, 2} = numbers{1};
end
catch me
end
end

%% Split data into numeric and cell columns.
rawNumericColumns = raw(:, 2);
rawCellColumns = raw(:, 1);


%% Replace non-numeric cells with NaN
R = cellfun(@(x) ~isnumeric(x) && ~islogical(x),
    rawNumericColumns); % Find non-numeric cells
rawNumericColumns(R) = {NaN}; % Replace non-numeric cells

%% Create output variable
input = raw;
```

F

TEST PROGRAM FOR PHYSICAL MODEL TESTS

In this chapter a method is described how to find conclusive answers using physical model tests. Figure 79 shows what relations can be used for finding P, the dashed lines represent the relations that have not been validated yet and were investigated in this thesis. Solid lines depict the way P has been defined.

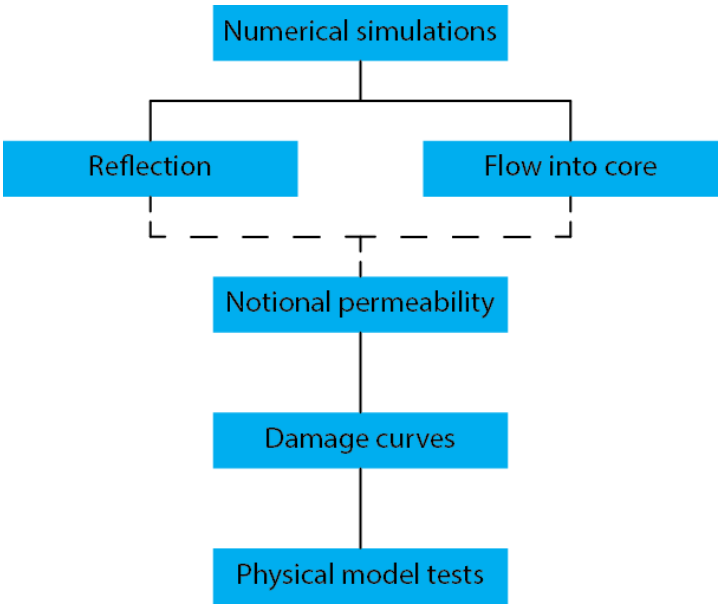

Figure 79: Scheme showing proven and unproven relations

F.1 GOAL

Physical model tests are a necessary step to discern between, and to validate the hypotheses. As can be seen in the scheme depicted in figure 79, physical model testing is the only *proven* way of finding P-values. The method of predicting these values is described in 2.1.1. A numerical model can be used to easily calculate K_r and Q, and more importantly, change the structure quickly and investigate its influence.

The goal of the physical tests is to see whether the hypotheses of finding P based on interpolation of Q and K_r produces the same result. As performing physical tests is time-consuming, the numbers of tests that need to be executed should be limited. Results need to be representative however, so attention should be paid how to limit the

number of tests.

STRUCTURE As testing a whole range of structures would take too much time. A start is made by defining an interesting structure. An important region for structures can be defined based on the tests in which t_c was varied between known-P configurations, see 5.2 on page 54. The result of this exercise is summarized in figure 80. Here, the blue line shows the results based on Q and the red those based on K_r. It can be seen that scatter is much larger in the red region and that the blue line follows a clearer trend as it is more steadily increasing. For values of $\frac{t_c}{D_{n50,a}} > 5$ the scatter around the blue line becomes very small, indicating the influence of T on the results becomes negligible. From $\frac{t_c}{D_{n50,a}} > 7$ the results are not increasing anymore. For the red line scatter is particularly large for $\frac{t_c}{D_{n50,a}} < 5$. The mean of the values when averaged over all wave periods seems to be higher for the red line compared to the blue line. Thus, an interesting region to investigate would be $1 < \frac{t_c}{D_{n50,a}} < 4$, specifically $\frac{t_c}{D_{n50,a}} = 4$, as the difference between the two methods is largest here, and it represents a situation that could be designed in practice.

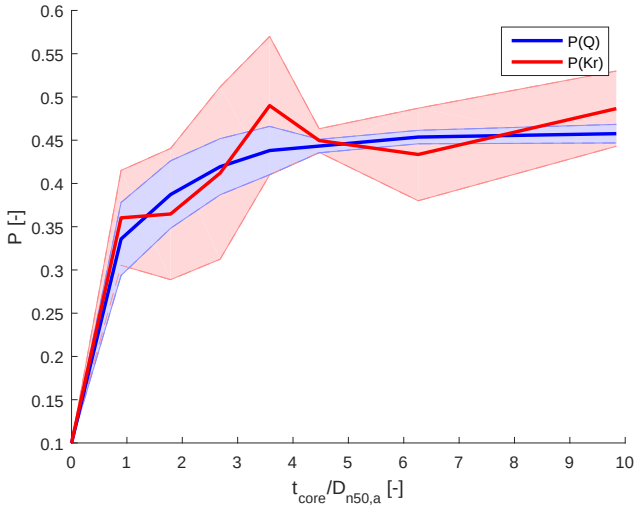

Figure 80: Plot showing mean values found for P, together with the range found in outcomes

Specific dimensions of the structure match those of the structures tested in this thesis, as stone diameters and layer thicknesses for the simulations were already selected with the purpose of being tested physically in a later stage. For the structure designs used in this thesis see 4.2.

Varying slope angle is recommended provided that the time is available. It would benefit the research as slope angle has a significant effect on stone stability and the parameter $\cot\alpha$ is part of the van der Meer-formula, thus varying it would provide a better fit of P. However, when time is critical, it is recommended to choose a fixed value for α. Moreover, the influence of α should first be investigated using numerical simulations.

HOW TO ASSIGN A P-VALUE TO A STRUCTURE This is a critical step and determines the tests to be executed. For images of the process, see 2.1.1.

In the end, P is a fit parameter in order to fit a curve through points on $H_s/\Delta D_{n50}$-ξ, graphs, for various damage levels and only for the surging part, as for those waves the Iribarren number could not incorporate the influence of the slope angle. A minimal test program would thus only include tests in the surging region (e.g. $\xi > 2.5-4$, depending on slope angle). To define multiple points in this plot, multiple damage curves are needed, as each curve provides one point per damage level. Such a curve relates H_s to a damage level S for a specific wave period. A range of wave heights and wave periods thus need to be tested.

This is an important difference with the method of [Kik, 2011]. In this research the shape of the fitted curve was kept similar and its position was fitted using a range of varied Iribarren numbers. While this is a very effective method, as it predicts a P-value using a relatively small number of tests, its validity in the *intermediate*-P region is uncertain, so it is better to maintain the original method. Moreover, the influence of T could be investigated using the results.

Other important lessons from [Kik, 2011] can be used however. In this research multiple structures were tested in order to validate the way of conducting tests (e.g. measuring damage). For structures $P = 0.1$ and $P = 0.5$ this method yielded good results as there was a reasonable match between measured and predicted S-values.

The recommendation for future research is thus to invest modeling time available in a wide range of T- vs. H_s-values, in order to construct sufficient damage curves for further analysis.

F.2 TEST PROGRAM

A *minimal* test program can be found in table 19, in which an example is provided for a minimal test program. Here, one structure is modeled. Adding more structures is beneficial for results if time is available, but when time is limited it is recommended to use provided wave conditions. This program will yield 5 damage curves based on 3 values of $\frac{H_s}{\Delta D_{n50}}$.

Table 19: Example of minimal test program

$\cot\alpha$	$t_c/D_{n50,a}$	# of tests	$H_s/\Delta D_{n50}$	Range T	Range s
2	8	5	1.5	1.5-4	0.01-0.025
2	8	5	1.9	1.5-4	0.012-0.031
2	8	5	2.3	1.5-4	0.014-0.038

As a comparison, the amount of damage that can be expected, depending on the method used is shown in table 20. The damage S is predicted using the van der Meer-formula [Van der Meer, 1988] and is calculated using a number of 1000 waves. In order to provide an estimation of the damage to be expected, S is calculated for both a permeable and an impermeable structure, as S for above tests is expected to be somewhere in between.

Table 20: Table showing damage that can be expected during tests.

$H_s/\Delta D_{n50}$	T [s]	S(P=0.5)	S(P=0.1)
1.5	1.5	1.50	5.55
	4	0.13	3.40
1.9	1.5	6.0	18
	4	0.52	11
2.3	1.5	19	46
	4	1.63	28

The values found for S cover a rather large range. However, as the expected value of P of the structure to be tested ($\frac{t_c}{D_{n50,a}} = 4$) will be between 0.1 and 0.5, so will the damage S.

The values for T that would be used in this program are the same in this thesis, so $T = 1.5,\ 2.0,\ 3.0,\ 4.0$. However, it is recommended to add a fifth wave period, $T = 2.5s$, as it appears to be an important range to model, see for example figures 30 where a relatively large

gap in results could potentially be explained using these values, and 34 where results are only found for wave periods of $T = 2.0s$ and $T = 3.0s$. Adding a fifth wave period also has the advantage of having an extra damage curve to fit data through.

F.3 RESULTS

With the resulting data the aforementioned damage-wave height curves can be constructed, relating $H_s/\Delta D_{n50}$ to damage levels S, per wave period T. Exponential curves are fitted through this data and then $H_s/\Delta D_{n50}$-values (rewritten to ξ) for certain predefined damage levels can be obtained. These ξ-values are grouped for certain fixed damage levels in order to create $H_s/\Delta D_{n50}$-ξ plots per damage level S.

It is expected that a curve with function $H_s/\Delta D_{n50} = \alpha\xi^P$ can be drawn through these points for the surging region, as was done in [Van der Meer, 1988].

The next step is now to compare this obtained P-value with outcomes of the numerical model. The process of predicting P-values using either Q or K_r is described in chapter 3 and 4. The goal is to find a way of interpolating the values of the governing parameters in such a way that a P-value matching the one found in physical tests is obtained. One method, with corresponding governing parameter, might be better able to describe the behavior for intermediate P-structures than the other.

G

RESULTS

In table 21 below, all the data obtained in this thesis is presented for future reference.

Table 21: All results obtained in the numerical simulations

Layout	Tp	Dn50,c	tc/dn50,a	P_Q	P_Kr	Q	Kr
A	1.5	*	*	0.1	0.1	0	0.3566
	2	*	*	0.1	0.1	0	0.4268
	3	*	*	0.1	0.1	0	0.6141
	4	*	*	0.1	0.1	0	0.7871
B	1.5	0.005	∞	0.5	0.5	0.0141	0.28
	2	0.005	∞	0.5	0.5	0.0262	0.2971
	3	0.005	∞	0.5	0.5	0.0457	0.4527
	4	0.005	∞	0.5	0.5	0.0607	0.627
C	1.5	0.04	∞	0.6	0.6	0.015	0.2813
	2	0.04	∞	0.6	0.6	0.0299	0.2941
	3	0.04	∞	0.6	0.6	0.0538	0.4276
	4	0.04	∞	0.6	0.6	0.073	0.6126
D	1.5	0.005	∞	0.49	0.46	0.0137	0.2877
	2	0.005	∞	0.47	0.47	0.0241	0.306
	3	0.005	∞	0.46	0.42	0.041	0.482
	4	0.005	∞	0.45	0.46	0.0531	0.6432
E	1.5	*	*	0.1	0.24	0	0.33
	2	*	*	0.1	0.2	0	0.3926
	3	*	*	0.1	0.13	0	0.601
	4	*	*	0.1	0.13	0	0.7745
F	1.5	0.005	0.89	0.378	0.3319	0.0098	0.3122
	2	0.005	0.89	0.3321	0.3054	0.0152	0.3602
	3	0.005	0.89	0.3171	0.3444	0.0248	0.5155
	4	0.005	0.89	0.3161	0.4593	0.0328	0.6433
G	1.5	0.005	1.79	0.4262	0.37	0.0115	0.3049
	2	0.005	1.79	0.3885	0.4143	0.0189	0.3249
	3	0.005	1.79	0.3705	0.2888	0.0309	0.5379
	4	0.005	1.79	0.3636	0.3856	0.04	0.6728

Table 21 – continued from previous page

Layout	Tp	Dn50,c	tc/dn50,a	P_Q	P_Kr	Q	Kr
H	1.5	0.005	2.68	0.4518	0.464	0.0124	0.2869
	2	0.005	2.68	0.4252	0.4328	0.0213	0.3189
	3	0.005	2.68	0.4072	0.3124	0.0351	0.5284
	4	0.005	2.68	0.3932	0.4388	0.045	0.6515
I	1.5	0.005	3.58	0.466	0.5	0.0129	0.28
	2	0.005	3.58	0.445	0.47	0.0226	0.3067
	3	0.005	3.58	0.4282	0.41	0.0375	0.4891
	4	0.005	3.58	0.413	0.58	0.0475	0.6155
J	1.5	0.005	4.47	0.451	**	0.0124	0.2717
	2	0.005	4.47	0.4435	0.4766	0.0225	0.3047
	3	0.005	4.47	0.437	0.4363	0.0385	0.4784
	4	0.005	4.47	0.4414	0.436	0.0519	0.6526
K	1.5	0.005	6.26	0.4543	**	0.0125	0.2779
	2	0.005	6.26	0.4496	0.487	0.0229	0.3012
	3	0.005	6.26	0.4492	0.38	0.04	0.5012
	4	0.005	6.26	0.4614	**	0.0548	0.6056
L	1.5	0.005	9.84	0.4555	**	0.0125	0.2778
	2	0.005	9.84	0.4511	0.53	0.023	0.2962
	3	0.005	9.84	0.4553	0.443	0.0406	0.4757
	4	0.005	9.84	0.4683	**	0.0559	0.6113
K	1.5	0.001	6.26	0.3958	0.4645	0.0104	0.2868
	2	0.001	6.26	0.3668	0.4944	0.0175	0.2989
	3	0.001	6.26	0.3551	0.2849	0.0292	0.5395
	4	0.001	6.26	0.3562	0.4633	0.0389	0.6418
K	1.5	0.007	6.26	0.4593	0.4828	0.0127	0.2833
	2	0.007	6.26	0.4569	0.4747	0.0234	0.3053
	3	0.007	6.26	0.4552	0.4361	0.0406	0.4785
	4	0.007	6.26	0.4637	0.4725	0.0552	0.638
K	1.5	0.01	6.26	0.4691	**	0.013	0.2765
	2	0.01	6.26	0.4719	0.488	0.0244	0.301
	3	0.01	6.26	0.4732	0.4591	0.0426	0.4692
	4	0.01	6.26	0.4818	**	0.0579	0.6013
K	1.5	0.013	6.26	0.474	**	0.0132	0.2727
	2	0.013	6.26	0.4815	**	0.025	0.2938
	3	0.013	6.26	0.4862	0.3265	0.0441	0.5227
	4	0.013	6.26	0.4973	0.5083	0.0603	0.6258

Table 21 – continued from previous page

Layout	Tp	Dn50,c	tc/dn50,a	P_Q	P_Kr	Q	Kr
K	1.5	0.016	6.26	0.4779	**	0.0133	0.2754
	2	0.016	6.26	0.4895	**	0.0255	0.2933
	3	0.016	6.26	0.4961	0.5323	0.0453	0.4446
	4	0.016	6.26	0.5106	0.477	0.0623	0.6362
K	1.5	0.1	6.26	0.4956	**	0.014	0.2715
	2	0.1	6.26	0.5369	**	0.0279	0.2855
	3	0.1	6.26	0.5791	0.5518	0.0519	0.4397
	4	0.1	6.26		**	0.0726	0.5789

* Undefined

** Interpolation based on K_r unsuccessful

∞ Whole structure consists of core material